

Thales Alenia Space  
Politecnico di Torino  
ISAE Supaero

---



**Aerospace Engineering master's thesis**

**Validation and further development of a tool  
for attitude perturbation analysis on satellites**

**Thesis supervisors:**

Eng. Andrea SITA (Thales Alenia Space)

Prof. Paolo MAGGIORE (Politecnico di Torino)

Prof. Joël BORDENEUVE-GUIBÉ (ISAE Supaero)

**Student:**

Pietro CRUCIANI

**November 2018**

Open

*This page is intentionally left blank.*

Open

# Abstract

Satellites encounter different kinds of attitude perturbations on orbit. Attitude perturbations are essentially torques that can be generated inside the satellite (sloshing of liquids, movable mechanisms...) or can derive from the space environment the satellite is in. This second class of perturbation torques can be subdivided in four groups: gravity gradient torque, magnetic torque, solar radiation pressure torque and aerodynamic torque. The estimation of these perturbations is crucial for the design of the Attitude and Orbit Control System (AOCS) of a satellite. Moreover, disturbing forces have an influence on the mission analysis of the satellite, in terms of propellant consumption and mission profile. This master's thesis, carried out at Thales Alenia Space in France, concerns the validation of a generic tool for the calculation of the solar radiation pressure perturbation acting on a satellite, and the development of an add-on of this tool for the computation of the aerodynamic disturbance as well. The tool consists in different modules that interact with each other. A module has been developed to propagate the orbit and the attitude of the satellite. Then, space environment models have been integrated in the modules aiming at estimating the attitude disturbances. Furthermore, a graphical user interface has been implemented to facilitate the insertion of the necessary inputs to set up a simulation. The tool has been validated by comparison with ESABASE, which is a software provided by the European Space Agency.

**Keywords:** space environment, perturbation torque, shadowing, solar radiation pressure, atmospheric density

*This page is intentionally left blank.*

**Open**

# Contents

<b>I</b>	<b>Introduction</b>	<b>1</b>
<b>1</b>	<b>General context</b>	<b>2</b>
1.1	Attitude and Orbit Control System (AOCS) . . . . .	2
1.2	The <i>Multi-physics analysis and modelization</i> team of Thales Alenia Space in France . . . . .	4
1.3	The necessity of a new tool for attitude perturbation analysis . . . . .	4
1.4	The scope of my internship . . . . .	5
<b>2</b>	<b>Planning and expected outcomes</b>	<b>6</b>
2.1	Planning . . . . .	6
2.2	Expected outcomes . . . . .	7
2.3	Report outline . . . . .	7
<b>II</b>	<b>Basic notions</b>	<b>8</b>
<b>3</b>	<b>Time conventions</b>	<b>9</b>
3.1	Solar time . . . . .	9
3.2	Sidereal time . . . . .	9
3.3	Solar day vs Sidereal day . . . . .	9
3.4	Universal Time (UT) . . . . .	10
3.5	Terrestrial Time (TT) . . . . .	11
3.6	International Atomic Time ( <i>Temps Atomique International</i> - TAI) . . . . .	11
3.7	Julian day . . . . .	11
<b>4</b>	<b>Reference frames used in TAPAS</b>	<b>12</b>
4.1	EME2000 . . . . .	12
4.2	Earth Centered-Earth Fixed (ECEF) frame . . . . .	13
4.3	Geocentric and geodetic coordinates . . . . .	13

4.3.1	Geocentric coordinates . . . . .	13
4.3.2	Geodetic coordinates . . . . .	14
4.4	Local Orbital Frame (LOF) . . . . .	15
4.5	Local Orbital Frame at time 0 (LOF0) . . . . .	16
4.6	Satellite reference frame . . . . .	16
<b>5</b>	<b>Perturbation torques</b>	<b>17</b>
5.1	Magnetic torque . . . . .	17
5.2	Gravity gradient torque . . . . .	17
5.3	Aerodynamic torque . . . . .	18
5.4	Solar radiation pressure torque . . . . .	19
5.5	Disturbance torques summary . . . . .	20
<b>III</b>	<b>The inputs of the tool</b>	<b>22</b>
<b>6</b>	<b>Structure of TAPAS</b>	<b>23</b>
6.1	Interactions between the different modules of the tool . . . . .	24
<b>7</b>	<b>Creation of the geometric model of the satellite</b>	<b>25</b>
7.1	What is Gmsh? . . . . .	25
7.2	Gmsh routines linked to TAPAS . . . . .	25
7.2.1	Body of the satellite . . . . .	26
7.2.2	Yoke . . . . .	30
7.2.3	Solar arrays . . . . .	31
<b>8</b>	<b>Mesh file in input to TAPAS</b>	<b>32</b>
8.1	bdf file . . . . .	33
<b>9</b>	<b>Date, orbit and attitude definition</b>	<b>35</b>
9.1	Initial date, orbit and attitude law of the simulation, entered directly in TAPAS	35
9.2	Orbit and attitude taken from external files . . . . .	38
<b>10</b>	<b>Graphical User Interface</b>	<b>39</b>
10.1	Starting windows . . . . .	39
10.2	Inputs for disturbing torques calculation . . . . .	41

<b>IV</b>	<b>Main modules of the TAPAS tool</b>	<b>43</b>
<b>11</b>	<b>Orbital mechanics module</b>	<b>44</b>
11.1	Orekit library . . . . .	44
11.1.1	The keplerian propagator . . . . .	44
11.1.2	The Eckstein-Hechler propagator . . . . .	45
11.1.3	Numerical integration propagator . . . . .	45
11.2	Solar arrays rotation . . . . .	45
<b>12</b>	<b>Solar and aerodynamic disturbances module</b>	<b>47</b>
12.1	Shadowing algorithm . . . . .	47
12.2	Solar torque computation . . . . .	49
12.3	Aerodynamic torque computation . . . . .	50
12.3.1	Solar and geomagnetic activity . . . . .	50
12.3.2	Atmospheric density . . . . .	52
<b>V</b>	<b>Results and validation</b>	<b>56</b>
<b>13</b>	<b>Example of analysis</b>	<b>57</b>
13.1	Inputs of the analysis . . . . .	57
13.2	Solar perturbation results . . . . .	58
13.2.1	Visualization of the orbit . . . . .	58
13.2.2	Visualization of the shadowing . . . . .	58
13.2.3	Solar force . . . . .	59
13.2.4	Solar torque . . . . .	60
13.3	Aerodynamic perturbation results . . . . .	61
13.3.1	Visualization of the orbit . . . . .	61
13.3.2	Visualization of the shadowing . . . . .	62
13.3.3	Aerodynamic force . . . . .	63
13.3.4	Aerodynamic torque . . . . .	63
<b>14</b>	<b>Validation results</b>	<b>65</b>
14.1	Solar force and torque validation . . . . .	65
14.1.1	ESABASE - TAPAS comparison for solar perturbation . . . . .	66
14.2	Aerodynamic force and torque validation . . . . .	71
14.2.1	ESABASE - TAPAS comparison for aerodynamic perturbation . . . . .	72

---

<b>VI</b>	<b>Conclusions</b>	<b>77</b>
<b>15</b>	<b>Conclusions</b>	<b>78</b>
15.1	Current state of the TAPAS tool . . . . .	78
15.2	Way forward . . . . .	78
	<b>Appendices</b>	<b>80</b>
<b>A</b>	<b>Other space environment models</b>	<b>81</b>
A.1	Earth's gravitational field . . . . .	81
A.2	Earth's magnetic field models . . . . .	83
A.2.1	Dipole magnetic field . . . . .	83
A.2.2	IGRF (International Geomagnetic Reference Field) . . . . .	84
A.2.3	WMM (World Magnetic Model) . . . . .	84
A.3	Sun ephemeris model . . . . .	86
<b>B</b>	<b>Different ways of defining the attitude of a satellite</b>	<b>87</b>
B.1	Cardan angles . . . . .	87
B.2	Rotation matrix . . . . .	87
B.3	Quaternions . . . . .	88
<b>C</b>	<b>The Runge-Kutta 4 method</b>	<b>89</b>

# List of Figures

1.1	Typical closed loop AOCS of a satellite. . . . .	2
1.2	On the left, configuration of three reaction wheels having their rotation axis perpendicular to each other. On the right, configuration of four reaction wheels placed on the faces of a pyramid. . . . .	3
2.1	Gantt diagram related to the planning of the internship. . . . .	6
3.1	Difference between solar and sidereal days [1]. From position 1 to position 2, one sidereal day has elapsed, while from position 1 to position 3, one solar day has elapsed. . . . .	10
4.1	EME2000 reference frame. References are dated to the J2000 epoch (1 <sup>st</sup> January 2000 at 12:00 TT) [2]. . . . .	12
4.2	ECEF reference frame [3]. . . . .	13
4.3	Geocentric latitude ( $\phi$ ) and longitude ( $\lambda$ ) of a point on the surface of the Earth [4]. . . . .	14
4.4	Geodetic vs geocentric latitude [5]. The form of the Earth ellipsoid is exaggerated in this figure. . . . .	14
4.5	Geodetic coordinates of a point P [6]. . . . .	15
4.6	VVLH Local Orbital Frame (LOF) for a satellite orbiting around the Earth. IRF stands for Inertial Reference frame [7]. . . . .	15
4.7	Satellite reference frame [8]. . . . .	16
5.1	Magnitude of perturbation torques as a function of the altitude [9]. au stands for arbitrary unit. Real values depend on the spacecraft design. . . . .	20
6.1	Structure of the folders of TAPAS. . . . .	23
6.2	Interactions between the different modules of TAPAS . . . . .	24
7.1	Mesh of a satellite model created with the graphical user interface of Gmsh. . . . .	26
7.2	Typical yoke of a satellite. . . . .	27

7.3	Body of a satellite modeled as a simple parallelepiped. . . . .	27
7.4	Body of a satellite modeled with inclined surfaces. . . . .	27
7.5	Body of a satellite with extensions on one face. . . . .	28
7.6	Body of a satellite with extensions on two faces. . . . .	28
7.7	Body of a satellite with extensions on three faces. . . . .	28
7.8	$\alpha$ angle between the ellipse and the x axis of the reflector reference frame, in the xy plane. . . . .	29
7.9	On the left, reflector drawn with a few points. On the right, reflector drawn with a lot of points. . . . .	30
7.10	Mesh of a reflector created with the Gmsh routine of TAPAS . . . . .	30
7.11	Three different shapes of yoke, created with the Gmsh routines of TAPAS. . . . .	31
7.12	Convention for numbering the solar arrays. . . . .	31
8.1	On the left, rough mesh of a satellite. On the right, refined mesh of a satellite. . . . .	32
8.2	Definition of the direction of the normal of a triangular element based on the order of its elements, following the right hand rule [10]. . . . .	34
9.1	Explanation of the keplerian orbital elements [11]. . . . .	36
9.2	$\theta$ angle for Sun-synchronous orbits [12]. The red line is the intersection between the equatorial plane and the orbit plane. . . . .	36
9.3	Yaw steering attitude law . . . . .	37
10.1	First window that appears after launching the TAPAS_Main.m script. . . . .	39
10.2	Window that appears after pressing the Ok button of the first window. . . . .	40
10.3	Window where the user can enter the parameters of the external files to be read by TAPAS for the definition of the orbit and attitude of the simulation. . . . .	40
10.4	Window where the user can choose the orbit propagator and the attitude law of the simulation. . . . .	41
10.5	Definition of the inputs for the aerodynamic torque computation. . . . .	41
10.6	Association of a material to each element group. On the left column there are the element groups of the satellite model. . . . .	42
12.1	Sun oriented reference frame, defined by the declination ( $\delta$ ) and azimuth ( $\alpha$ ) angles. . . . .	48
12.2	Shadowing problem in the xy plane of the Sun oriented frame. The primary polygon is the one having the lowest z coordinate in this frame. . . . .	48
12.3	Eclipse phases that a satellite can encounter along its orbit [13]. . . . .	49

12.4	Angle $\alpha$ between the satellite-to-Sun direction and the satellite-to-Earth direction. This angle is evaluated to know if the satellite is in eclipse, penumbra, or if it is enlightened by the Sun. . . . .	50
12.5	Evolution of the $F10.7$ index from 1990 to 2020. The red part of the diagram is the predicted radio flux. The smoothed radio flux is the flux averaged over one month. [14] . . . . .	51
12.6	Evolution of the $Ap$ index. The black line is the observed 13-month smoothed $Ap$ index, while the blue, green and red lines are the predicted values, for different percentiles. [15] . . . . .	52
12.7	Exponential model of the atmospheric density $\rho$ . . . . .	53
12.8	Atmospheric density at $0^\circ$ latitude as a function of the altitude, according to the NRLMSISE-00 model. The $\rho$ values are averaged over one year. The red line corresponds to $F10.7 = F10.7_{av} = 65$ and $Ap = 0$ , while the blue line corresponds to $F10.7 = F10.7_{av} = 250$ and $Ap = 45$ . . . . .	54
12.9	Map of the atmospheric density according to the NRLMSISE-00 model. The altitude is $400\text{ km}$ , the date is 21 Mar 2012, 12:00 UTC and the solar and geomagnetic activities indexes are $F10.7 = 88$ and $Ap = 1$ [16]. . . . .	55
13.1	Satellite of the example of this chapter. . . . .	57
13.2	Orbit and attitude of the satellite for the chosen simulation. The blue vector is the vector normal to the solar arrays, while the orange vector is the Sun direction. In the figure, these two vectors are superposed, which means that solar arrays point perfectly towards the Sun. . . . .	59
13.3	Solar shadow at the second step of the simulation, from two different points of view. The elements that are exposed to the Sun are green, while the shadowed elements are orange. In the image on the left, the satellite is seen from the Sun direction. . . . .	60
13.4	Solar force acting on the satellite, expressed in the satellite reference frame. . . . .	61
13.5	Solar torque acting on the satellite, expressed in the satellite reference frame. . . . .	61
13.6	Orbit and attitude of the satellite for the chosen simulation. The blue vector is the vector normal to the solar arrays, while the orange vector is the direction of the satellite velocity with respect to the atmosphere. . . . .	62
13.7	Aerodynamic shadow at the second step of the simulation, from two different points of view. The elements that are exposed to the air flow are green, while the shadowed elements are orange. In the image on the left, the satellite is seen in the direction of its velocity with respect to the atmosphere. . . . .	63

13.8	Aerodynamic force acting on the satellite, expressed in the satellite reference frame. . . . .	64
13.9	Aerodynamic torque acting on the satellite, expressed in the satellite reference frame. . . . .	64
14.1	The ecliptic. On summer solstice, the Sun is at its maximum latitude, while on winter solstice, it is at its minimum latitude, as seen from the Earth [17].	66
14.2	Geometric model used for the validation case of this chapter. . . . .	67
14.3	ESABASE results of the solar force, expressed in the satellite reference frame. The x-axis of the diagram is the time in hours, while the y-axis is the force in Newton. . . . .	68
14.4	TAPAS results of the solar force, expressed in the satellite reference frame. The x-axis of the diagram is the time in hours, while the y-axis is the force in Newton. . . . .	69
14.5	ESABASE results of the solar torque, expressed in the satellite reference frame. The x-axis of the diagram is the time in hours, while the y-axis is the torque in Newton meters. . . . .	70
14.6	TAPAS results of the solar torque, expressed in the satellite reference frame. The x-axis of the diagram is the time in hours, while the y-axis is the torque in Newton meters. . . . .	71
14.7	ESABASE results of the aerodynamic force, expressed in the satellite reference frame. The x-axis of the diagram is the time in hours, while the y-axis is the force in Newton. . . . .	73
14.8	TAPAS results of the aerodynamic force, expressed in the satellite reference frame. The x-axis of the diagram is the time in hours, while the y-axis is the force in Newton. . . . .	73
14.9	ESABASE results of the aerodynamic torque, expressed in the satellite reference frame. The x-axis of the diagram is the time in hours, while the y-axis is the torque in Newton meters. . . . .	74
14.10	TAPAS results of the aerodynamic torque, expressed in the satellite reference frame. The x-axis of the diagram is the time in hours, while the y-axis is the torque in Newton meters. . . . .	74
A.1	Geoid height with respect to the mean sea level, according to the EGM2008 model [18]. . . . .	81
A.2	Three different spherical harmonics. . . . .	82

---

A.3	Shape of the Earth magnetic field lines [19]. The Sun and the Earth are not to scale. . . . .	83
A.4	Declination of the Earth's magnetic field lines, according to the WMM - Epoch 2015.0. . . . .	85
A.5	Intensity of the Earth's magnetic field, according to the WMM - Epoch 2015.0.	85
B.1	Cardan angles of a satellite around the Earth [20]. . . . .	87
C.1	Runge-Kutta 4 method [21]. . . . .	90

*This page is intentionally left blank.*

Open

# List of Tables

2.1	Number of days spent for each main activity of the internship. . . . .	6
14.1	Comparison between the results of the solar force components of ESABASE and TAPAS. . . . .	68
14.2	Comparison between the results of the solar torque x and z components of ESABASE and TAPAS. . . . .	70
14.3	Comparison between the results of the aerodynamic force components of ESABASE and TAPAS. The comparison is made taking into consideration the same atmospheric densities. . . . .	75
14.4	Comparison between the results of the aerodynamic torque x and z components of ESABASE and TAPAS. The comparison is made taking into consideration the same atmospheric densities. . . . .	76

*This page is intentionally left blank.*

Open

# Acronyms

<b>AOCS</b>	Attitude and Orbit Control System
<b>bdf</b>	bulk data file
<b>CAD</b>	Computer-Aided Design
<b>CAE</b>	Computer-Aided Engineering
<b>ECEF</b>	Earth Centered-Earth Fixed
<b>EME2000</b>	Earth Mean Equator and equinox at epoch J2000
<b>EOR</b>	Electric Orbit Raising
<b>ESA</b>	European Space Agency
<b>GEO</b>	Geostationary
<b>GUI</b>	Graphical User Interface
<b>IGRF</b>	International Geomagnetic Reference Field
<b>LEO</b>	Low Earth Orbit
<b>LOF</b>	Local Orbital Frame
<b>LST</b>	Local apparent Solar Time
<b>NRLMSISE-00</b>	US Naval Research Laboratory Mass Spectrometer and Incoherent Scatter Radar Exosphere 2000
<b>OREKIT</b>	ORbit Extrapolation KIT
<b>SFU</b>	Solar Flux Unit
<b>SI</b>	Système International (International System)
<b>TAI</b>	Temps Atomique International (International Atomic Time)
<b>TAPAS</b>	Tool for Attitude Perturbation Analysis
<b>TAS</b>	Thales Alenia Space
<b>TASinF</b>	Thales Alenia Space in France
<b>TT</b>	Terrestrial Time
<b>UT</b>	Universal Time
<b>UTC</b>	Universal Time Coordinated
<b>WMM</b>	World Magnetic Model

# Part I

## Introduction

# Chapter 1

## General context

### 1.1 Attitude and Orbit Control System (AOCS)

All satellites have specific pointing requirements, based on the mission to perform. Pointing requirements are expressed in terms of pointing directions of the three body axes of the satellite. Therefore, satellites' attitude must be controlled by means of actuators, sensors and control laws. The attitude and orbit control of satellites is a closed-loop system: that means that the control torque to apply to the satellite is calculated taking into account the difference between the desired and the measured attitudes of the satellite. A typical block diagram of an attitude control system is shown in fig. 1.1.

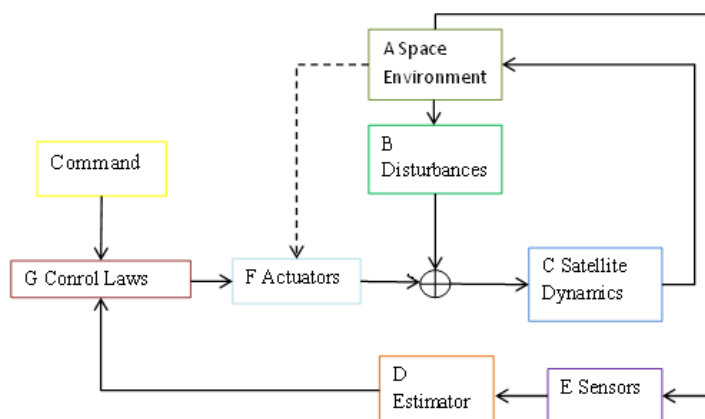


Figure 1.1: Typical closed loop AOCS of a satellite.

The control laws block evaluates the torque to apply to the satellite as a function of the attitude error, that is the difference between the command and the measured attitude of the satellite. This torque is applied by means of actuators. The satellite's attitude is measured with sensors. Since sensors are affected by noise and biases, estimators are included in the loop in order to find the best estimation of the real attitude. Estimators are also used to estimate variables that cannot be measured. In the block diagram of fig. 1.1, space

environment and disturbances play an important role. Indeed, they are responsible not only for pointing errors, but also for actuators sizing, as explained hereafter. Typically, reaction wheels are used as actuators. These wheels can rotate with respect to the satellite body by means of electric motors (stator plus rotor). Their functioning is based on the action reaction principle: if a wheel is accelerated in a certain direction, the satellite is submitted to the opposite angular acceleration. A satellite has typically three reaction wheels oriented so that their rotation axis form a Cartesian reference frame. To achieve a better pointing precision and for redundancy issues, some satellites have four reaction wheels. These two configurations are shown in fig. 1.2.

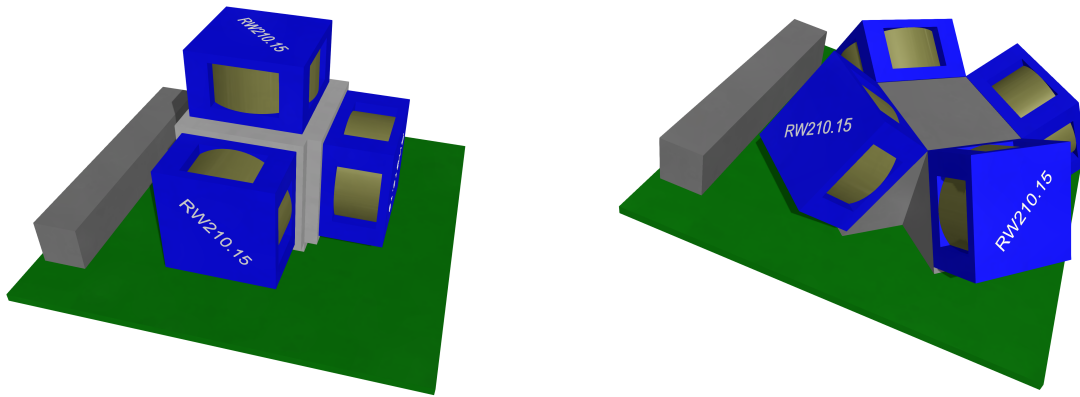


Figure 1.2: On the left, configuration of three reaction wheels having their rotation axis perpendicular to each other. On the right, configuration of four reaction wheels placed on the faces of a pyramid.

The dynamics equation of a rigid body satellite having reaction wheels as actuators is the following

$$\vec{t}_{ext} = \dot{\vec{h}}_{sat} + \dot{\vec{h}}_{RWS} + \vec{\omega}_{sat} \wedge (\vec{h}_{sat} + \vec{h}_{RWS}) \quad (1.1)$$

where  $\vec{t}_{ext}$  is the sum of all the external torques applied to the satellite,  $\dot{\vec{h}}_{sat}$  is the time derivative of the angular momentum of the satellite without taking into account the reaction wheels,  $\dot{\vec{h}}_{RWS}$  is the time derivative of the sum of all angular momenta of the reaction wheels, and  $\vec{\omega}_{sat}$  is the satellite's angular velocity. All the vectors in the eq. 1.1 are expressed in the satellite reference frame. It can be noticed that  $\vec{t}_{ext}$  has a direct influence on  $\dot{\vec{h}}_{RWS}$ , therefore it also influences the angular momentum of the wheels, which is the time integral of  $\dot{\vec{h}}_{RWS}$ . If the reaction wheels reach their maximum angular momentum (that means that they reach their maximum rotational speed), they lose their control capability. To avoid this, other actuators such as magnetorquers or thrusters are used. Thus, the estimation of perturbation torques is crucial to predict how frequently reaction wheels must be desaturated and how

to operate desaturation actions. From these aspects, trade-off choices about the sizing of the AOCS actuators are made.

## 1.2 The *Multi-physics analysis and modelization* team of Thales Alenia Space in France

During my internship, I worked in collaboration with the *Multi-physics analysis and modelization* team of Thales Alenia Space in France. This team carries out different types of analysis, such as the impact of the space environment on satellites and the interactions between the different subsystems of a spacecraft. This includes the propulsion, the structure, the power and thermal subsystems. The analysis conducted by the *Multi-physics analysis and modelization* team serve as support to the trade-off choices of the design of a satellite or mission. Within the company, the engineers of this team are the experts of orbital mechanics and disturbing torques and represent a reference for these subjects. Hence, they fill in the AOCS and Mission Analysis DataBank of a satellite project with the values of space environment disturbances.

## 1.3 The necessity of a new tool for attitude perturbation analysis

Until 2015, engineers at Thales Alenia Space in France used the software ESABASE, provided by ESA, for the calculation of the main kinds of perturbation torques. The use of ESABASE has various drawbacks:

1. ESABASE is a closed source program. It is not possible to see its source code, so debug actions are quite limited, and there is no possibility to develop and improve ESABASE internally.
2. ESABASE has very limited graphics capabilities. For instance, it is not possible to visualize the orbit or the attitude of the satellite. The satellite position and pointing information is saved only in a text file, by means of x-y-z coordinates.
3. It is an old tool: it is dated 1988. This means that the environment models (see appendix A and section 12.3) are not up-to-date, therefore solar activity and solar flux, as well as the atmospheric density estimation, are affected by relevant errors.
4. ESABASE runs on old servers that often have operational problems.
5. Because of their obsolescence, there is a potentially high risk of malfunctioning of the servers of ESABASE, with the possibility of loosing all the data inside them.

For these reasons the *Multi-physics analysis and modelization* team of TASinF decided to develop a tool internally, in order to replace ESABASE. This new tool is called TAPAS (Tool for Attitude Perturbation Analysis) and it is developed in the Matlab environment. My TAS tutor Andrea Sita started the development of this tool in 2015.

## 1.4 The scope of my internship

Within my internship, my main activities were to validate the solar torque module of TAPAS and to develop the aerodynamic torque module. Beside this, I was asked to change the meshing software used for TAPAS applications, to pass from a proprietary to an open source software. Moreover, other tasks of my internship were to improve the algorithm of the shadowing (see section 12.1) in order to make it faster, and to work on the user-friendliness of the tool.

## Chapter 2

# Planning and expected outcomes

### 2.1 Planning

The list of the main activities to carry out during my internship, in order of priority, is presented in table 2.1. The amount of time spent for each activity is indicated as well.

Task Name	Start	End	Duration [days]
Familiarization with the software to use	07/05/2018	08/06/2018	25
Integration of the software Gmsh into TAPAS	11/06/2018	20/06/2018	8
Validation of the solar torque module	21/06/2018	25/07/2018	25
Development of the aerodynamic torque module	26/07/2018	31/08/2018	27
Validation of the aerodynamic torque module	03/09/2018	20/09/2018	14
Better results comprehension	21/09/2018	28/09/2018	6
Graphical user interface	01/10/2018	05/10/2018	5
Report and user manual	08/10/2018	26/10/2018	15

Table 2.1: Number of days spent for each main activity of the internship.

The Gantt diagram related to the planning of the internship is presented in fig. 2.1

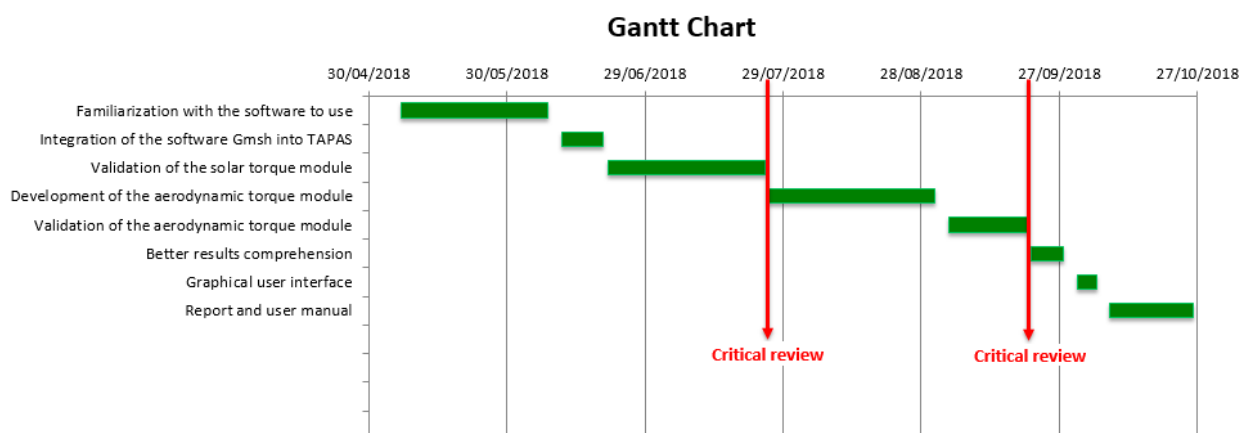


Figure 2.1: Gantt diagram related to the planning of the internship.

The two critical reviews of the internship were at the end of the validation phases of the

solar and aerodynamic torques modules. Indeed, the validation activities of the internship were crucial for its success.

## 2.2 Expected outcomes

The main expected outcome of the internship is a tool capable of calculating the solar and the aerodynamic forces and torques on a generic satellite. This also includes the user manual and the other documentation of the tool, such as the internship report and the validation files that can prove the proper functioning of TAPAS.

## 2.3 Report outline

This report is structured as follows. Chapters 3, 4 and 5 introduce the conventions used in the TAPAS tool as well as some basic theoretical notions necessary for the understanding of the report. Part III (that is, chapters 6 to 10) explains the structure of TAPAS, the creation and mesh of the geometric model of the satellite and the other inputs needed to set up a simulation. An explanation of the graphical user interface of the tool is given too. Chapters 11 and 12 show the main modules of TAPAS, i.e. the orbital mechanics and the disturbing torques modules. Finally, chapters 13 and 14 present an example of simulation and the validation results. Some possible ideas of improvement of the tool are detailed in part VI. The appendices contain specific theoretical insights to complement the document.

# Part II

## Basic notions

# Chapter 3

## Time conventions

There are different conventions to express an instant of time in space engineering. This chapter illustrates the ones used in the TAPAS tool.

### 3.1 Solar time

”Solar time is a calculation of the passage of time based on the position of the Sun in the sky. The fundamental unit of solar time is the day” [1]. The apparent solar time and the mean solar time can be distinguished as follows. Apparent solar time is based on the apparent motion of the actual Sun relative to the Earth. The fundamental time unit of the apparent solar time is the solar day, which corresponds to the time interval between two successive returns of the Sun to the local meridian [1]. Since the orbit of the Earth around the Sun is elliptical, the speed of the Earth throughout its orbit changes, therefore the duration of the solar day is not constant in a year. The mean solar time is the apparent solar time averaged throughout a year, so that the mean solar day remains constant.

### 3.2 Sidereal time

Sidereal time is a time scale that is based on Earth’s rate of rotation measured relative to the fixed stars. ”From a given observation point on the Earth, a star found at one location in the sky will be found at the same location on another night at the same sidereal time” [22].

### 3.3 Solar day vs Sidereal day

As explained previously, the duration of the solar day is the time interval between two successive returns of the Sun to the local meridian, so it is based on the Earth’s rotation motion as seen from the Sun. On the other hand, the sidereal day is the duration between

two successive returns of a fixed star to the local meridian, therefore it is based on the Earth's rotation motion as seen from the fixed stars (see fig. 3.1). On yearly average, the duration of a solar day is approximately 86400 UTC seconds, while the sidereal time lasts 86164.1 UTC seconds (see section 3.4 for the definition of UTC).

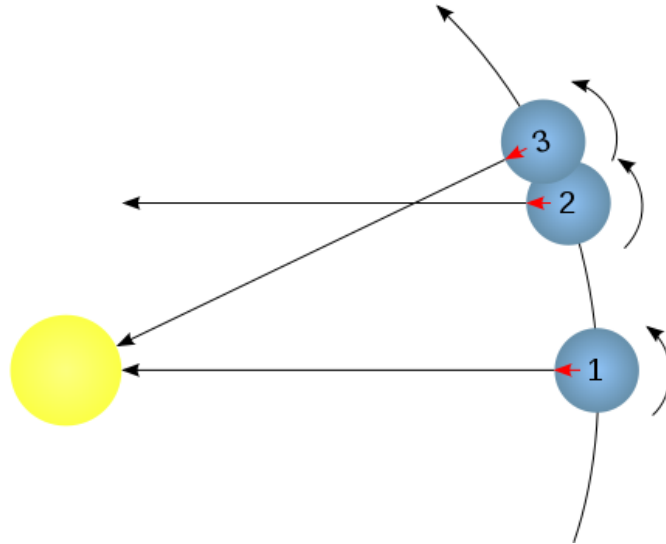


Figure 3.1: Difference between solar and sidereal days [1]. From position 1 to position 2, one sidereal day has elapsed, while from position 1 to position 3, one solar day has elapsed.

### 3.4 Universal Time (UT)

The most used time scale in the TAPAS tool is the Universal Time (UT) scale. This is also the most common time scale in space engineering. Universal time is a time standard based on Earth's rotation. Each instant of time is represented by the related year, month, day, hour, minute, second and millisecond. There are different versions of Universal Time [23]: the ones used in TAPAS are listed below.

1. **UT1**: "UT1 is the principal form of Universal Time" [23]. Conceptually, it coincides with the mean solar time at  $0^\circ$  longitude, therefore it is related to the Earth's rotation motion around its rotation axis, relative to the Sun. One second UT1 is equal to  $1/86400$  of a Solar Day (see section 3.1). Since precise measurements of the Sun direction are difficult, UT1 is computed from observations of distant quasars (Active Galactic Nucleus). Due to the slowdown of the Earth's rotation motion around its axis, the duration of one second UT1 is not constant over the years, but it increases of almost 2 milliseconds every 100 years.
2. **UTC**: UTC means Universal Time Coordinated and is the primary time standard by which the world regulates clocks and time [24]. It is an atomic timescale that approximates UT1. The duration of one UTC second is constant over time and coincides with

the duration of one second as defined by the International System of Units (SI). The duration of one UTC second is slightly smaller than the duration of one UT1 second and, due to the slowdown of the Earth's rotation motion, this difference increases over the years. In order to maintain the difference between the UTC and UT1 time scales smaller than one UTC second, leap seconds are occasionally added to the UTC time.

### 3.5 Terrestrial Time (TT)

Terrestrial Time is an ideal time scale used for time-measurements of astronomical observations made from the surface of the Earth [25]. One TT second coincides with one SI second.

### 3.6 International Atomic Time (*Temps Atomique International* - TAI)

"International Atomic Time is a high-precision atomic coordinate time standard" [26]. It is the principal realization of Terrestrial Time, except for a fixed offset. The duration of one TAI second is equal to the duration of one UTC second. TAI and UTC time scales coincided in 1958. Since then, leap seconds were added to the UTC, but not to the TAI time scale. Therefore, the difference between the TAI and UTC time scales increases over the years due to the addition of UTC leap seconds. The current and historical difference between TAI and UTC is also a reference of all the leap seconds added to the UTC scale over time. Nowadays, the TAI time scale is ahead the UTC of 37 SI seconds and behind the Terrestrial Time scale of about 32.184 SI seconds.

### 3.7 Julian day

Julian day is the continuous count of days since a specific starting date [27]. Each instant of time is associated to a Julian day number. This number can be integer or decimal. Decimal Julian day numbers express fractions of days. Julian days are used in different space engineering applications such as the Sun ephemeris calculation (see appendix A.3). There are different variants of Julian day depending on the time scale and on the starting date chosen to count days.

## Chapter 4

# Reference frames used in TAPAS

The following reference frames are used in the TAPAS tool. All the cartesian reference frames used within this tool are right-handed.

### 4.1 EME2000

The most used Earth-centered inertial reference system in space engineering is the EME2000 (also called J2000). Its origin is at the center of mass of the Earth. The x-axis of this frame is directed towards the Sun at the Spring equinox (approximately on 20<sup>th</sup> March), and the z-axis is aligned with the Earth's spin axis (towards the north pole). The y-axis completes the cartesian frame (see fig. 4.1). Since the Earth rotation is affected by precession and nutation, the convention for this frame is to take the J2000 epoch (1<sup>st</sup> January 2000 at 12:00 TT) as reference for the Earth rotation axis and the Earth-to-Sun direction at Spring equinox.

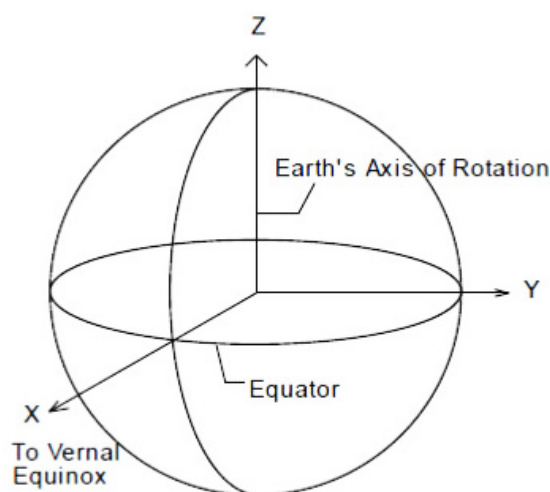


Figure 4.1: EME2000 reference frame. References are dated to the J2000 epoch (1<sup>st</sup> January 2000 at 12:00 TT) [2].

## 4.2 Earth Centered-Earth Fixed (ECEF) frame

The origin of the ECEF frame is the center of the Earth. Its x-axis corresponds to the intersection between the plane defined by the Greenwich meridian (or Prime Meridian) and the equatorial plane. The z-axis is directed from the South to the North Pole of the Earth and the y-axis completes the Cartesian reference frame (see fig. 4.2).

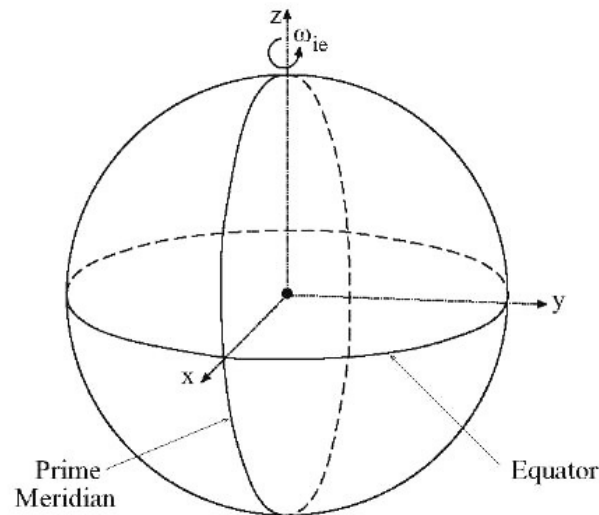


Figure 4.2: ECEF reference frame [3].

## 4.3 Geocentric and geodetic coordinates

The geocentric and geodetic coordinates are two similar ways of defining the position of a satellite by exploiting angular measures.

### 4.3.1 Geocentric coordinates

The geocentric coordinates are the geocentric latitude ( $\phi$ ) and longitude ( $\lambda$ ) referred to the center of the Earth, as shown in fig. 4.3. Note that

$$-90^\circ \leq \phi \leq 90^\circ \quad (4.1)$$

and

$$-180^\circ \leq \lambda < 180^\circ \quad (4.2)$$

To completely define the position of a point with respect to the Earth, a third coordinate is necessary. This third parameter is often the radius from the Earth's center to the considered point.

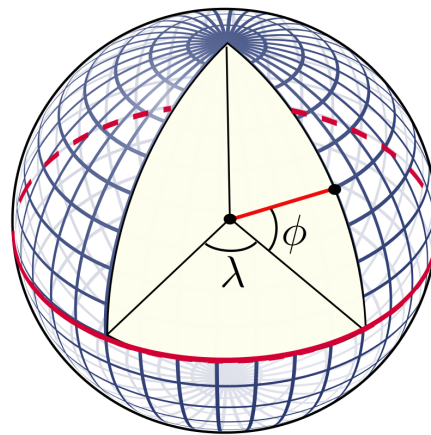


Figure 4.3: Geocentric latitude ( $\phi$ ) and longitude ( $\lambda$ ) of a point on the surface of the Earth [4].

### 4.3.2 Geodetic coordinates

The geodetic coordinates are similar to the geocentric ones, but, in this case, the reference is the axis which is normal to the spheroid representing the Earth and passes through the point under consideration (fig. 4.4). In fact, the Earth is not a perfect sphere, being slightly flattened at the poles.

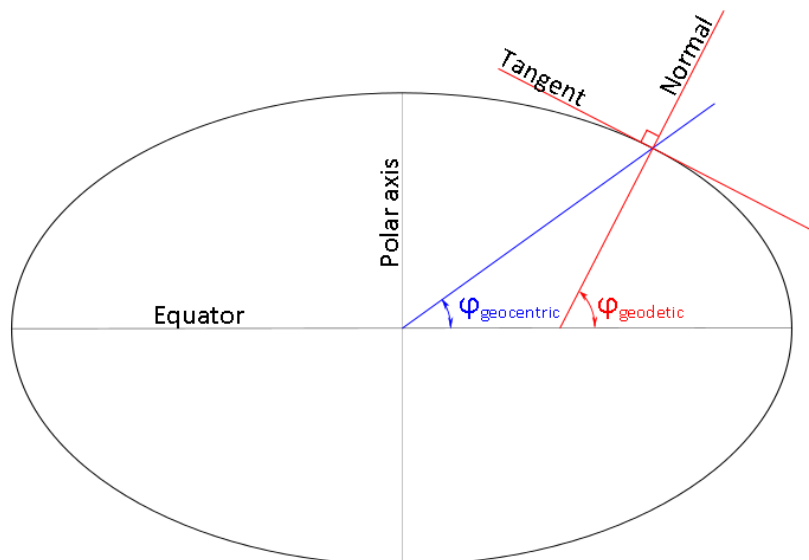


Figure 4.4: Geodetic vs geocentric latitude [5]. The form of the Earth ellipsoid is exaggerated in this figure.

For the geodetic coordinates, the third parameter used to define completely the position of a point P is the altitude ( $h$ ), evaluated along the direction normal to the spheroid modelling the Earth's surface (see fig. 4.4 and 4.5).

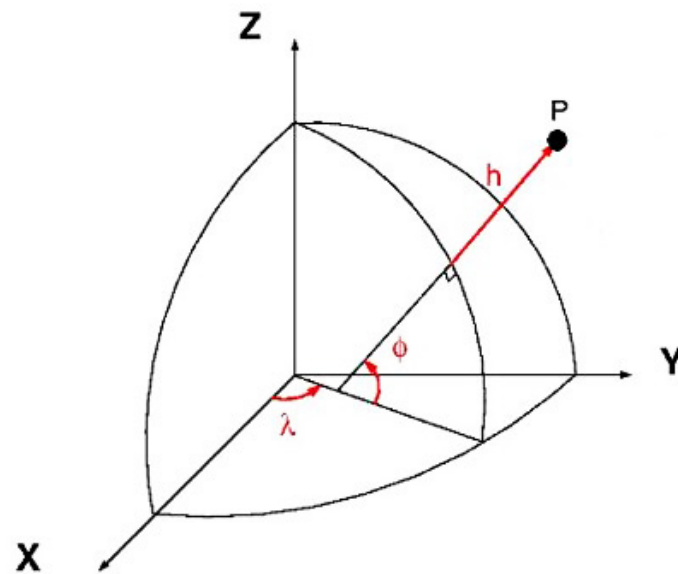


Figure 4.5: Geodetic coordinates of a point P [6].

#### 4.4 Local Orbital Frame (LOF)

The Local Orbital Frame is centered at the satellite's center of gravity. There are different types of Local Orbital Frames. The one which is used in TAPAS is called VVLH, that stands for Vehicle Velocity, Local Horizontal. The z-axis of this frame is directed towards the Earth's center of gravity, and the y-axis is perpendicular to the orbital plane so that the x-axis forms an acute angle with the velocity of the satellite (see fig. 4.6).

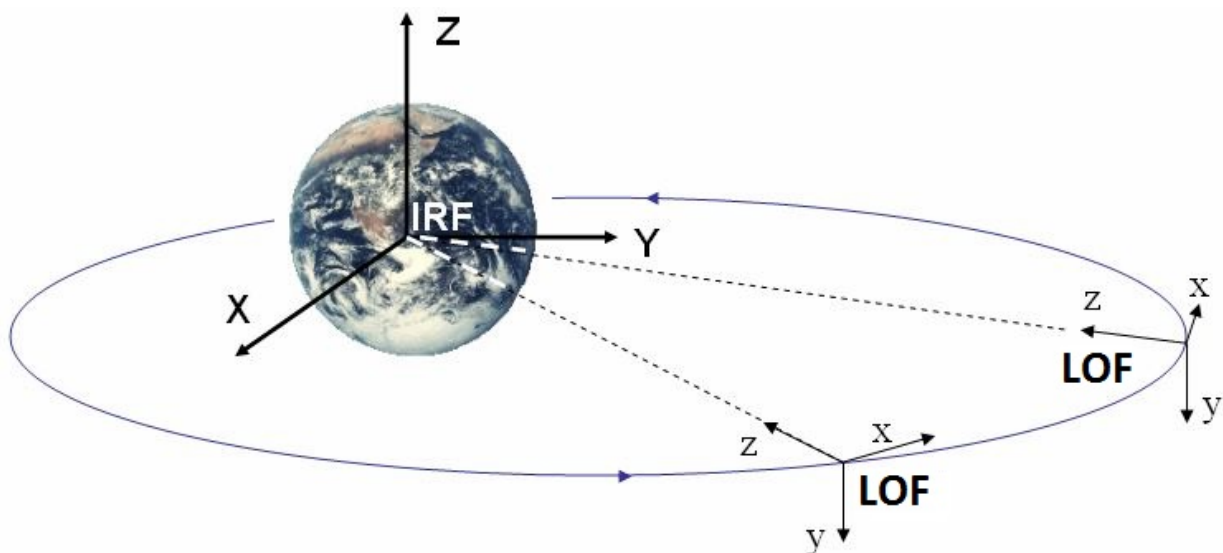


Figure 4.6: VVLH Local Orbital Frame (LOF) for a satellite orbiting around the Earth. IRF stands for Inertial Reference frame [7].

## 4.5 Local Orbital Frame at time 0 (LOF0)

The Local Orbital Frame 0 (LOF0) is simply the Local Orbital Frame at the first instant of the simulation. This reference frame is important because it does not rotate, therefore it can be considered as inertial. In an inertial reference frame, the equation 1.1 becomes

$$\vec{t}_{ext} = \dot{\vec{h}}_{sat,tot} \quad (4.3)$$

where  $\vec{h}_{sat,tot}$  is the global angular momentum of the satellite. One can notice that the time integration of external torques in an inertial reference system, from the start to the end of the simulation, is equal to the global angular momentum that the spacecraft accumulates all over the simulation period. This is a clear index for the sizing of the actuators of the AOCS of the satellite.

## 4.6 Satellite reference frame

The satellite reference system is a frame of reference which is linked to the body of the satellite. Its origin is usually the satellite's center of gravity, but can be any other point of the satellite's body. This reference system is important because all the satellite's equipment, including the AOCS actuators and sensors, is linked to this frame. The fig. 4.7 shows a typical example of satellite reference frame, where solar panels are along the y-axis.

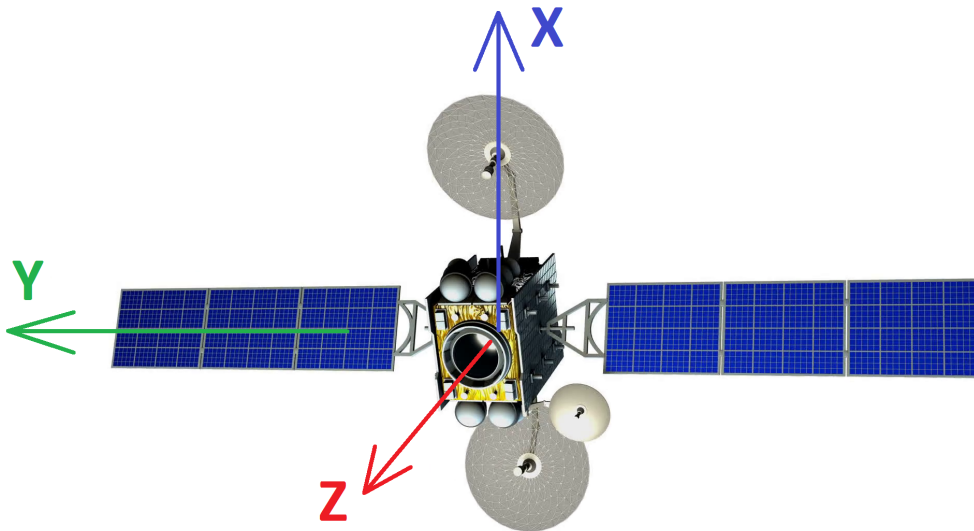


Figure 4.7: Satellite reference frame [8].

# Chapter 5

## Perturbation torques

A satellite encounters different kinds of attitude perturbation on orbit. In this chapter, all the possible types of external attitude perturbations are listed, explaining the physical phenomena underlying these perturbations, and the equations to estimate them.

### 5.1 Magnetic torque

The Earth, like many others planets of the solar system, is surrounded by a magnetic field that originates at its core.

Inside a satellite, there are usually a lot of electronic components that can create a magnetic moment. Due to the presence of the Earth's magnetic field, these magnetic moments generate a torque on the satellite, according to the following law

$$\vec{t}_B = \vec{M} \wedge \vec{B} \quad (5.1)$$

where  $\vec{t}_B$  is the magnetic torque,  $\vec{B}$  is the magnetic field of the Earth and  $\vec{M}$  is magnetic moment inside the satellite [28]. This kind of perturbation torque is significant only for LEO satellites, because the intensity of the magnetic field of the Earth decreases proportionally to  $1/r^3$  (see eq. A.6), therefore it becomes negligible in high orbits.

### 5.2 Gravity gradient torque

The Earth gravity acts on the satellite and, due to its non-uniform mass distribution along its three axes, a gravity gradient torque is created. This torque is the sum of the forces acting on each infinitesimal mass element having a lever arm with respect to the center of gravity of the satellite [29]. The resulting gravity gradient torque,  $\vec{t}_{GG}$ , is described by the following cross product.

$$\vec{t}_{GG} = 3 \frac{\mu}{r^3} \vec{e}_{E-sat} \wedge (\mathbf{I}_{sat} \cdot \vec{e}_{E-sat}) \quad (5.2)$$

where  $\mu$  is the gravitational parameter  $GM$  of the Earth,  $r$  is the distance between the satellite's and the Earth's centers of gravity,  $\mathbf{I}_{sat}$  is the inertia matrix of the satellite and the  $\vec{e}_{E-sat}$  is the unit vector in the direction Earth-satellite. This kind of torque is important for LEO satellites whose inertia around one axis is much smaller than the inertia around the other two axis. As the magnetic torque, the gravity gradient torque becomes negligible in high orbits, due to the presence of  $1/r^3$  in its expression (eq. 5.2).

### 5.3 Aerodynamic torque

Satellites in LEO are exposed to atmospheric forces too. Even if the atmospheric density decreases exponentially with the altitude, it has a non-negligible effect on satellites under 1000 *km* of altitude. The estimation of the aerodynamic force acting on a plane surface of a satellite is calculated by the following equation

$$\vec{F}_{aero} = \frac{1}{2} \rho \|\vec{V}\|^2 A (C_t \sin(\alpha) \cos(\alpha) \vec{t} - C_n \cos^2(\alpha) \vec{n}) \quad (5.3)$$

where  $\rho$  is the atmospheric density,  $\vec{V}$  is the velocity of the satellite with respect to the atmosphere,  $A$  is the dimension of the surface ( $m^2$ ),  $C_t$  is the tangential aerodynamic coefficient,  $\alpha$  is the angle between the normal to the surface and the vector  $\vec{V}$  ( $0 \leq \alpha \leq 90^\circ$ ),  $\vec{t}$  is the unit vector which is tangent to the surface and is in the same plane as the vector  $\vec{V}$ ,  $C_n$  is the normal aerodynamic coefficient and  $\vec{n}$  is the unit vector normal to the surface. The eq. 5.3 is valid under the hypothesis of free molecular flow, which is linked to the Knudsen number as follows [30]

$$Kn = \frac{\lambda}{L} > 1 \quad (5.4)$$

where  $\lambda$  is the mean free path of the atmosphere molecules and  $L$  is the representative physical length scale of the problem under consideration. For spacecraft applications, the hypothesis of free molecular flow is applicable above 140 *km* of altitude [30].

The values of the aerodynamic coefficients  $C_t$  and  $C_n$  are difficult to estimate. Typically, a good approximation is  $C_t = 1.7$  and  $C_n = 2.3$  [31]. The estimation of the atmospheric density is another crucial aspect in the eq. 5.3. The atmospheric density at high altitudes depends widely on the solar and geomagnetic activities. The stronger these two activities, the denser the atmosphere is.

It is assumed that the force  $\vec{F}_{aero}$  is applied to the geometric center of the surface under consideration. Therefore, the resulting torque about the satellite's center of gravity, deriving from this force, is

$$\vec{t}_{aero} = \vec{v}_{GO} \wedge \vec{F}_{aero} \quad (5.5)$$

where  $\vec{v}_{GO}$  is the vector going from the center of gravity of the satellite to the geometric center of the surface on which  $\vec{F}_{aero}$  acts. In estimating the aerodynamic force with the eq. 5.3, one has to consider only those surfaces of the satellite which are exposed to the air flow. For this, an algorithm capable of calculating the shadowing on the satellite's external surfaces (see section 12.1) is necessary. The estimation of the global torque acting on the satellite is made by integration of all the contributions of each infinitesimal elementary surface:

$$\vec{t}_{aero} = \int_{surf} \vec{r} \wedge d\vec{F}_{aero} \quad (5.6)$$

where  $d\vec{F}_{aero}$  is the aerodynamic force acting on the elementary surface, and  $\vec{r}$  is the lever arm of  $d\vec{F}_{aero}$  with respect to the point around which the torque is evaluated. The integral in eq. 5.6 is applied to the external surfaces of the satellite which are exposed to the airflow. In TAPAS, a finite elements model of the satellite must be created using triangle elements. The overall aerodynamic torque acting on the satellite is then calculated as the sum of the contributions of the forces applied to all the  $N$  triangle elements which are exposed to the airflow.

$$\vec{t}_{aero, tot} = \sum_{i=1}^N \vec{t}_{aero, i} = \sum_{i=1}^N \vec{v}_{GOi} \wedge \vec{F}_{aero, i} \quad (5.7)$$

## 5.4 Solar radiation pressure torque

While all the other kinds of disturbing torques are considerable only for LEO satellites, the solar radiation pressure torque is predominant in high orbits. This is the main perturbation torque for geostationary satellites. The cause of this kind of torque on a satellite is the impacts of solar photons on the satellite's surfaces. To estimate the solar radiation pressure force acting on a plane surface, the following expression is used

$$\vec{F}_{solar} = p A \cos(\alpha) \left\{ - \left[ (1 + C_S) \cos(\alpha) + \frac{2}{3} C_D \right] \vec{n} + (1 - C_S) \sin(\alpha) \vec{t} \right\} \quad (5.8)$$

where  $p$  is the solar pressure (near the Earth,  $p \simeq 4.66 \cdot 10^{-6} N/m^2$ ),  $A$  is the dimension of the surface under consideration ( $m^2$ ),  $\alpha$  is the angle between the vector which goes from the satellite's center of gravity to the Sun's center of gravity and the normal to the surface ( $0^\circ \leq \alpha \leq 90^\circ$ ),  $C_S$  is the specular coefficient of the material of the surface,  $C_D$  its diffuse coefficient,  $\vec{n}$  is the unit vector normal to the surface and  $\vec{t}$  is the unit vector tangent to the surface and in the same plane as the satellite-to-Sun vector. As for the aerodynamic force, it is assumed that the force  $\vec{F}_{solar}$  is applied to the geometric center of the considered surface, so a torque about the satellite's center of gravity is created, according to the following

expression

$$\vec{t}_{solar} = \vec{v}_{GO} \wedge \vec{F}_{solar} \tag{5.9}$$

where  $\vec{v}_{GO}$  is the vector going from the center of gravity of the satellite to the geometric center of the surface on which  $\vec{F}_{solar}$  acts. Also in this case, one has to consider only those surfaces of the satellite which are enlightened by the Sun, therefore a shadowing algorithm is necessary (see section 12.1). The global solar torque is estimated by integration of all the contributions of each infinitesimal elementary surface:

$$\vec{t}_{solar} = \int_{surf} \vec{r} \wedge d\vec{F}_{solar} \tag{5.10}$$

where  $d\vec{F}_{solar}$  is the solar force acting on the elementary surface, and  $\vec{r}$  is the lever arm of  $d\vec{F}_{solar}$  with respect to the point around which the torque is evaluated. The integral in the eq. 5.10 is applied to all the enlightened surfaces of the satellite.

As already mentioned, in TAPAS a finite elements model of the satellite must be created using triangle elements. The overall solar torque acting on the satellite is then calculated as the sum of the contributions of the forces applied to all the  $N$  enlightened triangle elements.

$$\vec{t}_{solar, tot} = \sum_{i=1}^N \vec{t}_{solar, i} = \sum_{i=1}^N \vec{v}_{GOi} \wedge \vec{F}_{solar, i} \tag{5.11}$$

## 5.5 Disturbance torques summary

The fig. 5.1 shows a typical dependence of the four types of disturbance torques on the altitude.

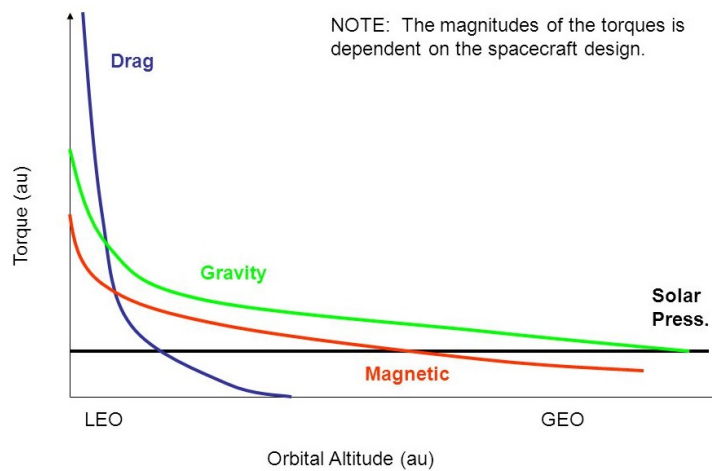


Figure 5.1: Magnitude of perturbation torques as a function of the altitude [9]. au stands for arbitrary unit. Real values depend on the spacecraft design.

The TAPAS tool only estimates the aerodynamic and solar torques on a satellite, because

these are the most complex ones, especially because of the shadowing of some surfaces of the satellite. The magnetic and the gravity gradient torques can be simply calculated by analytical equations.

## Part III

# The inputs of the tool

# Chapter 6

## Structure of TAPAS

The structure of the folders of the TAPAS tool is shown in fig. 6.1.

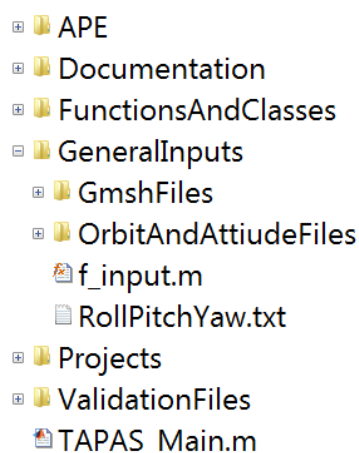


Figure 6.1: Structure of the folders of TAPAS.

All the folders in the fig. 6.1 are contained inside the main folder which is called TAPAS. The tool can be launched by running the script TAPAS\_Main.m. The central core of the tool is inside the *APE* folder. *APE* stands for Attitude Perturbation Estimation. The *Documentation* folder contains the user manual and other documentation about the tool. The folder *FunctionsAndClasses* contains all the functions of TAPAS, including those for the environmental models, orbit propagation and disturbing torques estimation. The folder *GeneralInputs* contains some general input files of the tool, such as the Gmsh files and the function *f.input.m* (see chapter 7 and section 9.1). Before running the TAPAS\_Main.m script, the user has to create a folder, inside *Projects*, with a specific name, where TAPAS stores all the results of the analysis at the end of the simulation. This folder contains also the input files of the analysis to perform. The *ValidationFiles* folder contains all the validation files (see chapter 14).

## 6.1 Interactions between the different modules of the tool

The fig. 6.2 shows the interactions between the different modules of the TAPAS tool.

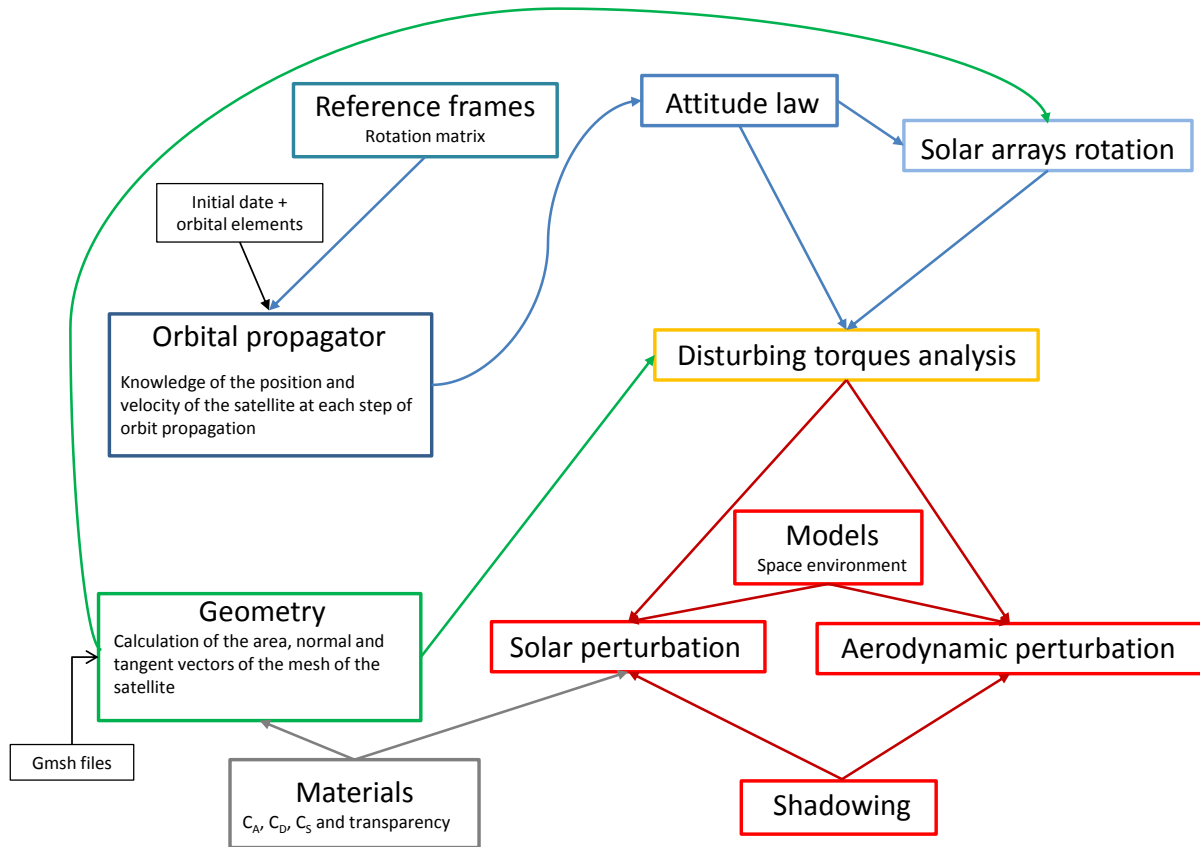


Figure 6.2: Interactions between the different modules of TAPAS

When the user launches a new simulation, the first calculations carried out by TAPAS are the orbit and attitude propagations. Once the position and attitude of the satellite are known at each propagation step, knowing the shape of the spacecraft, the tool can evaluate the disturbing forces and torques acting on it. For this, the space environment models and a shadowing algorithm are necessary. This is explained in more detail in chapter 12.

## Chapter 7

# Creation of the geometric model of the satellite

Since solar and aerodynamic perturbation torques depend on the external shape of the satellite, a CAD model of the satellite must be created and meshed with finite elements. The mesh is necessary to approximate the integrals 5.6 and 5.10 with sums, and to evaluate the shadows on the satellite. TAPAS tool uses the open source software Gmsh to create the satellite's geometric model and to mesh it.

### 7.1 What is Gmsh?

As already mentioned, Gmsh is a finite-element mesh generator. Released under the GNU General Public License, Gmsh is a free software. It contains 4 modules: geometry description, meshing, solving and post-processing. Gmsh supports parametric input and has advanced visualization mechanisms [32]. The graphical user interface of Gmsh (see fig. 7.1) allows a user-friendly utilization of this software.

### 7.2 Gmsh routines linked to TAPAS

To simplify the creation of the geometric model of the satellite, some Gmsh routines have been developed within Thales Alenia Space. When the geometric model is created, one has to mesh it with finite triangular elements. The images that follow show different meshes created with Gmsh. The implemented routines are called by a main script, which is structured as follows. The user can decide whether he or she wants to include or not the following items in the geometric model of the satellite:

1. The satellite's central body, including any possible parabolic reflector.
2. The yoke, which is the support structure for solar panels (see fig. 7.2).
3. The solar arrays.

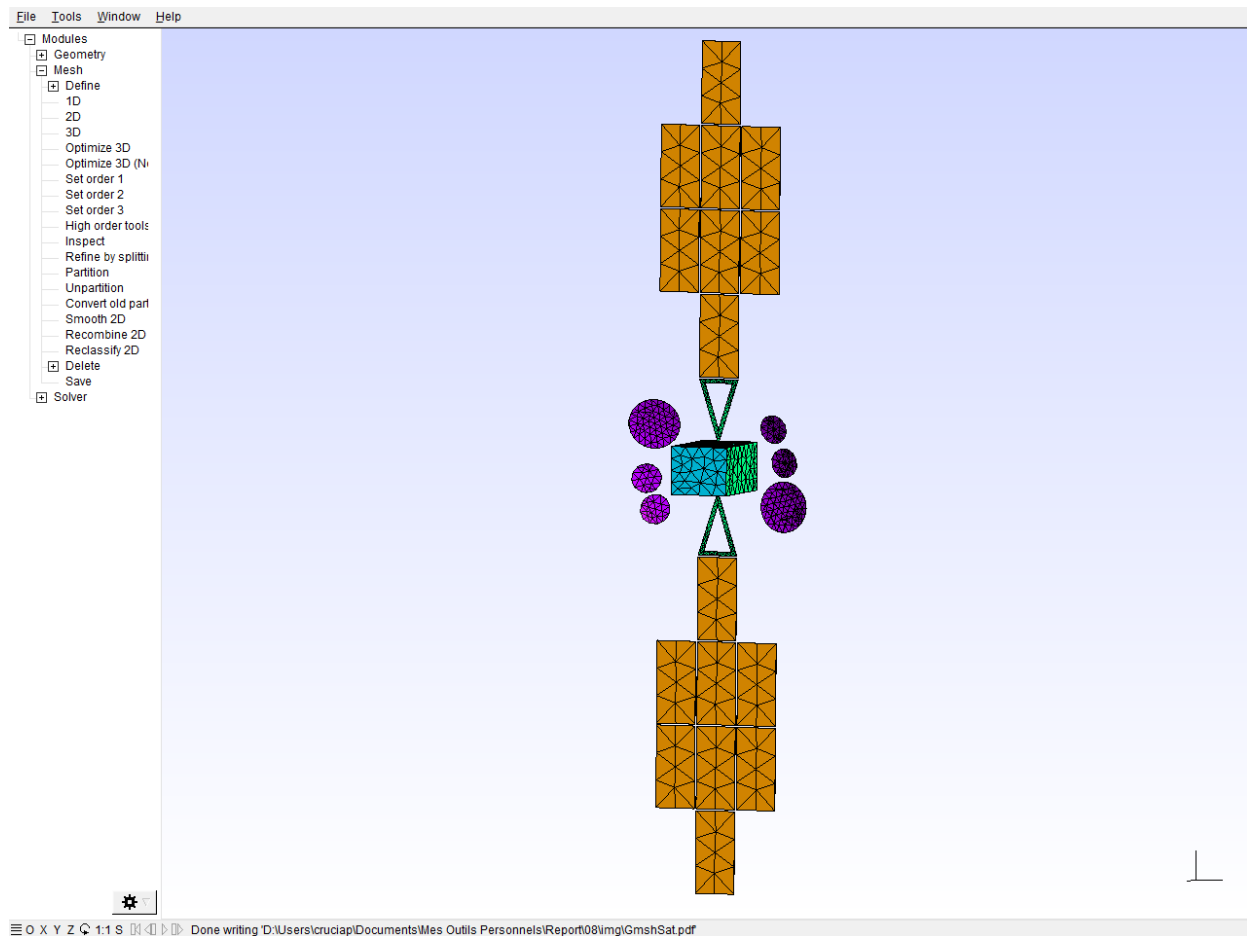


Figure 7.1: Mesh of a satellite model created with the graphical user interface of Gmsh.

### 7.2.1 Body of the satellite

The implemented Gmsh routines include five different kinds of satellite central bodies.

- (A) Simple parallelepiped (fig. 7.3)
- (B) Body with inclined surfaces (fig. 7.4)
- (C) Body with extensions of one face (fig. 7.5)
- (D) Body with extensions on two faces (fig. 7.6)
- (E) Body with extensions on three faces (fig. 7.7)

In addition to this, the user can add as many parabolic reflectors as needed. To add a parabolic reflector, the user has to enter its dimensions in the main file. In particular, one has to define:

- (a) The focal of the reflector
- (b) The semi-major and semi-minor axis of the reflector, as seen in plan view
- (c) The position and the orientation of the antenna, in the satellite reference frame

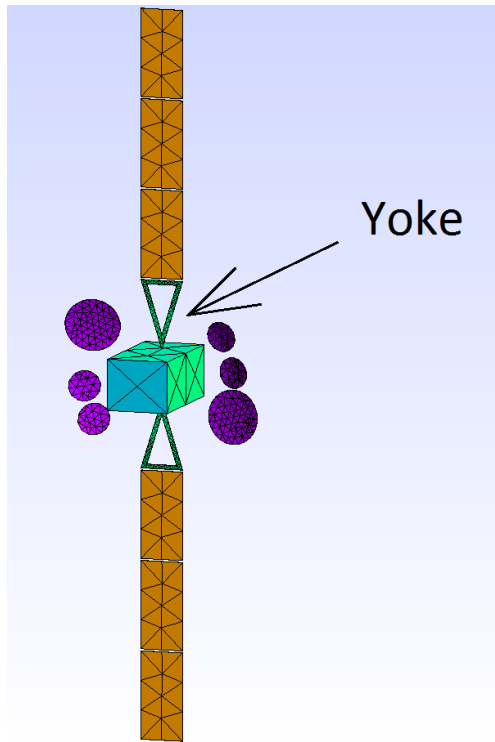


Figure 7.2: Typical yoke of a satellite.

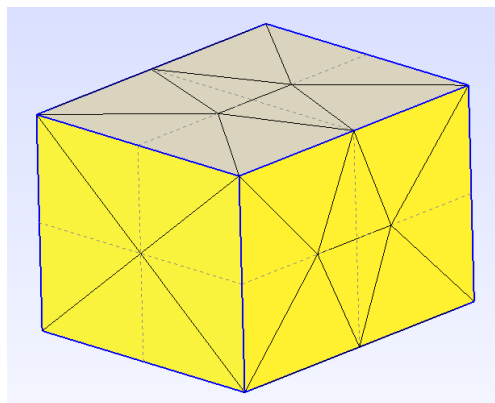


Figure 7.3: Body of a satellite modeled as a simple parallelepiped.

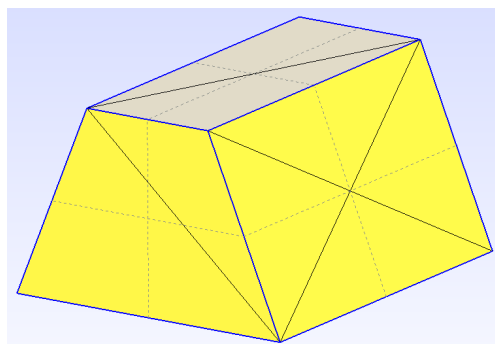


Figure 7.4: Body of a satellite modeled with inclined surfaces.

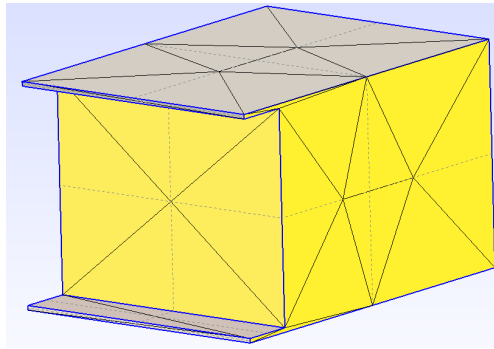


Figure 7.5: Body of a satellite with extensions on one face.

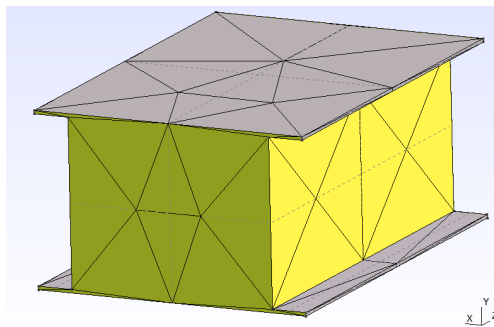


Figure 7.6: Body of a satellite with extensions on two faces.

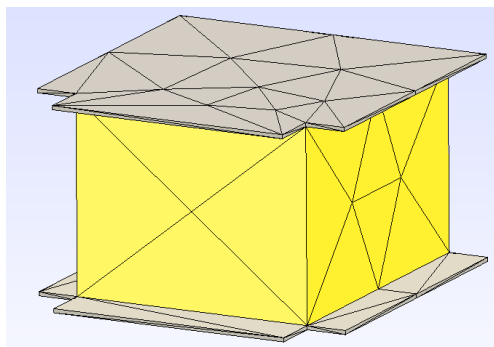


Figure 7.7: Body of a satellite with extensions on three faces.

The satellite in fig. 7.1 has six parabolic reflectors.

### Geometric equations to draw a parabolic reflector

The parabolic reflector, in the Gmsh routines of TAPAS, is drawn as the intersection of a paraboloid and a cylinder. The base of the cylinder can be circular or elliptical.

First of all, one defines the  $x$  and  $y$  coordinates of the center of the circular or elliptical base of the cylinder, in the  $x$ - $y$  plane of the reference system linked to the reflector. Then, the  $z$  coordinate of the center of the reflector is calculated through the equation of the paraboloid:

$$z_c = \frac{x_c^2 + y_c^2}{4f} \quad (7.1)$$

where  $x_c$ ,  $y_c$  and  $z_c$  are, respectively, the  $x$ ,  $y$  and  $z$  coordinates of the center of the reflector, and  $f$  its focal. Next, the contour of the reflector is defined by means of the following parametric equations

$$\begin{cases} x = x_c + a \cos(\theta) \cos(-\alpha) + b \sin(\theta) \sin(-\alpha) \\ y = y_c - a \cos(\theta) \sin(-\alpha) + b \sin(\theta) \cos(-\alpha) \\ z = \frac{x^2 + y^2}{4f} \end{cases} \quad (7.2)$$

where  $a$  and  $b$  are, respectively, the semi-axis along  $x$  and  $y$ ,  $\theta$  is the angular parameter of the equations ( $0 \leq \theta < 2\pi$ ) and  $\alpha$  is the angle shown in fig. 7.8.

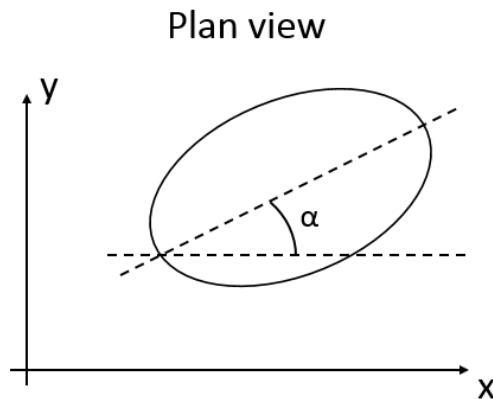


Figure 7.8:  $\alpha$  angle between the ellipse and the  $x$  axis of the reflector reference frame, in the  $xy$  plane.

An angular step of  $\theta$  has to be chosen based on how precisely one wants to draw the reflector. The shorter this step, the higher the number of points drawn and the more precise the shape of the reflector is. Indeed, the points defined by the equations 7.2 are then interconnected with splines, exploiting the spline command of Gmsh. The fig. 7.9 illustrates a reflector drawn with few geometric points and a reflector drawn with more geometric points.

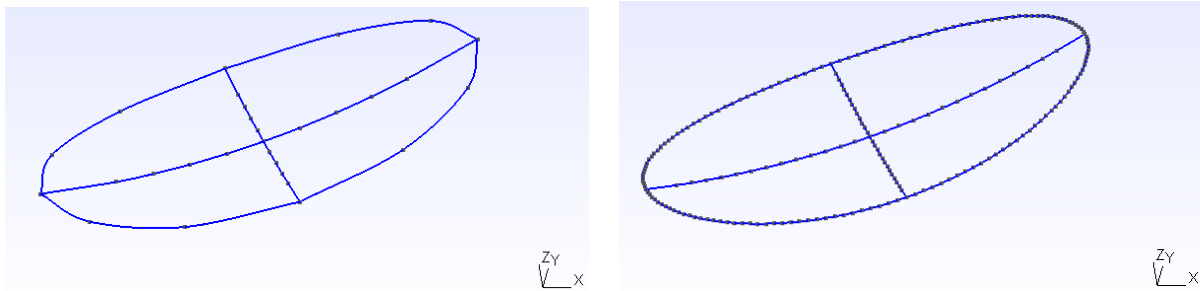


Figure 7.9: On the left, reflector drawn with a few points. On the right, reflector drawn with a lot of points.

Once the contour of the reflector is drawn, one has to define some internal points to give the reflector its parabolic shape. An example of a mesh of a parabolic reflector is shown in fig. 7.10.

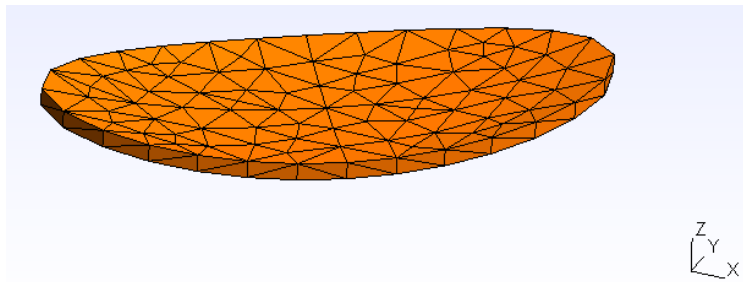


Figure 7.10: Mesh of a reflector created with the Gmsh routine of TAPAS

Initially, the reflector is drawn in its own reference frame and, later, the relative position of this frame with respect to the satellite reference frame is taken into account.

## 7.2.2 Yoke

The TAPAS Gmsh routines allow the user to draw the yoke shape by defining the position of its contour points. Therefore, different shapes can be drawn, as shown in fig. 7.11.

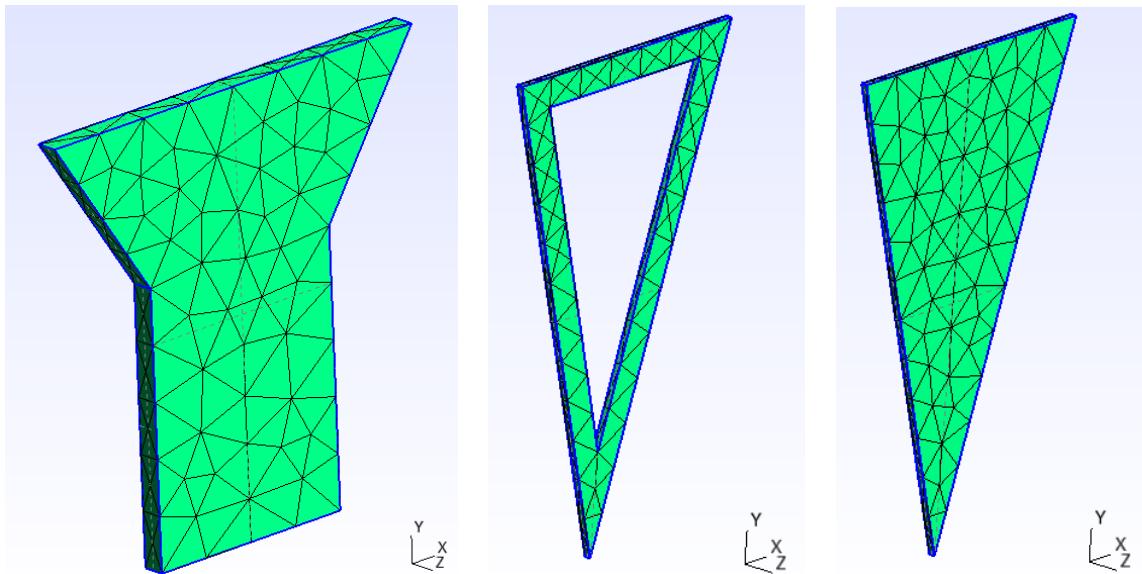


Figure 7.11: Three different shapes of yoke, created with the Gmsh routines of TAPAS.

### 7.2.3 Solar arrays

The user can choose how many solar panels the satellite has. The maximum number of solar panels is 16 (see fig. 7.1). Moreover, one can choose which solar panels to include in the model. The convention for numbering the solar arrays is shown in fig. 7.12.

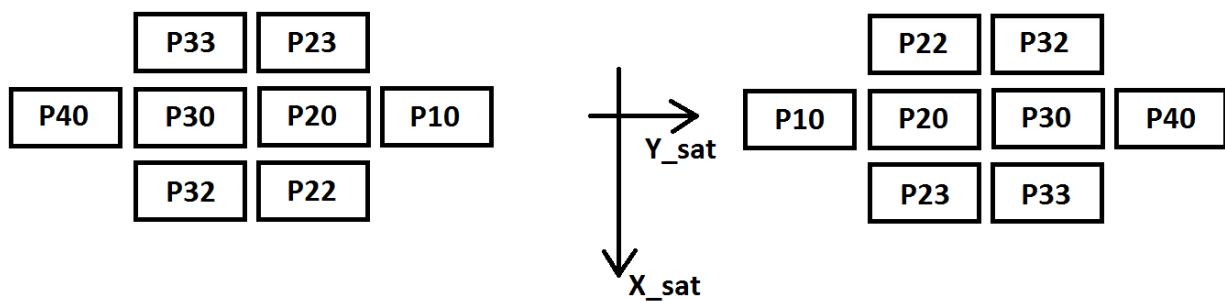


Figure 7.12: Convention for numbering the solar arrays.

## Chapter 8

# Mesh file in input to TAPAS

As already mentioned, once the geometric model of the satellite is defined, the user has to mesh it with finite triangular elements. This can be done easily with the Gmsh GUI. The TAPAS Gmsh routines allow the user to define the mean dimension of the triangular elements, for each part of the model: central body, antennas, yoke and solar panels. The fig. 8.1 shows the same satellite meshed with two different mean element sizes.

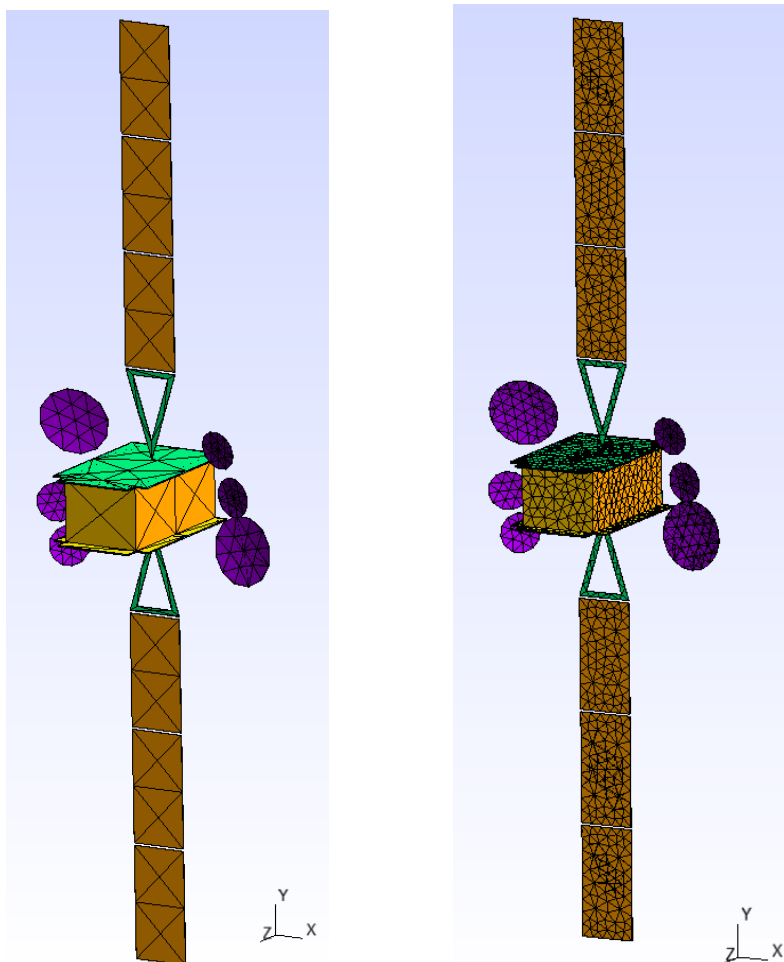


Figure 8.1: On the left, rough mesh of a satellite. On the right, refined mesh of a satellite.

Having a refined mesh is important in particular for the reflectors because they have a parabolic surface, while each singular finite triangular element has a plane surface, so the approximation of the paraboloid would be bad if the mesh was rough. Moreover, a refined mesh is also important to calculate the shadows on the satellite precisely (see section 12.1).

## 8.1 bdf file

The format of the mesh file in input to TAPAS is the bdf format. This is a standard format for mesh data used by the finite elements solver NASTRAN, which can be obtained by pre and post-processing CAE software such as FEMAP or PATRAN. An example of a simple bdf file created by Gmsh is shown hereafter.

```
$ Created by Gmsh
GRID      1      0      0.00E+000.00E+001.000000
GRID      2      0      0.00E+000.00E+000.00E+00
GRID      3      0      0.00E+001.0000001.000000
GRID      4      0      0.00E+001.0000000.00E+00
GRID      5      0      1.0000000.00E+001.000000
GRID      6      0      1.0000000.00E+000.00E+00
GRID      7      0      1.0000001.0000001.000000
GRID      8      0      1.0000001.0000000.00E+00
CTRIA3    129     100001  2      1      4
CTRIA3    130     100001  4      1      3
CTRIA3    131     100002  6      8      5
CTRIA3    132     100002  8      7      5
CTRIA3    133     100002  2      6      1
CTRIA3    134     100002  1      6      5
CTRIA3    135     100001  4      3      8
CTRIA3    136     100001  3      7      8
CTRIA3    137     110999  2      4      6
CTRIA3    138     110999  6      4      8
CTRIA3    139     110999  1      5      3
CTRIA3    140     110999  5      7      3
ENDDATA
```

The first part of the file, that is the lines starting with GRID, contains a list of all the nodes of the mesh. The first number of each of these lines is the node identification number, the second number indicates the reference system in which the coordinates of each node are expressed (this number is always zero for TAPAS applications), while the remaining numbers are the x, y and z coordinates of the node. Each coordinate number takes eight characters. The second part of the file, that is the lines starting with CTRIA3, contains the list of all the elements of the model. The expression CTRIA3 indicates that the line refers to a triangular element. The first number that follows the expression CTRIA3 is

the element identification number. These numbers may not be ordered when exporting in bdf format from Gmsh. The second number is the group the element belongs to. This is especially important for the attribution of a material to each elements group. Indeed, it is necessary to have the properties of the material of each element to calculate the solar force and torque on the satellite (see the  $C_D$  and  $C_S$  coefficients in the eq. 5.8). The last three numbers are the identification numbers of the nodes of the element into account. The order of the nodes of each element defines the direction of the element's normal vector, following the right hand rule (fig. 8.2).

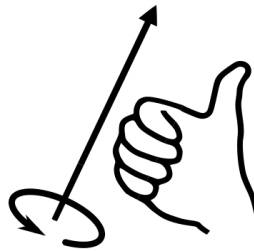


Figure 8.2: Definition of the direction of the normal of a triangular element based on the order of its elements, following the right hand rule [10].

The advantage of using triangular elements is that the triangle is a planar geometric figure, so its normal can always be defined uniquely. TAPAS reads the bdf file associated to the satellite into account, and retrieves the surface area and the normal of all its elements.

## Chapter 9

# Date, orbit and attitude definition

Three fundamental inputs of all simulations are the initial date, the orbit and attitude law of the satellite. These can be directly entered in TAPAS or in external files, as explained in sections 9.1 and 9.2.

### 9.1 Initial date, orbit and attitude law of the simulation, entered directly in TAPAS

The starting date and the satellite orbit for the simulation to perform can be defined in the file *f\_input.m* of the tool (see chapter 6). The date is defined in the UTC time scale, in terms of starting year, month, day, hour, minute and second. After this, one has to enter the orbit of the satellite. For this, four different formats are possible:

1. Six keplerian orbital elements. In this case, the user has to enter
  - (A) the longitude of the ascending node of the orbit ( $\Omega$ ) in the EME2000 reference frame
  - (B) the inclination of the orbit ( $i$ )
  - (C) the semi-major axis ( $a$ )
  - (D) the eccentricity ( $e$ )
  - (E) the argument of perigee ( $\omega$ )
  - (F) the starting anomaly ( $\nu$ )

The fig. 9.1 shows the meaning of the terms above.

2. State vector, so the initial position and velocity of the satellite, in the EME2000 reference frame.

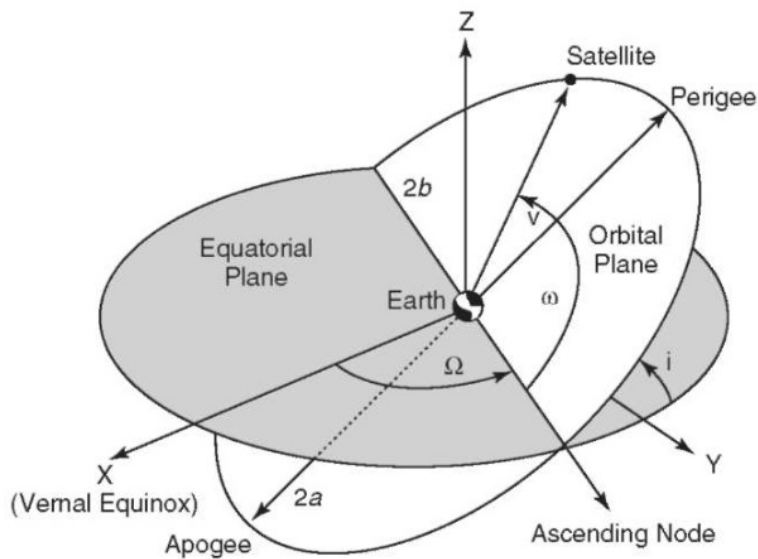


Figure 9.1: Explanation of the keplerian orbital elements [11].

3. Geostationary orbit, for which the user has to define only the longitude of the geostationary position of the satellite, in the ECEF frame.
4. Sun-synchronous orbit, for which one has to enter only the altitude, the  $\theta$  angle (shown in fig. 9.2) and the initial anomaly of the satellite.

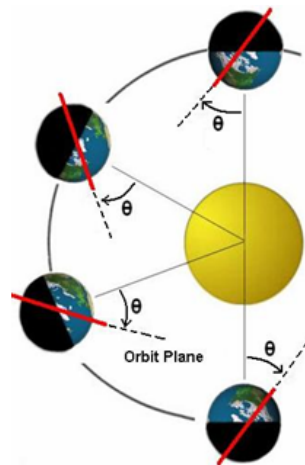


Figure 9.2:  $\theta$  angle for Sun-synchronous orbits [12]. The red line is the intersection between the equatorial plane and the orbit plane.

Once the orbit is defined, the user has to choose the attitude law for the simulation. This is done with a graphical user interface (section 10). Three choices are possible:

1. Classical Earth pointing (LOF), where the z-axis of the satellite points towards the center of the Earth, the y-axis is perpendicular to the orbit plane and the x-axis is

towards the velocity of the satellite and completes the right-handed frame (see fig. 4.6).

2. Yaw steering pointing law (fig. 9.3), where the z axis of the satellite is towards the center of the Earth, the -x axis points towards the Sun 'at best', and the y axis completes the right-handed frame. The x axis points 'at best' towards the Sun because the constraint on the z axis pointing towards the Earth's center must always be satisfied. This kind of attitude law allows the solar arrays of the satellite, which are usually along the y axis of the satellite reference system, to be pointed perpendicularly to the Sun direction, thus maximizing the solar energy received. The yaw steering is only possible if the mission doesn't have specific requirements in the yaw angle of the satellite.

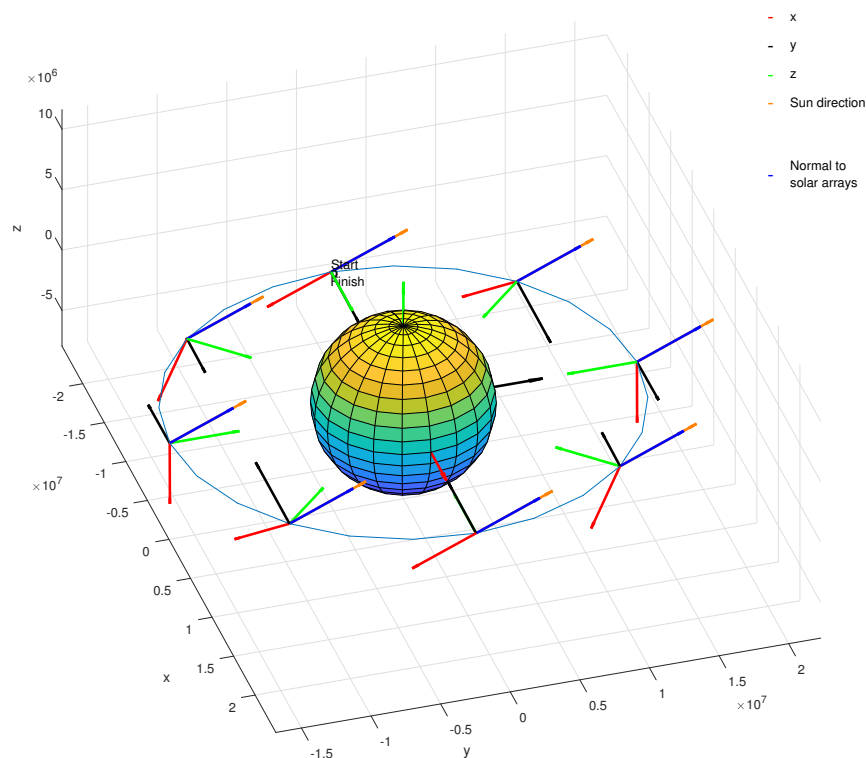


Figure 9.3: Yaw steering attitude law

3. Attitude file (see the file *RollPitchYaw.txt* in the fig. 6.1), that is a file containing the attitude information of the satellite, for all the duration of the simulation, in terms of Cardan angles and solar arrays rotation. The format of the attitude file read by TAPAS is shown herein.

Open

t [mn]	Roll [deg]	Pitch [deg]	Yaw [deg]	SA_rotation [deg]
0	12.65	85.48	15	180
0.5	15.80	74.68	13.83	180
1	16.23	65.43	11.13	180
1.5	17.97	60.67	9.97	180
2	19.02	58.71	8.14	175.94
2.5	20.94	55.45	6.77	170.05
3	22.13	52.21	5.11	168.89
3.5	24.05	49.88	4.01	165.07
4	25.51	46.50	2.48	161.79
4.5	28.06	43.40	1.03	155.55
5	30.62	40.81	0.06	153.02

## 9.2 Orbit and attitude taken from external files

As already mentioned, date, orbit and attitude can also be defined in two different text files (one for the orbit and one for attitude) which can be read by TAPAS. Each row of the orbit file must contain the simulation time and the six orbital elements of the osculating orbit, while the attitude file must contain the simulation time and the attitude of the satellite, by means of quaternions (see appendix B.3). In this case, the user has to define, for each of these two files, the start and the end line to read, and the line step. TAPAS then reads these files and transforms the six orbital elements into a state vector (position and velocity) and converts the quaternion into roll, pitch and yaw angles.

# Chapter 10

## Graphical User Interface

As mentioned in the section 1.4, one of the scope of my internship was to work on the user-friendliness of the tool. For this, a graphical user interface (GUI) has been developed. In this chapter, the different windows of this interface are shown.

### 10.1 Starting windows

Just after launching the TAPAS\_Main.m script (see fig. 6.1), the fig. 10.1 appears.

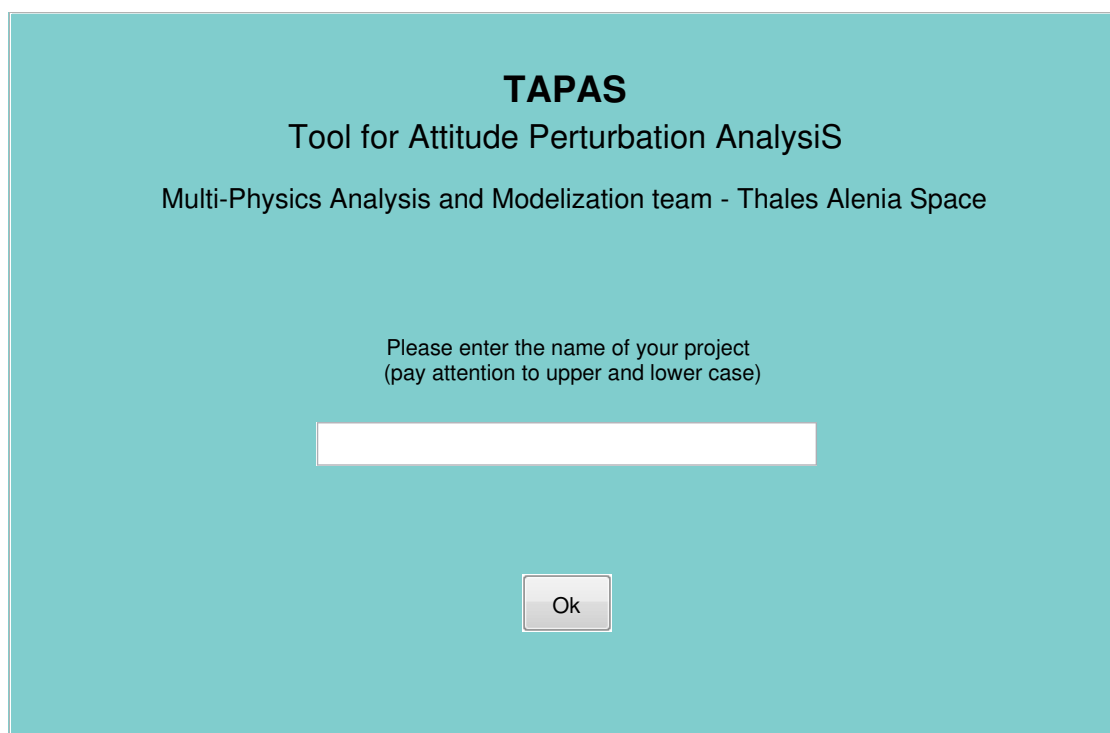


Figure 10.1: First window that appears after launching the TAPAS\_Main.m script.

In this window, the user has to enter the name of the folder related to the analysis to perform, where all the relevant input files are stocked. This folder must be inside the *Projects* folder of TAPAS (see fig. 6.1). This is a necessary step of the execution of TAPAS, because it lets

Open

TAPAS know where the input files are and in which folder the tool creates the output files at the end of the simulation. When one presses the Ok button, a second window appears, as shown in fig. 10.2.

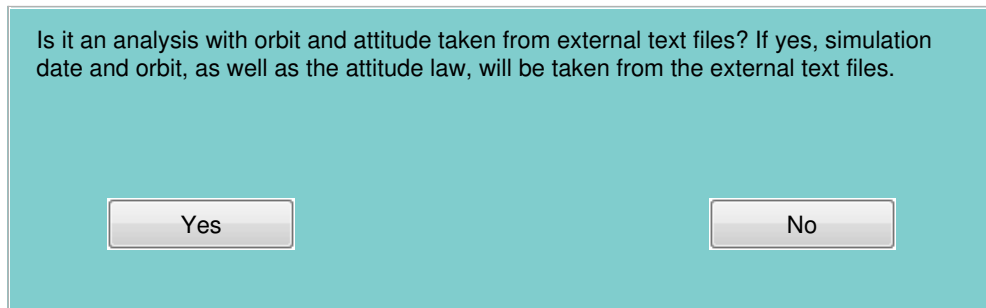


Figure 10.2: Window that appears after pressing the Ok button of the first window.

With the window 10.2, the user decides if taking the orbit and attitude law for the simulation from external files, or if taking the parameters entered in the `f_input.m` file. If the user presses the Yes button, the fig. 10.3 appears, otherwise, if one presses No, the fig. 10.4 shows.

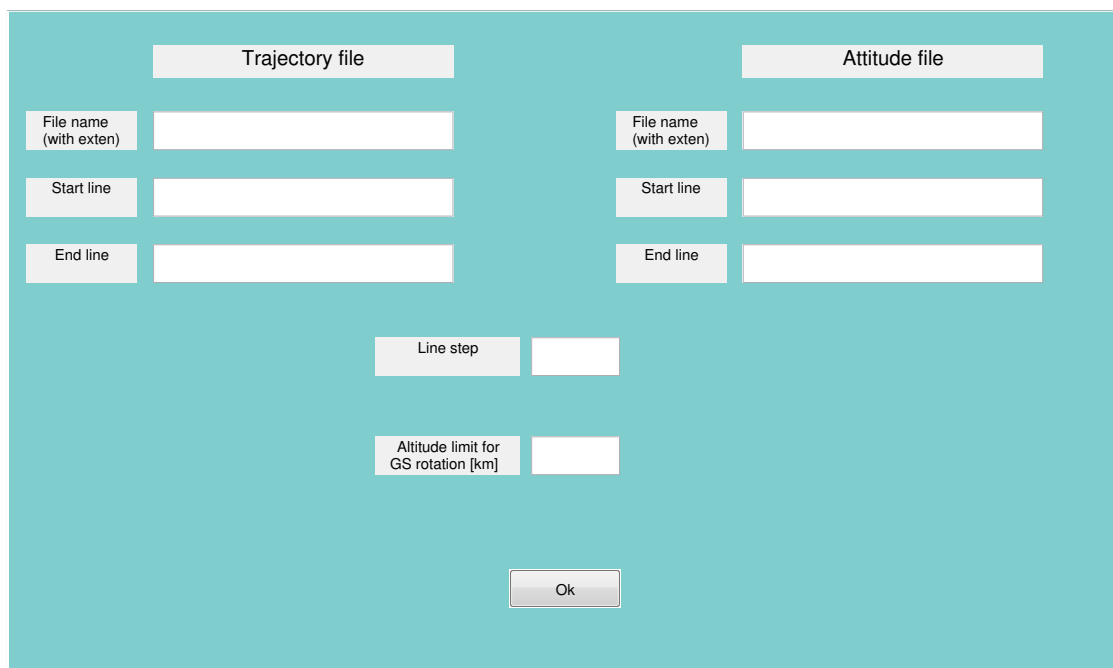


Figure 10.3: Window where the user can enter the parameters of the external files to be read by TAPAS for the definition of the orbit and attitude of the simulation.

The window 10.3 allows the user to enter the parameters of the external files that define the orbit and attitude of the simulation. The text field *Altitude limit for GS rotation [km]* is used to set specific orientations of the solar panels for low perigee passages.

On the other hand, if one defines the initial date and orbit in the `f_input.m` file, the window 10.4 allows to choose the orbit propagator and the attitude law, as explained in section 9.1.

Open

Figure 10.4: Window where the user can choose the orbit propagator and the attitude law of the simulation.

If the attitude is read from an external file, one has to enter the starting and the ending line of this file. The user can choose between three different orbit propagators: the numerical, the keplerian and Eckstein-Hechler propagator. This is explained more in detail in section 11.1.

## 10.2 Inputs for disturbing torques calculation

Finally, one has to enter the specific parameters of the analysis to carry out. Therefore, for the aerodynamic torque the user has to enter the normal and tangential coefficients  $C_n$  and  $C_t$  (see eq. 5.3), and the intensity of the solar activity. This is done through the window 10.5. Possible choices for the solar activity intensity are strong, average or weak.

Figure 10.5: Definition of the inputs for the aerodynamic torque computation.

For the solar torque analysis, the user has to associate each element group to a material with specific properties. This can be done in the window 10.6.

Open

**Materials association**

Physical surface	Material	CA	CD	CS	Transparency
100001	user-defined	0.48	0.31	0.21	0
100002	OSR	0.5	0.2	0.3	0
110999	Alluminium	0.4	0.6	0	0
Yoke	Alluminium	0.4	0.6	0	0
SA edges	Alluminium	0.4	0.6	0	0
SA +z face	Solar cells	0.35	0.45	0.2	0
SA -z face	kapton	0.28	0.47	0.25	0

Ok

Figure 10.6: Association of a material to each element group. On the left column there are the element groups of the satellite model.

In fig. 10.6, the  $C_A$  coefficient is the absorption coefficient of the material and the transparency is the ratio between the solar flux that passes through the material and the total solar flux that hits the material. One can also enter the four coefficients  $C_A$ ,  $C_D$ ,  $C_S$  and the transparency manually. Note that  $C_A + C_D + C_S = 1$ , and  $0 \leq Transparency \leq 1$ .

## Part IV

# Main modules of the TAPAS tool

# Chapter 11

## Orbital mechanics module

In this chapter, the orbital mechanics module of TAPAS is explained.

### 11.1 Orekit library

The TAPAS tool exploits the Orekit library for the orbit and attitude modules. Orekit is an Open Source Java library of orbital mechanics, developed by *CS Systèmes d'information*. It has different Java methods and classes to define and propagate the orbit and attitude of a satellite, as well as for the calculation of the ephemeris of different celestial bodies of the solar system. Orekit provides accurate and efficient low level components for the development of flight dynamics applications. It is designed to be easily used in very different contexts, from quick studies up to critical operations. Orekit has already been successfully used during the real time monitoring of the rendez-vous phase between the Automated Transfer Vehicle (ATV) and the International Space Station (ISS) by the Centre National d'Études Spatiales (CNES, the French space agency) and the European Space Agency (ESA). It has been selected in early 2011 by CNES to be the basis of its next generation space flight dynamics systems, including operational systems, study systems and mission analysis systems. Furthermore, Orekit has been used for several studies and ground systems developments by various industrial actors such as EUMETSAT [33]. This library is used also in other departments of Thales Alenia Space. All TAPAS modules are developed under the Matlab environment, so the Java Orekit library has been imported in Matlab.

Orekit proposes three different kinds of orbit propagation: the keplerian, the Eckstein-Hechler and the numerical integration propagator. The propagation time step can be entered by the user. For each propagation time instant, TAPAS stores the position and the velocity of the satellite, in the EME2000 reference frame.

#### 11.1.1 The keplerian propagator

The keplerian propagator is the simplest propagator of the Orekit library. It is an analytic

solution of the following differential equation:

$$\ddot{\vec{r}} = -\frac{\mu}{r^3}\vec{r} \quad (11.1)$$

where  $\vec{r}$  is the vector representing the satellite position in the EME2000 reference frame,  $\ddot{\vec{r}}$  its second time derivative and  $\mu$  the Earth's standard gravitational parameter. This is a simple model and it does not take into account disturbing effects of the Earth's gravitational potential (see appendix A.1). However, it is important to have it because, since satellites' orbits are controlled by the AOCS, the actual orbit of a satellite is nearly keplerian.

### 11.1.2 The Eckstein-Hechler propagator

The Eckstein-Hechler propagator is another analytical propagator [34]. It can take into account the zonal harmonics coefficients of the gravitational potential of the Earth up to the sixth order (see appendix A.1), so it is more precise than the simple keplerian propagator. However, the Eckstein-Hechler propagator is valid only for orbits whose eccentricity is less than 0.05, and whose inclination is not equatorial nor critical ( $i \neq 0$  and  $i \neq 63.4^\circ$ ). This kind of propagator is based on the differential Lagrange equations, which take into account only conservative disturbing effects of the Earth's gravitational potential.

### 11.1.3 Numerical integration propagator

This propagator is based on a numerical integration of the dynamics equation of the motion of the satellite. The TAPAS tool uses the numerical integrator Runge-Kutta 4 (see appendix C). The gravitational potential model for this propagator takes into account the spherical harmonics coefficients up to the order and index 10. The most important coefficient of the spherical harmonics expansion is the J2 term of the equation A.1 because it is the term at the basis of Sun-synchronous orbits.

## 11.2 Solar arrays rotation

For each point of the orbit, solar panels must be rotated so that solar cells are towards the Sun. The axis of rotation of solar arrays is usually parallel to the y-axis of the satellite reference frame (see fig. 4.7). A null angle of rotation of solar arrays coincides with the solar cells being oriented towards the z axis of the satellite reference frame. In order to find the angle of rotation of the solar arrays, one needs to know the Sun direction in the satellite reference frame. Then, this direction is projected in the x-y plane of the satellite reference frame, and the angle between this projected direction and the z axis of the satellite

is evaluated. This angle is the solar arrays' angle of rotation that makes solar cells point towards the Sun.

# Chapter 12

## Solar and aerodynamic disturbances module

The solar and the aerodynamic disturbances modules are the main parts of the TAPAS tool. The computation of these kinds of perturbations requires an algorithm for the shadowing due to the presence of some external parts of the satellite between the Sun or the aerodynamic flux (depending on which analysis one is performing) and other parts.

### 12.1 Shadowing algorithm

The basis of the shadowing algorithm has been taken from R. Mukundan [35]. First of all, one needs to know all the elements and the coordinates of the nodes of the satellite mesh. Herein, the example of the solar perturbation is presented, but everything is also valid for the aerodynamic disturbance. Once all the coordinates of the nodes in the satellite reference frame are known, they must be expressed in a new reference frame, which is called Sun-oriented and which is defined by the declination ( $\delta$ ) and the azimuth ( $\alpha$ ) angles, as shown in fig. 12.1.

To pass from the satellite to the Sun oriented reference frame, the following matrix equation is used

$$\begin{bmatrix} X \\ Y \\ Z \end{bmatrix} = \begin{bmatrix} \cos(\delta) \cos(\alpha) & \cos(\delta) \sin(\alpha) & -\sin(\delta) \\ -\sin(\alpha) & \cos(\alpha) & 0 \\ \sin(\delta) \cos(\alpha) & \sin(\delta) \sin(\alpha) & \cos(\delta) \end{bmatrix} \begin{bmatrix} x \\ y \\ z \end{bmatrix} \quad (12.1)$$

where  $(x, y, z)$  are the coordinates of the node in the satellite reference frame, while  $(X, Y, Z)$  are the coordinates of the same node in the Sun oriented reference frame. After this transformation, TAPAS calculates the coordinates of the geometric center and the normal of the elements, and it orders the elements in the descending order of the  $z$  coordinate of their geometric centers. Next, it transforms the problem in a 2D problem in the  $x$ - $y$  plane of the Sun oriented frame, and it searches for possible superposition of the elements in this plane. If a superposition occurs, it means that the superposed element having the

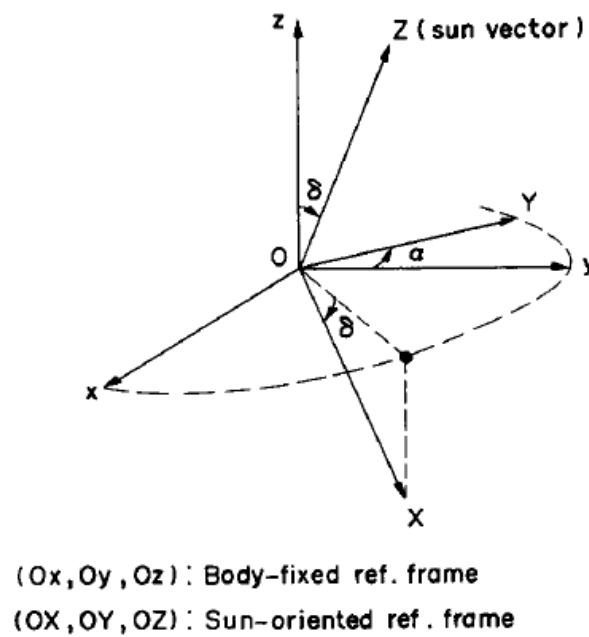


Figure 12.1: Sun oriented reference frame, defined by the declination ( $\delta$ ) and azimuth ( $\alpha$ ) angles.

lowest  $z$  coordinate is shadowed (see fig. 12.2). To find if an element is shadowed (that is, a superposition occurs), TAPAS checks if the center of the element into account is inside another element having a higher  $z$  coordinate. This check is done in the  $x$ - $y$  plane of the Sun-oriented reference frame.

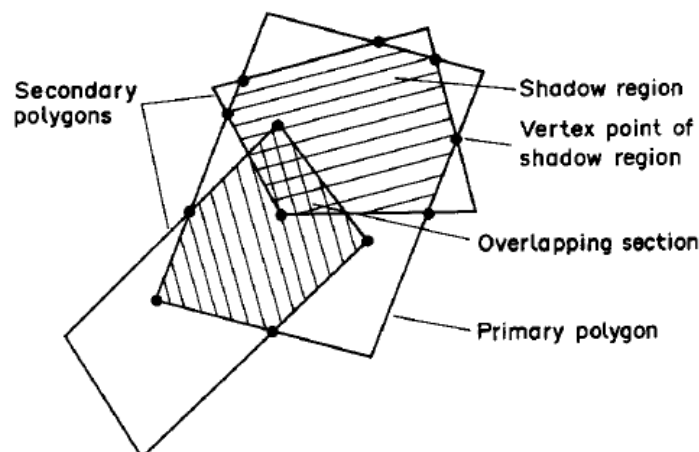


Figure 12.2: Shadowing problem in the  $xy$  plane of the Sun oriented frame. The primary polygon is the one having the lowest  $z$  coordinate in this frame.

To calculate the shadowing for the aerodynamic perturbation, the algorithm is the same, but the Sun direction is replaced with the satellite velocity with respect to the air.

## 12.2 Solar torque computation

To compute the solar force acting on the satellite, one has to sum up the solar forces acting on all the enlightened elements, following the eq. 5.8:

$$\vec{F}_{solar} = p A \cos(\alpha) \left\{ - \left[ (1 + C_S) \cos(\alpha) + \frac{2}{3} C_D \right] \vec{n} + (1 - C_S) \sin(\alpha) \vec{t} \right\}$$

where, in this case,  $A$ ,  $\vec{n}$  and  $\vec{t}$  refer to a single finite element. In this equation, the value of the solar pressure  $p$  has to be evaluated. The expression of  $p$  is

$$p = \frac{\phi_{Sun}}{c} \quad (12.2)$$

where  $\phi_{Sun}$  is the solar flux expressed in  $W/m^2$ , and  $c$  is the speed of light ( $c \simeq 3 \cdot 10^8 m/s$ ). The value of  $\phi_{Sun}$  depends essentially on the distance between the Sun and the satellite. At  $1 AU \simeq 1.495 \cdot 10^{11} m$ ,  $\phi_{Sun} = 1367.5 W/m^2$  and it changes proportionally to the inverse of the square power of the distance between the satellite and the Sun. Finally, the global solar torque on the satellite is computed with the eq. 5.11, represented below.

$$\vec{t}_{solar, tot} = \sum_{i=1}^N \vec{t}_{solar, i} = \sum_{i=1}^N \vec{v}_{GOi} \wedge \vec{F}_{solar, i}$$

An important aspect for the solar perturbation is the evaluation of the eclipse of the satellite. When the satellite is in eclipse, the solar perturbation is null. The passage from enlightened to eclipse phase (and vice versa) is not instantaneous. Indeed, as shown in fig. 12.3, the satellite passes through a penumbra phase where only a portion of the Sun disk is shadowed by the Earth.

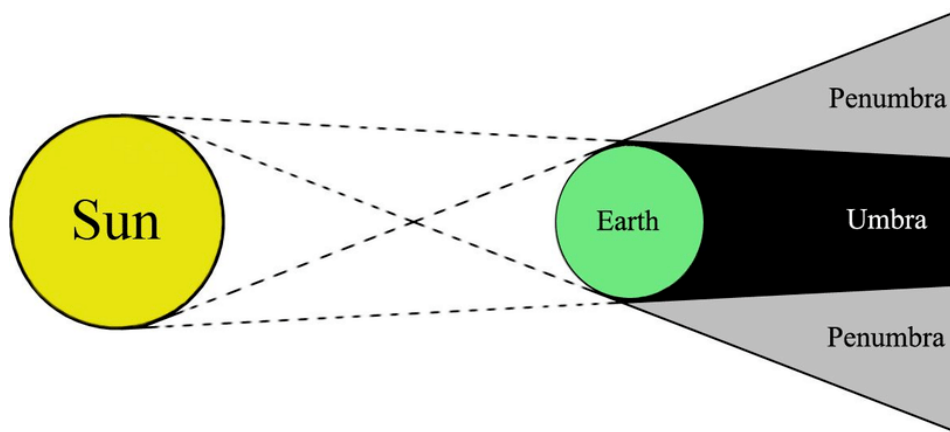


Figure 12.3: Eclipse phases that a satellite can encounter along its orbit [13].

The evaluation of the eclipse and penumbra phases of the simulation is carried out by calculating the angle  $\alpha$  between the satellite-to-Sun and the satellite-to-Earth vectors (see fig. 12.4), and comparing it with the angles of the cones that define the eclipse and penumbra phases.

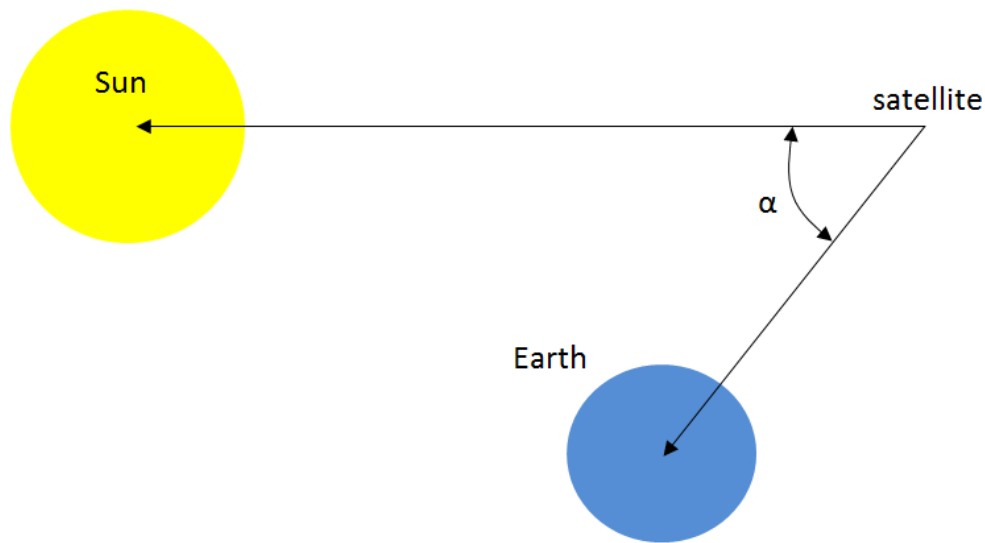


Figure 12.4: Angle  $\alpha$  between the satellite-to-Sun direction and the satellite-to-Earth direction. This angle is evaluated to know if the satellite is in eclipse, penumbra, or if it is enlightened by the Sun.

## 12.3 Aerodynamic torque computation

For the calculation of the aerodynamic torque, similarly to the solar torque, TAPAS evaluates the aerodynamic force and torque acting on each element of the satellite mesh, and it eventually sums up all these contributions to find the global aerodynamic force and torque on the satellite. The equations used for this are presented in chapter 5.3. Hereafter there is a summary of these expressions.

$$\vec{F}_{aero} = \frac{1}{2} \rho \|\vec{V}\|^2 A (C_t \sin(\alpha) \cos(\alpha) \vec{t} - C_n \cos^2(\alpha) \vec{n})$$

$$\vec{t}_{aero, tot} = \sum_{i=1}^N \vec{t}_{aero, i} = \sum_{i=1}^N \vec{v}_{GOi} \wedge \vec{F}_{aero, i}$$

In this case,  $A$ ,  $\vec{n}$  and  $\vec{t}$  refer to a single finite element. As one can see from these equations, the aerodynamic perturbation is directly proportional to the value of the atmospheric density. So, in order to have good estimations of this kind of perturbation, one needs to use an accurate model for this. Moreover, a model for the intensity of the solar and geomagnetic activities must be implemented, because they influence significantly the density of the higher layers of the atmosphere.

### 12.3.1 Solar and geomagnetic activity

The electromagnetic radiation emitted by the Sun is not constant over the years. This concerns especially the UV solar flux, that varies between a minimum and a maximum

value. The duration of a cycle of solar activity is 11 years. The UV solar flux has a relevant influence on the temperature and density of the higher layers of the atmosphere, therefore it plays an important role in the determination of the aerodynamic force and torque acting on a satellite.

The variation in the solar activity are due to the presence of sunspot on the Sun's surface. The more numerous these sunspots are, the higher the intensity of the solar activity is. To determine the intensity of the solar activity, the  $F10.7$  index is used, which is the solar radio flux emitted by the Sun at 2800 MHz (10.7 cm wavelength) [36]. The physical units of  $F10.7$  are  $10^{-22} W m^{-2} Hz^{-1}$ , which corresponds to a Solar Flux Unit (SFU). This index is used because it is well correlated to the sunspot number. The fig. 12.5 shows the evolution of the observed and monthly-smoothed  $F10.7$  index over the last two and a half solar cycles.

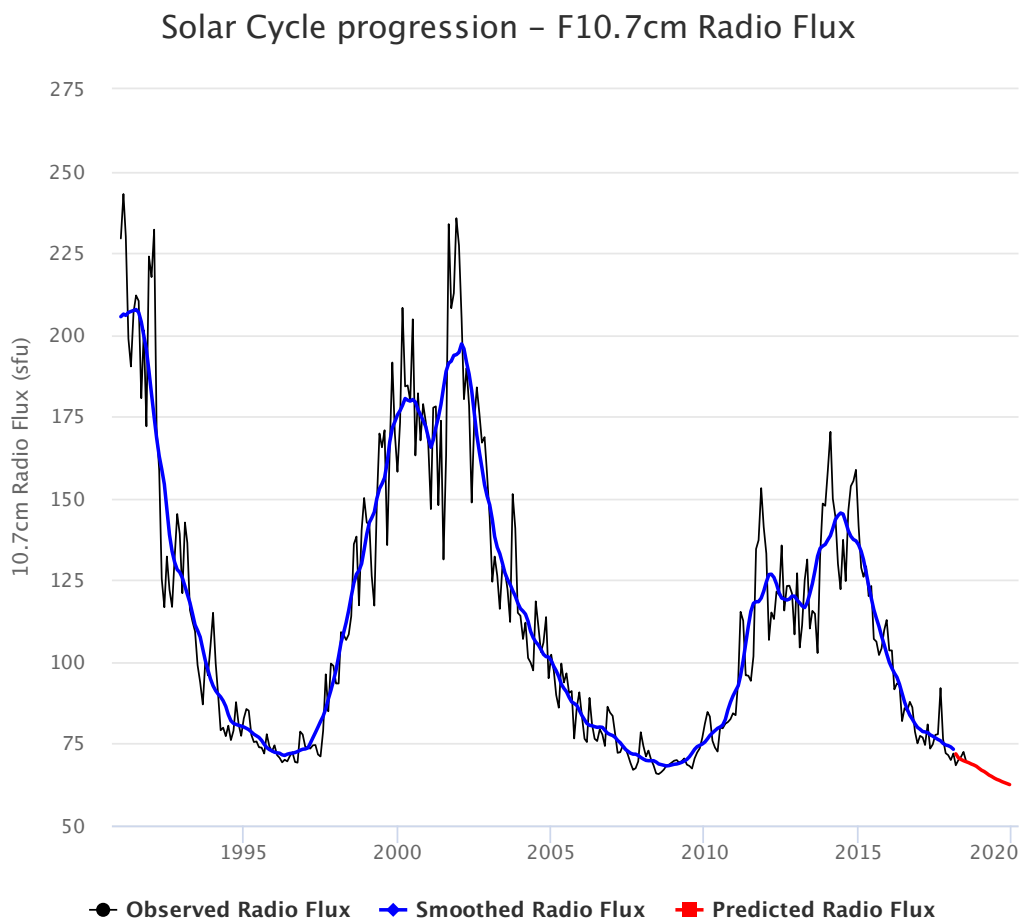


Figure 12.5: Evolution of the  $F10.7$  index from 1990 to 2020. The red part of the diagram is the predicted radio flux. The smoothed radio flux is the flux averaged over one month. [14]

Also the geomagnetic activity has a strong influence on the temperature and density of the atmosphere. To describe the intensity of the geomagnetic activity, the ap index is used.

This index is derived from measurements made at a number of stations world-wide of the variation of the geomagnetic field due to currents flowing in the earth's ionosphere and, to a lesser extent, in the earth's magnetosphere [37]. Values of  $ap$  range from 0 to 400 and are expressed in units of 2 nT [36]. The  $ap$  index is updated every three hours. Its daily average is the  $Ap$  index. The fig. 12.6 shows the evolution of the 13-month smoothed  $Ap$  index and its predicted values until the year 2031.

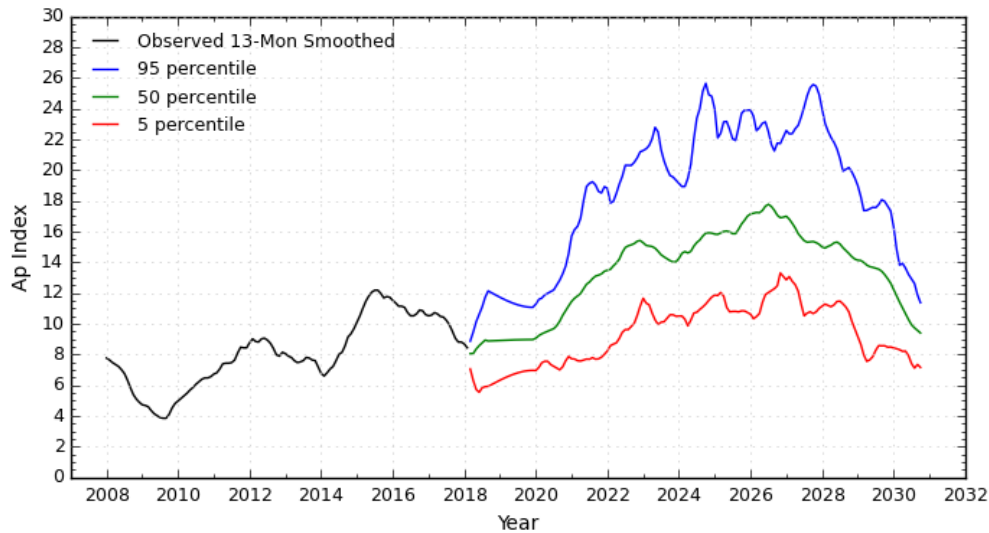


Figure 12.6: Evolution of the  $Ap$  index. The black line is the observed 13-month smoothed  $Ap$  index, while the blue, green and red lines are the predicted values, for different percentiles. [15]

Past, current and predicted values of the  $F10.7$  and  $Ap$  indexes are given by the NASA Marshall Space Flight Center [15].

### 12.3.2 Atmospheric density

As already mentioned, the knowledge of the value of the atmospheric density is fundamental for the estimation of the atmospheric perturbation.

#### Exponential model

The most simple way to estimate the atmospheric density at a given altitude  $h$  is to use the following exponential model [21]

$$\rho(h) = \rho(h_0) e^{-\beta(h-h_0)} \quad (12.3)$$

where  $h_0 = 200 \text{ km}$ ,  $\rho(h_0) = 10^{-10} \text{ kg/m}^3$  and  $\beta = 0.016 \text{ km}^{-1}$ . This model is valid for  $300 \text{ km} \leq h \leq 800 \text{ km}$ . The fig. 12.7 shows the graph of the eq. 12.3.

This exponential model does not take into account the solar and geomagnetic activities.

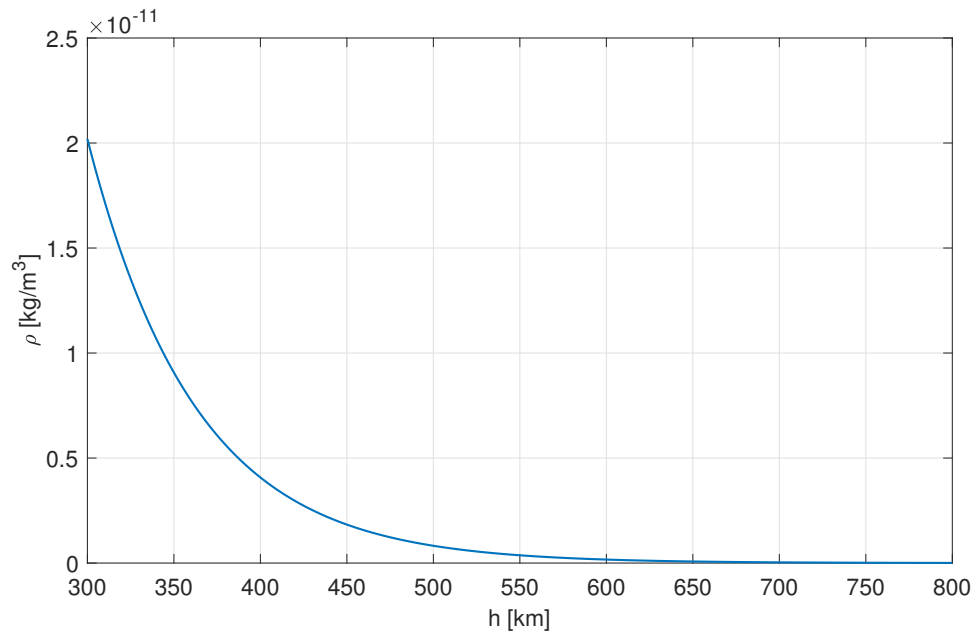


Figure 12.7: Exponential model of the atmospheric density  $\rho$ .

### NRLMSISE-00 model

To have more accurate estimations of the atmospheric density, TAPAS uses the NRLMSISE-00 model [38]. This model is valid from 0 to about 1000 km of altitude. 'NRL' stands for US Naval Research Laboratory, 'MSIS' stands for Mass Spectrometer and Incoherent Scatter Radar, 'E' indicates that the model extends from the ground to the exosphere, and '00' means that the model was released in 2000. The NRLMSISE-00 model is an update of the earlier models MSIS-86 and MSISE-90 [39]. This model makes use of a lot of data measured by satellites, rockets and instruments on ground, over the years. The NRLMSISE-00 model takes into account the solar and geomagnetic activities. The inputs of this model are:

1. The date of the simulation
2. The altitude of the satellite
3. The geodetic latitude and longitude of the satellite
4.  $F10.7_{av}$ , which is the 81-day average of  $F10.7$  index, centered on the day of the simulation
5. The daily  $F10.7$  index of the day before the one of the simulation
6. The daily and averaged geomagnetic ap indexes

The output of this model is the density of the atmosphere at the point under consideration. The figure 12.8 shows the values of the atmospheric density at  $0^\circ$  latitude, obtained with

the NRLMSISE-00 model, for low and high solar and geomagnetic activities. The values shown are averaged over one year.

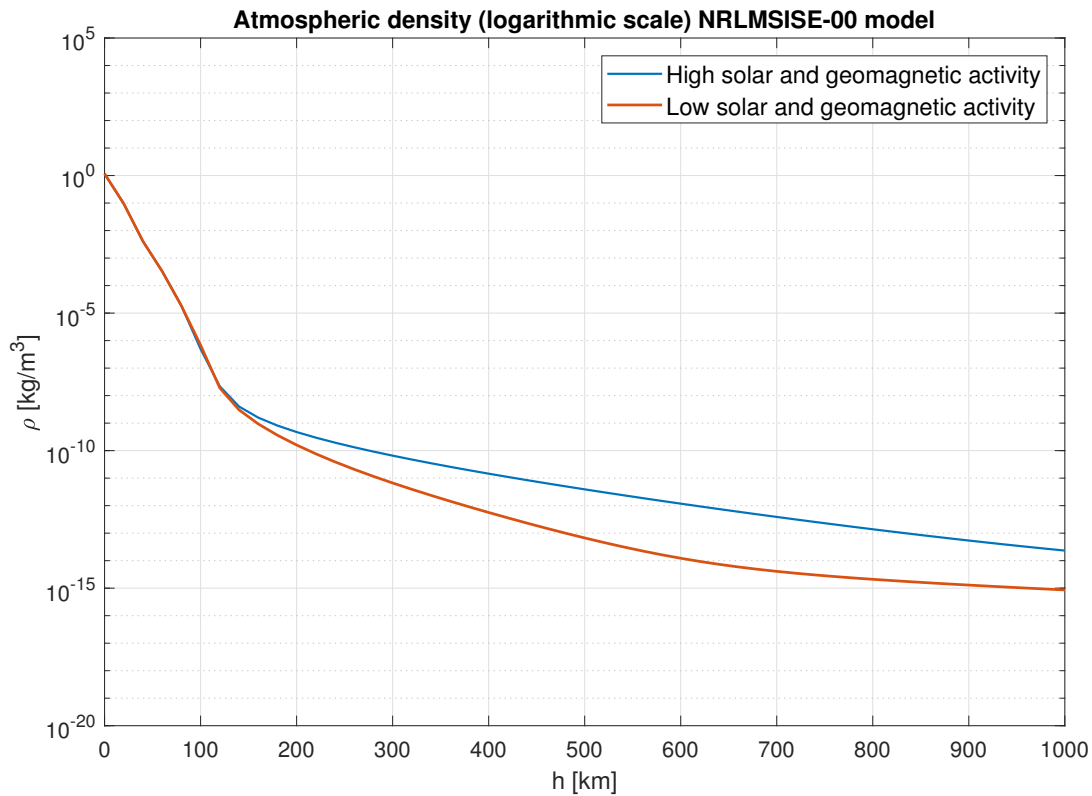


Figure 12.8: Atmospheric density at  $0^\circ$  latitude as a function of the altitude, according to the NRLMSISE-00 model. The  $\rho$  values are averaged over one year. The red line corresponds to  $F10.7 = F10.7_{av} = 65$  and  $Ap = 0$ , while the blue line corresponds to  $F10.7 = F10.7_{av} = 250$  and  $Ap = 45$ .

The fig. 12.9 shows a map of the atmospheric density values, according to the NRLMSISE-00 model, at 400 km of altitude. One can notice that the density is higher during daylight and lower during the night.

TAPAS uses a Matlab function that implements the NRLMSISE-00 model. This function can be found in the Mathworks file exchange website [40].

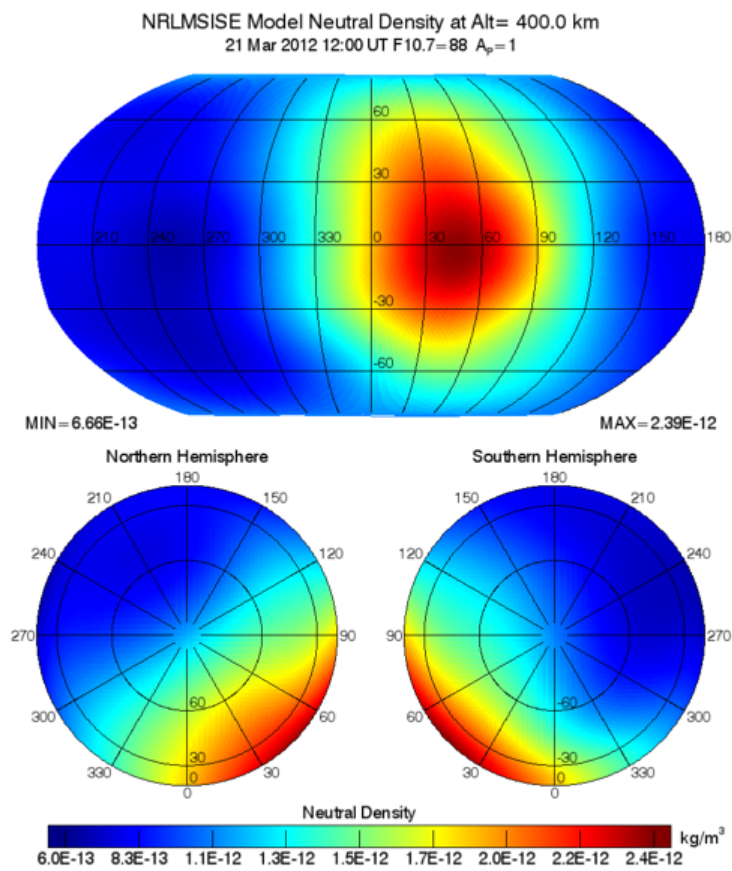


Figure 12.9: Map of the atmospheric density according to the NRLMSISE-00 model. The altitude is  $400 \text{ km}$ , the date is 21 Mar 2012, 12:00 UTC and the solar and geomagnetic activities indexes are  $F10.7 = 88$  and  $A_p = 1$  [16].

# Part V

## Results and validation

# Chapter 13

## Example of analysis

This chapter contains an example of analysis on a generic satellite.

### 13.1 Inputs of the analysis

The satellite taken into account is the one in fig. 13.1.

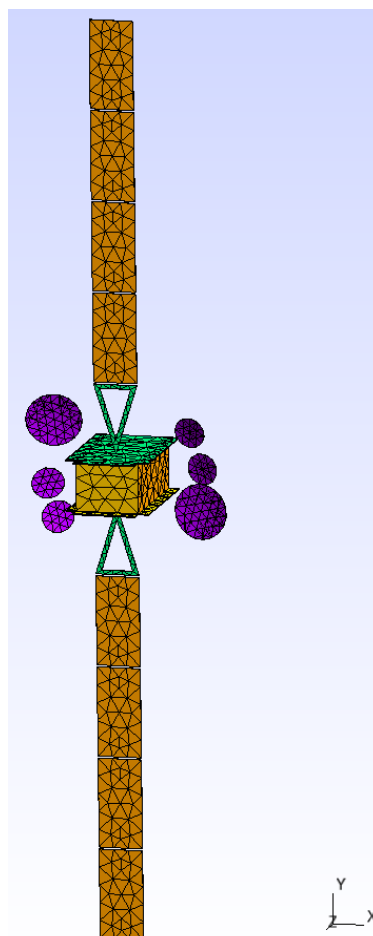


Figure 13.1: Satellite of the example of this chapter.

This satellite presents extensions on three faces of its body, six parabolic reflectors and four

Open

solar panels on each side.

The orbit chosen for this analysis is the following:

1.  $\Omega = 40^\circ$
2.  $\omega = 0^\circ$
3.  $i = 58^\circ$
4.  $a = 13756 \text{ km}$
5.  $e = 0.1$
6.  $\nu = 0^\circ$

The attitude law is the yaw steering and the solar arrays are pointed towards the Sun. The starting date of the simulation is 21<sup>st</sup> June 2001 at 00:00:00 UTC. The duration of the simulation covers a complete orbit of the satellite. Aerodynamic and solar torques are evaluated with respect to the center of the -z face of the satellite central body.

## 13.2 Solar perturbation results

In this chapter, the results concerning the solar disturbance are presented.

### 13.2.1 Visualization of the orbit

The fig. 13.2 shows the orbit and the attitude of the satellite for the simulation taken into account. Moreover, it shows that the solar arrays of the satellite point perfectly towards the Sun, thus maximizing the solar energy received. This is possible thanks to the choice of the yaw steering attitude law.

### 13.2.2 Visualization of the shadowing

At the end of each simulation, the TAPAS tool creates some bdf files to visualize the shadows on the satellite at each propagation time step. The visualization of the shadowing is done by assigning two different colors to the elements which are enlightened and to the elements which are shadowed, and visualizing it in the Gmsh GUI. The fig. 13.3 shows the solar shadows on the satellite, at the second step of the simulation, from two different points of view. The enlightened elements are green, while the shadowed elements are orange.

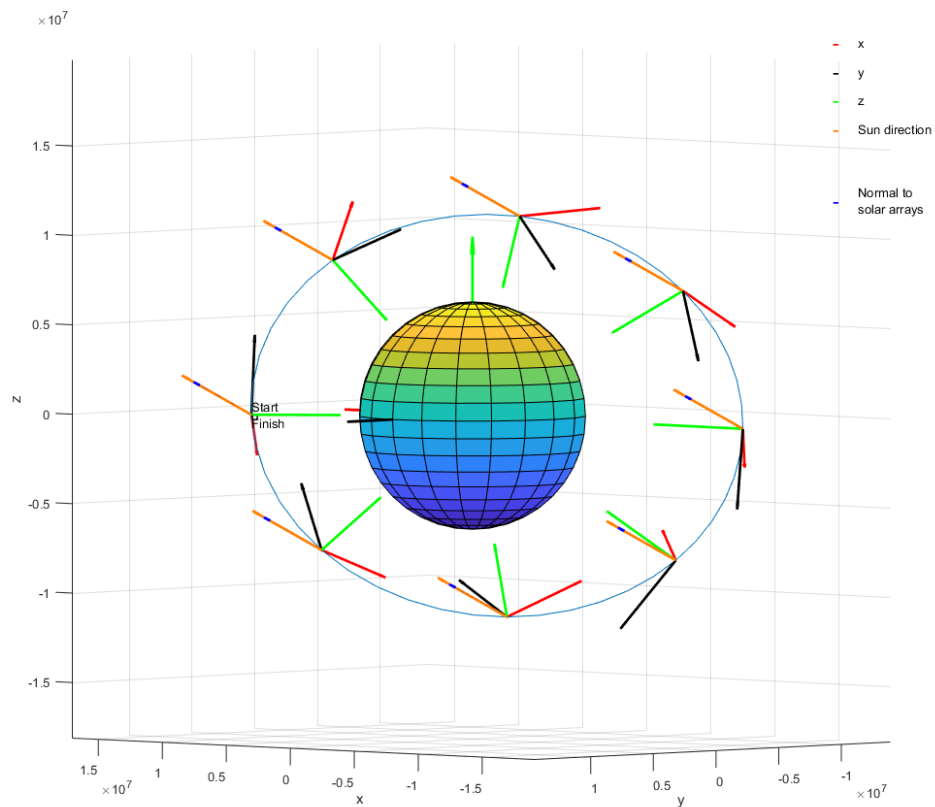


Figure 13.2: Orbit and attitude of the satellite for the chosen simulation. The blue vector is the vector normal to the solar arrays, while the orange vector is the Sun direction. In the figure, these two vectors are superposed, which means that solar arrays point perfectly towards the Sun.

### 13.2.3 Solar force

The fig. 13.4 shows the results obtained for the solar force acting on the satellite, expressed in the satellite reference frame. In this picture, one can notice that the satellite is in eclipse for about 30 minutes during its orbit.

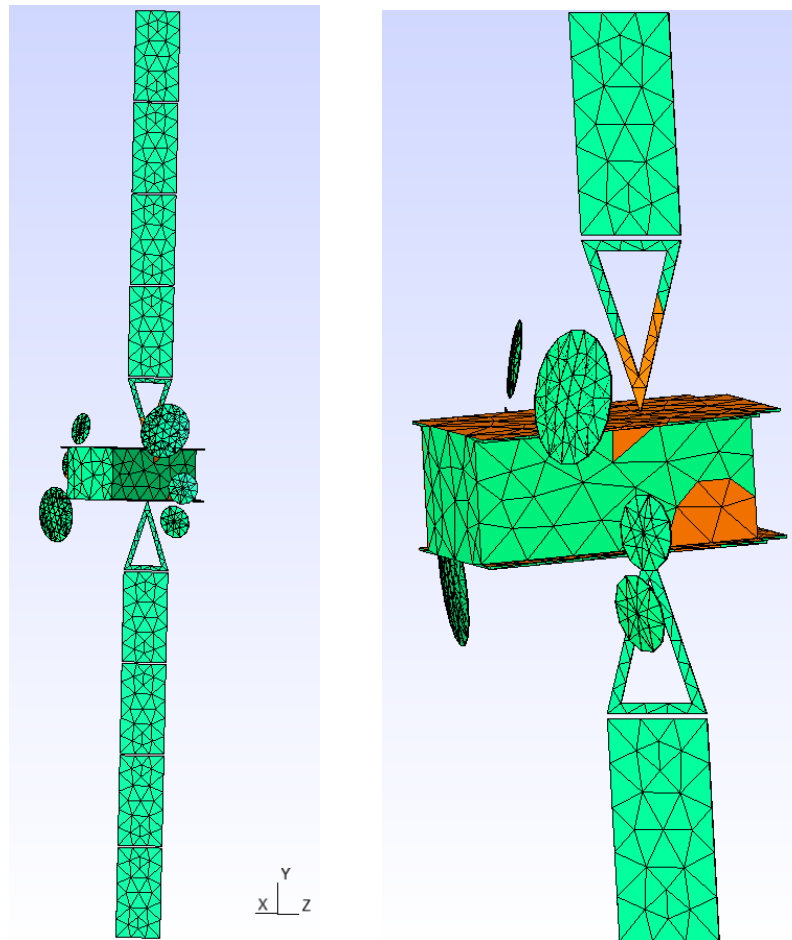


Figure 13.3: Solar shadow at the second step of the simulation, from two different points of view. The elements that are exposed to the Sun are green, while the shadowed elements are orange. In the image on the left, the satellite is seen from the Sun direction.

### 13.2.4 Solar torque

The fig. 13.5 shows the results of the analysis of the solar torque acting on the satellite, expressed in the satellite reference frame. During the eclipse phase, the solar torque is null. For this simulation, the predominant component of the solar torque is the one around the y-axis of the satellite reference frame, because it is the axis parallel to the axis of rotation of solar panels. Indeed, solar panels have a very big surface exposed to the Sun and they have a lever arm with respect to the point of calculation of the solar torque, so their contribution to the overall torque is predominant.

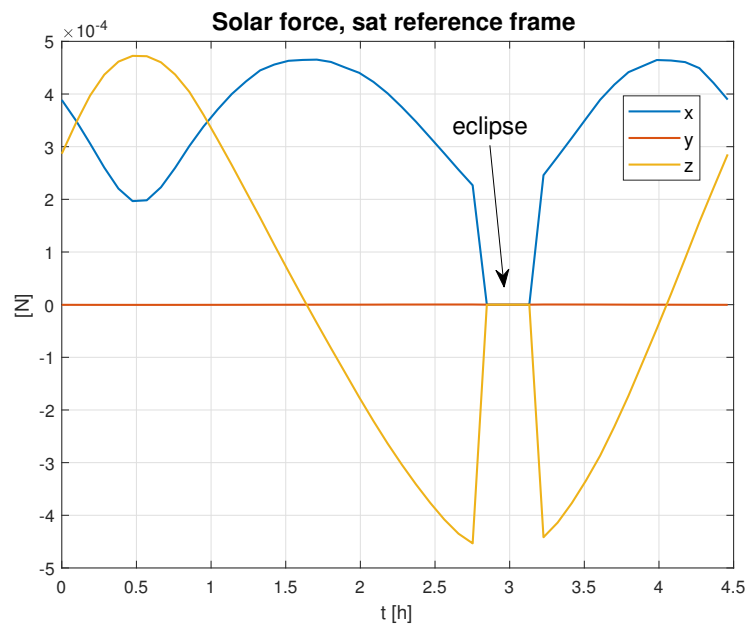


Figure 13.4: Solar force acting on the satellite, expressed in the satellite reference frame.

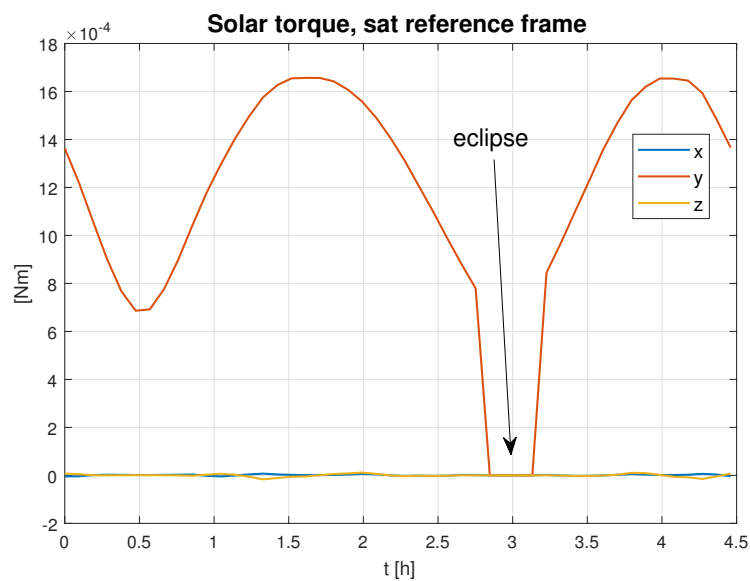


Figure 13.5: Solar torque acting on the satellite, expressed in the satellite reference frame.

### 13.3 Aerodynamic perturbation results

In this section, the results concerning the attitude perturbation linked to the aerodynamic effects are presented.

#### 13.3.1 Visualization of the orbit

The fig. 13.6 shows the orbit and the orientation of the satellite body axes for the simulation taken into account.

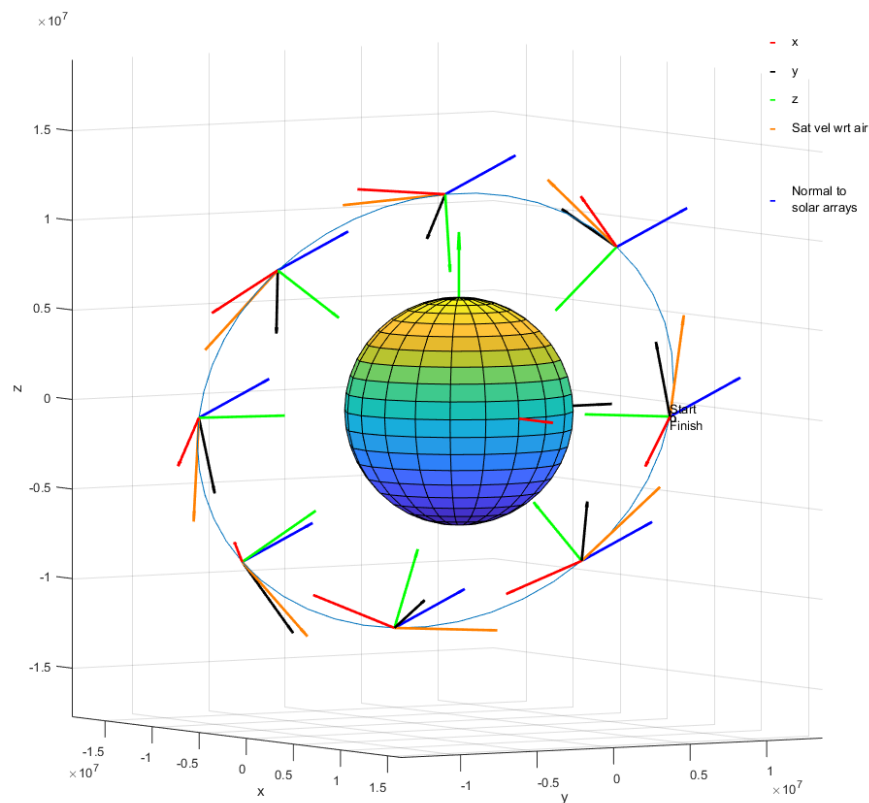


Figure 13.6: Orbit and attitude of the satellite for the chosen simulation. The blue vector is the vector normal to the solar arrays, while the orange vector is the direction of the satellite velocity with respect to the atmosphere.

### 13.3.2 Visualization of the shadowing

As for the solar shadows, the TAPAS tool allows the visualization of aerodynamic shadows on the satellite too. The fig. 13.7 shows the aerodynamic shadows on the satellite at the second simulation step, from two different points of view. The elements that are exposed to the air flow are green, while the shadowed elements are orange.

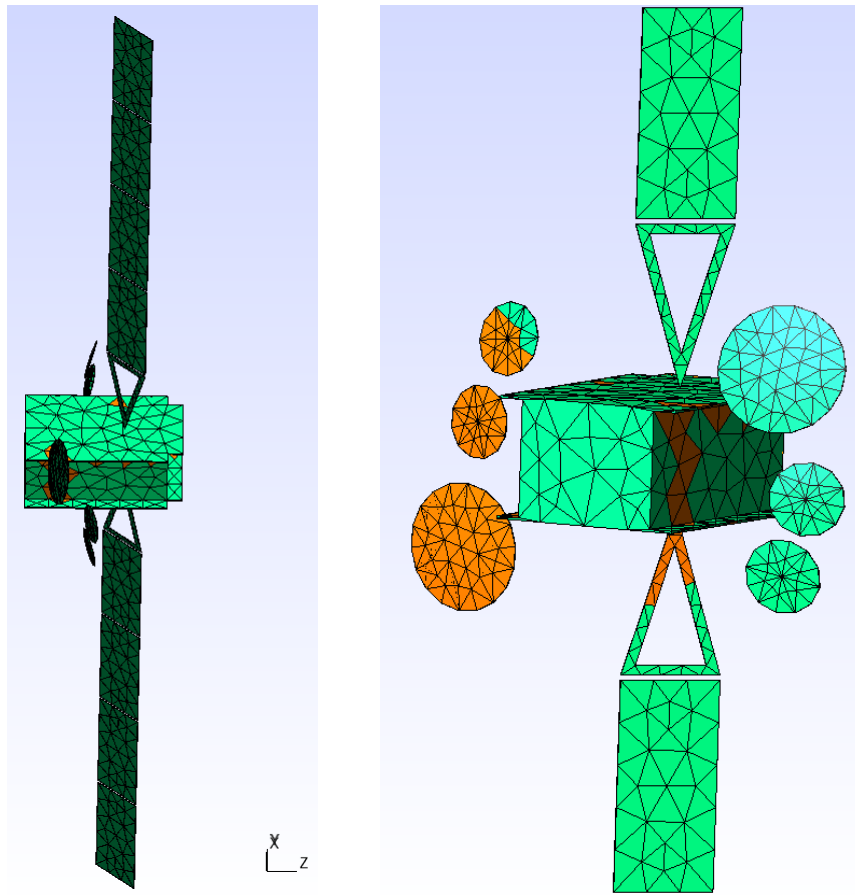


Figure 13.7: Aerodynamic shadow at the second step of the simulation, from two different points of view. The elements that are exposed to the air flow are green, while the shadowed elements are orange. In the image on the left, the satellite is seen in the direction of its velocity with respect to the atmosphere.

### 13.3.3 Aerodynamic force

The fig. 13.8 shows the results obtained for the aerodynamic force acting on the satellite, expressed in the satellite reference frame.

### 13.3.4 Aerodynamic torque

The fig. 13.9 shows the results obtained for the aerodynamic torque acting on the satellite, expressed in the satellite reference frame.

One can notice that, since the orbit is quite high, the aerodynamic perturbation is very low. Indeed, the semi major-axis of the orbit is  $13756 \text{ km}$ , which corresponds to a mean altitude of about  $1000 \text{ km}$ . At this altitude, the atmosphere is quite rarefied ( $\rho \simeq 10^{-14} \text{ kg/m}^3$ ).

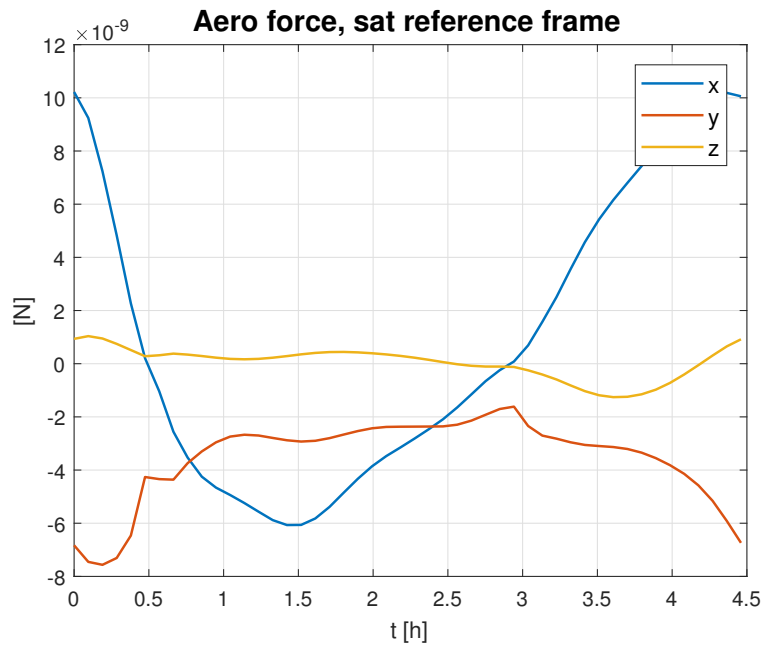


Figure 13.8: Aerodynamic force acting on the satellite, expressed in the satellite reference frame.

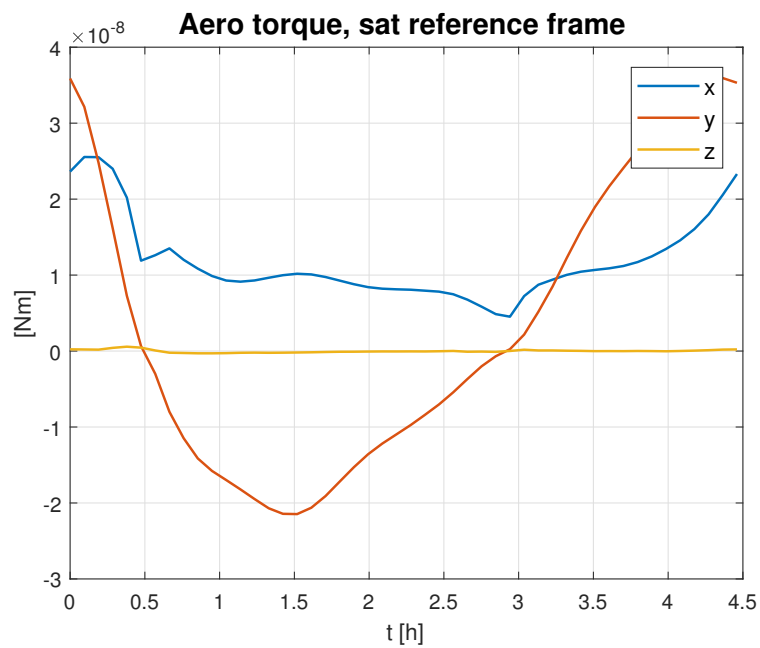


Figure 13.9: Aerodynamic torque acting on the satellite, expressed in the satellite reference frame.

# Chapter 14

## Validation results

In this chapter, some results of the validation of TAPAS are presented. Validation has been performed to ensure the proper functioning of the tool, as regards the calculation of the aerodynamic and solar perturbations. The software ESABASE has been used to validate TAPAS. As already mentioned, ESABASE is a software delivered by ESA in 1988. It allows the execution of different analysis such as the out-gassing, contamination and disturbing torques calculations. ESABASE is a closed source program, so it is not possible to see the equations and the algorithm used by this software.

### 14.1 Solar force and torque validation

To validate the solar torque, different case studies have been selected, with different geometric models, as explained below:

1. Plane plate, in GEO orbit with LOF attitude law
2. Cube, in GEO orbit with LOF attitude law
3. Cube plus two plane plates, in GEO orbit with LOF attitude law. The two plane plates represent the solar panels and are pointed towards the Sun.
4. Complete geostationary satellite with LOF attitude law
5. Complete satellite in LEO (about  $50^\circ$  of inclination) with yaw steering attitude law

Each case has been studied in three different initial dates:

- (a) Spring equinox (21<sup>st</sup> March) 2001
- (b) Summer solstice (21<sup>st</sup> June) 2001
- (c) Winter solstice (21<sup>st</sup> December) 2001

These dates are significant because, on 21<sup>st</sup> March, 21<sup>st</sup> June and 21<sup>st</sup> December, the Sun is respectively at its mean, maximum and minimum latitudes as seen from the Earth. This is illustrated in fig. 14.1.

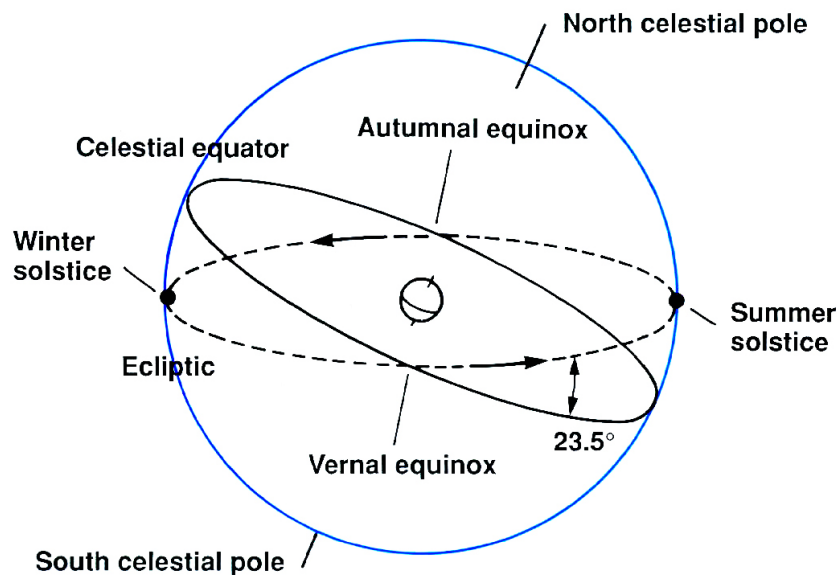


Figure 14.1: The ecliptic. On summer solstice, the Sun is at its maximum latitude, while on winter solstice, it is at its minimum latitude, as seen from the Earth [17].

For all these cases, the results of ESABASE and TAPAS have been compared. The names of the satellites, as well as the results obtained for them, are omitted for confidentiality issues. The selected cases have different orbits and attitude laws, which allows a complete validation of the tool. This section illustrates the comparison between the results of ESABASE and TAPAS for the first case: plane plate, in GEO orbit, with LOF attitude law.

### 14.1.1 ESABASE - TAPAS comparison for solar perturbation

The geometrical model chosen for this case is shown in fig. 14.2.

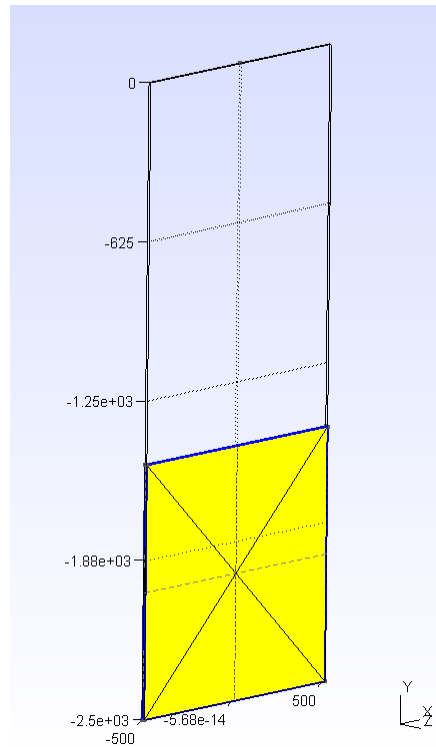


Figure 14.2: Geometric model used for the validation case of this chapter.

The point with respect to which solar perturbation is calculated is the origin of the satellite reference frame. The plate is not centered at the origin of this frame, because its center has a negative  $y$ -coordinate. If the plate was centered on the origin of the satellite reference frame, the disturbing torque would have been null, so the case would not have been interesting. The side of the plate is  $1\text{ m}$  long, and the thickness is  $1\text{ cm}$ . The initial date of the simulation is 21<sup>st</sup> June 2001 at 00:00:00 UTC. The simulation covers a complete orbit period. The orbit is geostationary and the longitude of the plate in the ECEF frame is  $0^\circ$ . The attitude law is the LOF. The material of the plate is solar cells, having the following features

1.  $C_A = 0.905$
2.  $C_D = 0.038$
3.  $C_S = 0.057$

### Solar force

For a quick comparison, the table 14.1 contains the values of the solar force components calculated by ESABASE and TAPAS, while the fig. 14.3 and 14.4 show the solar force for this analysis, obtained respectively with ESABASE and TAPAS.

The main differences between ESABASE and TAPAS results occur when the diagrams cross the  $x$ -axis. Indeed, when the value of the force component is almost null, the relative error between the two software increases significantly.

t [h]	Fx ESABASE [N]	Fx TAPAS [N]	Fy ESABASE [N]	Fy TAPAS [N]	Fz ESABASE [N]	Fz TAPAS [N]
0	-1,91E-08	2,63E-08	1,51E-06	1,53E-06	-4,00E-06	-4,05E-06
1	-8,89E-07	-8,60E-07	1,46E-06	1,48E-06	-3,73E-06	-3,80E-06
2	-1,53E-06	-1,52E-06	1,31E-06	1,34E-06	-3,01E-06	-3,09E-06
3	-1,76E-06	-1,78E-06	1,07E-06	1,10E-06	-2,02E-06	-2,10E-06
4	-1,53E-06	-1,57E-06	7,64E-07	7,91E-07	-1,02E-06	-1,08E-06
5	-9,00E-07	-9,53E-07	4,02E-07	4,28E-07	-2,87E-07	-3,20E-07
6	-7,46E-08	-8,40E-08	3,13E-08	3,54E-08	9,88E-10	-1,50E-09
7	-9,34E-07	-9,04E-07	4,19E-07	4,04E-07	3,11E-07	2,86E-07
8	-1,55E-06	-1,55E-06	7,78E-07	7,70E-07	1,06E-06	1,03E-06
9	-1,76E-06	-1,78E-06	1,09E-06	1,09E-06	2,06E-06	2,03E-06
10	-1,51E-06	-1,55E-06	1,32E-06	1,33E-06	3,05E-06	3,04E-06
11	-8,54E-07	-9,09E-07	1,46E-06	1,48E-06	3,75E-06	3,77E-06
12	2,11E-08	-2,89E-08	1,51E-06	1,53E-06	4,00E-06	4,05E-06
13	8,91E-07	8,58E-07	1,46E-06	1,48E-06	3,73E-06	3,81E-06
14	1,53E-06	1,52E-06	1,31E-06	1,34E-06	3,00E-06	3,09E-06
15	1,76E-06	1,78E-06	1,07E-06	1,10E-06	2,02E-06	2,10E-06
16	1,53E-06	1,58E-06	7,63E-07	7,92E-07	1,02E-06	1,09E-06
17	8,98E-07	9,53E-07	4,01E-07	4,28E-07	2,86E-07	3,20E-07
18	7,71E-08	8,44E-08	3,24E-08	3,55E-08	-1,13E-09	1,53E-09
19	9,36E-07	9,04E-07	4,20E-07	4,04E-07	-3,12E-07	-2,85E-07
20	1,55E-06	1,55E-06	7,79E-07	7,70E-07	-1,07E-06	-1,03E-06
21	1,76E-06	1,78E-06	1,09E-06	1,08E-06	-2,07E-06	-2,03E-06
22	1,51E-06	1,55E-06	1,32E-06	1,32E-06	-3,05E-06	-3,03E-06
23	8,52E-07	9,10E-07	1,46E-06	1,48E-06	-3,75E-06	-3,77E-06

Table 14.1: Comparison between the results of the solar force components of ESABASE and TAPAS.

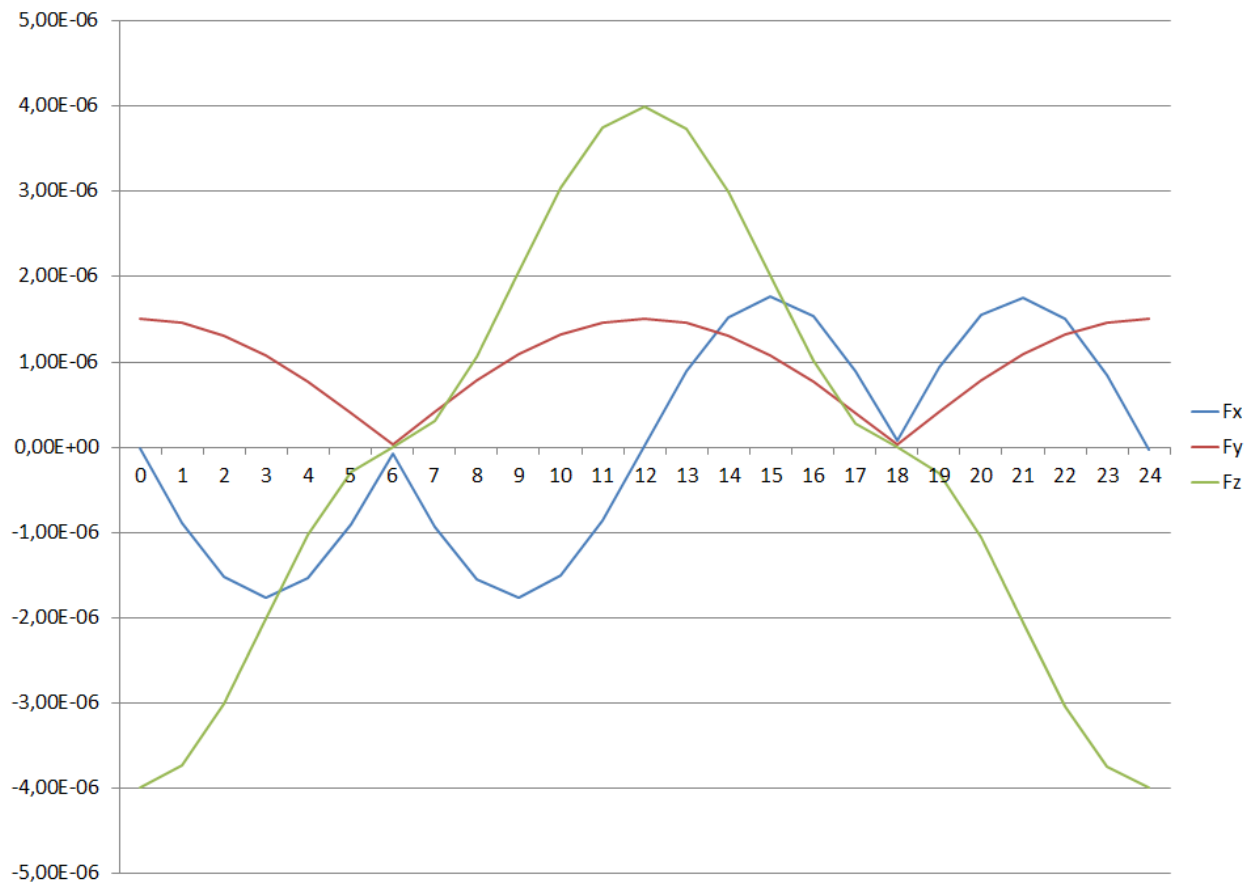


Figure 14.3: ESABASE results of the solar force, expressed in the satellite reference frame. The x-axis of the diagram is the time in hours, while the y-axis is the force in Newton.

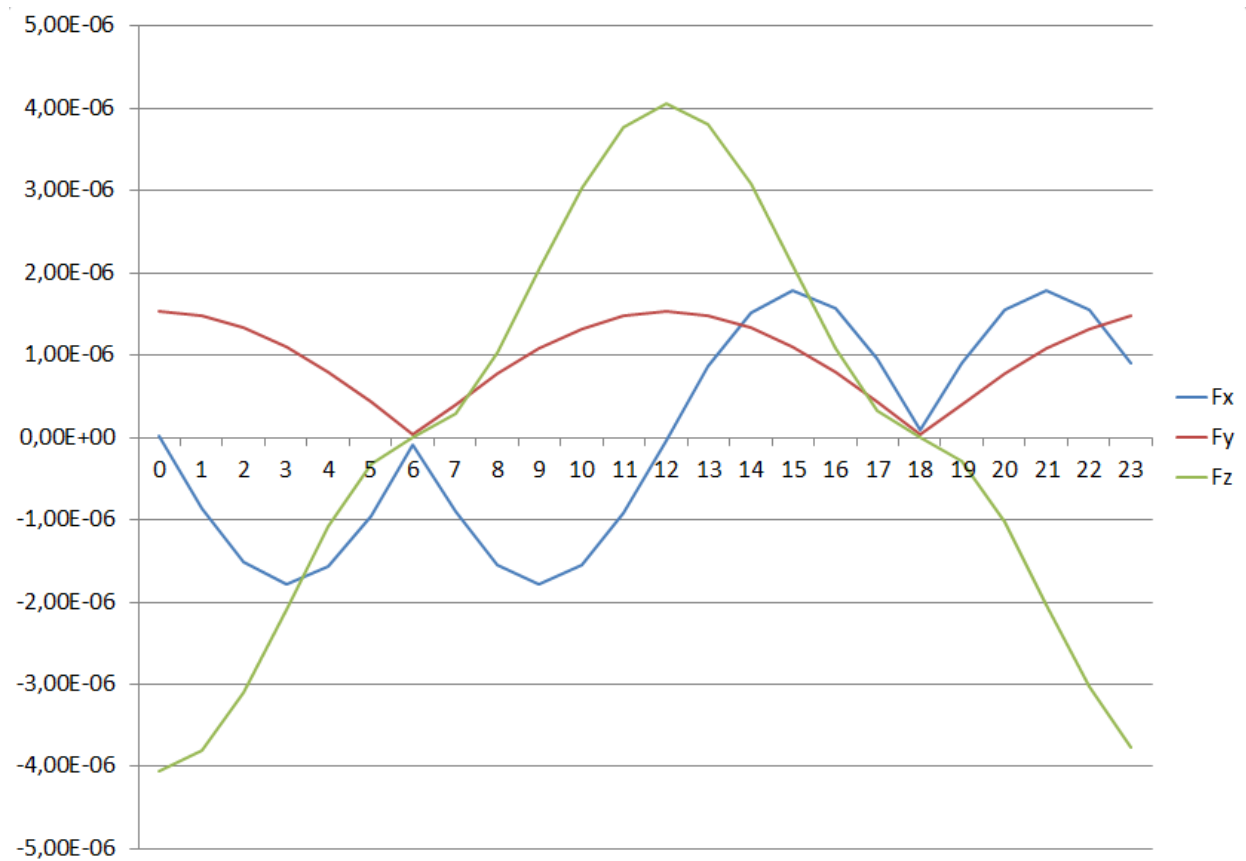


Figure 14.4: TAPAS results of the solar force, expressed in the satellite reference frame. The x-axis of the diagram is the time in hours, while the y-axis is the force in Newton.

### Solar torque

The table 14.2 contains the results of the x and z components of the solar torque on the satellite, calculated by ESABASE and TAPAS. The y component of the torque being null, it is not included in the table. The fig. 14.5 and 14.6 show the solar torque for this analysis, obtained respectively with ESABASE and TAPAS.

Also for the solar torque, the main differences between ESABASE and TAPAS occur when the torque is close to zero, because near these points the relative error between the two software can reach high values. In general, the fig. 14.3-14.6 show that the results obtained with the two software are very similar. Indeed, the ratio between ESABASE and TAPAS results is between 0.9 and 1.1 for all simulation time instants. The validation showed good results for all the case studies analyzed.

t [h]	Cx ESABASE [Nm]	Cx TAPAS [Nm]	Cz ESABASE [Nm]	Cz TAPAS [Nm]
0	7,99E-06	8,09E-06	-3,82E-08	5,27E-08
1	7,46E-06	7,60E-06	-1,78E-06	-1,72E-06
2	6,01E-06	6,18E-06	-3,05E-06	-3,04E-06
3	4,04E-06	4,19E-06	-3,52E-06	-3,57E-06
4	2,05E-06	2,17E-06	-3,06E-06	-3,15E-06
5	5,74E-07	6,39E-07	-1,80E-06	-1,91E-06
6	-1,98E-09	3,01E-09	-1,49E-07	-1,68E-07
7	-6,22E-07	-5,71E-07	-1,87E-06	-1,81E-06
8	-2,13E-06	-2,06E-06	-3,10E-06	-3,10E-06
9	-4,13E-06	-4,07E-06	-3,52E-06	-3,57E-06
10	-6,09E-06	-6,07E-06	-3,01E-06	-3,10E-06
11	-7,51E-06	-7,55E-06	-1,71E-06	-1,82E-06
12	-7,99E-06	-8,10E-06	4,22E-08	-5,77E-08
13	-7,46E-06	-7,61E-06	1,78E-06	1,72E-06
14	-6,01E-06	-6,19E-06	3,06E-06	3,04E-06
15	-4,03E-06	-4,20E-06	3,52E-06	3,57E-06
16	-2,04E-06	-2,17E-06	3,06E-06	3,15E-06
17	-5,71E-07	-6,40E-07	1,80E-06	1,91E-06
18	2,26E-09	-3,05E-09	1,54E-07	1,69E-07
19	6,25E-07	5,70E-07	1,87E-06	1,81E-06
20	2,13E-06	2,05E-06	3,11E-06	3,09E-06
21	4,13E-06	4,06E-06	3,52E-06	3,57E-06
22	6,10E-06	6,07E-06	3,01E-06	3,10E-06
23	7,51E-06	7,54E-06	1,70E-06	1,82E-06
24				

Table 14.2: Comparison between the results of the solar torque x and z components of ESABASE and TAPAS.

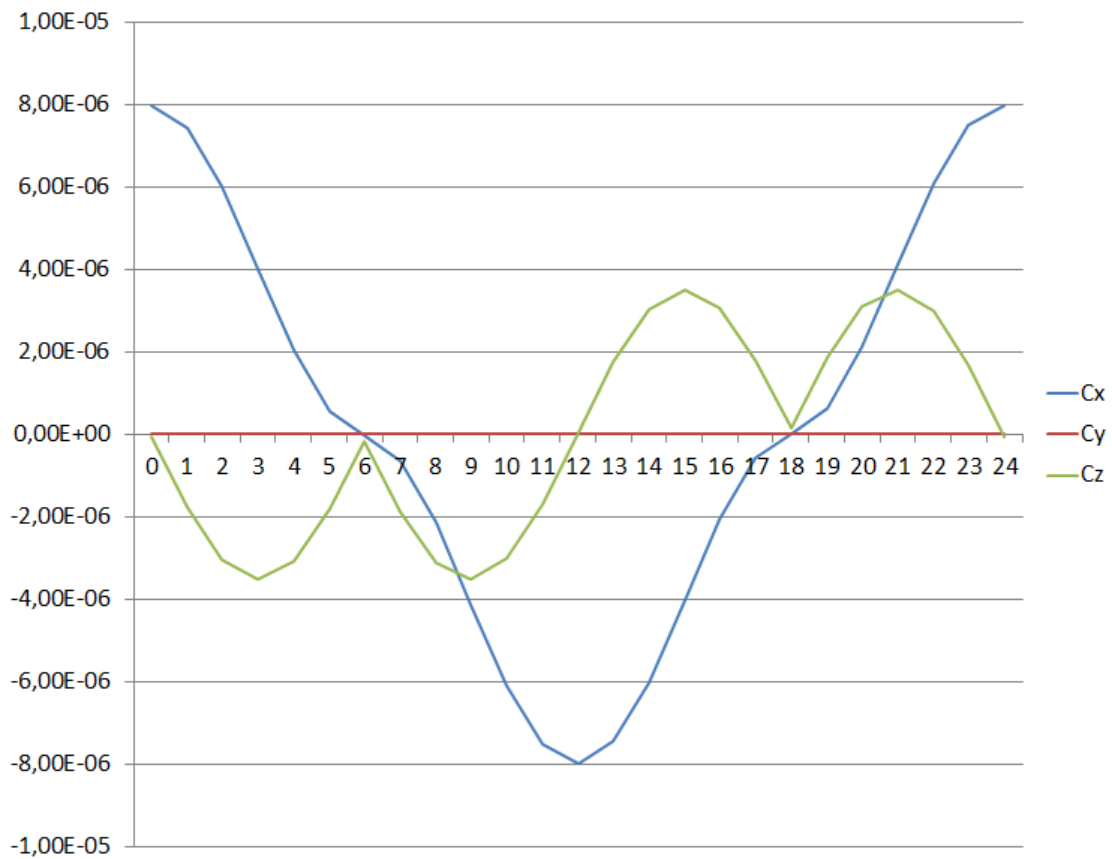


Figure 14.5: ESABASE results of the solar torque, expressed in the satellite reference frame. The x-axis of the diagram is the time in hours, while the y-axis is the torque in Newton meters.

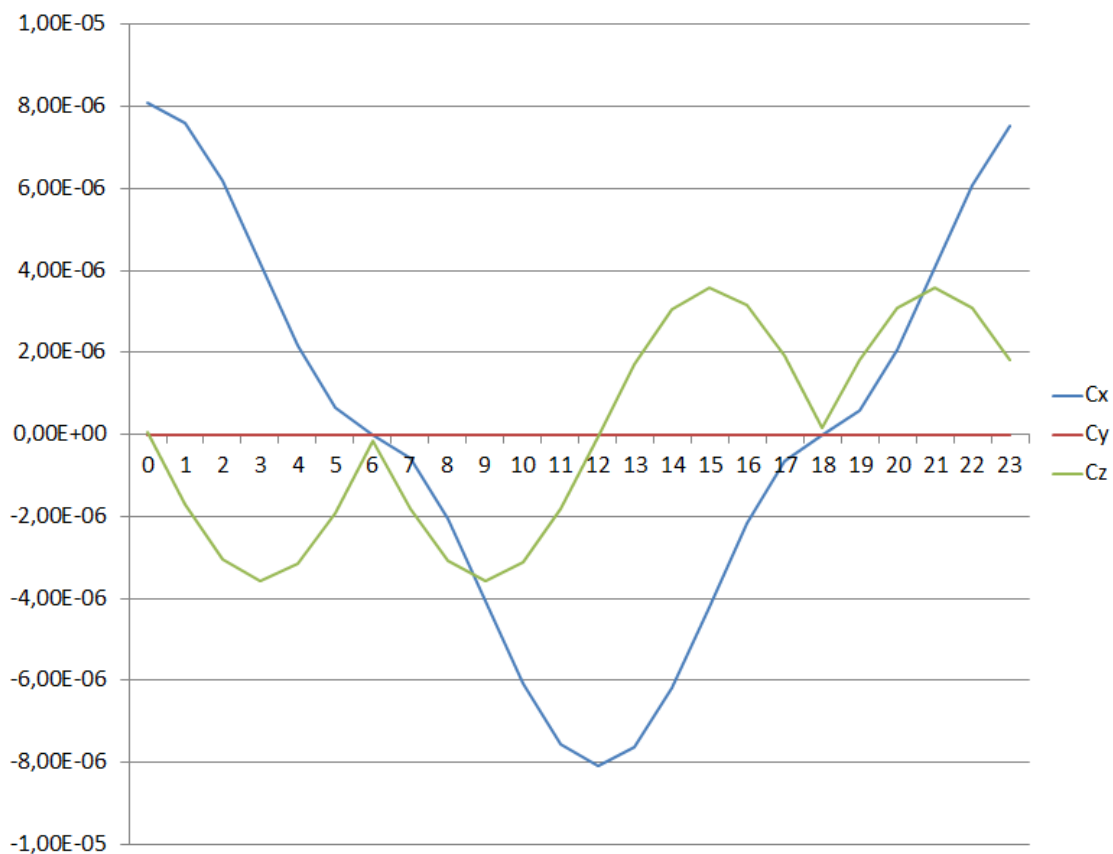


Figure 14.6: TAPAS results of the solar torque, expressed in the satellite reference frame. The x-axis of the diagram is the time in hours, while the y-axis is the torque in Newton meters.

## 14.2 Aerodynamic force and torque validation

The validation of the aerodynamic perturbation has been carried out in the following cases:

1. Plane plate, in LEO orbit (about  $50^\circ$  of inclination) with LOF attitude law
2. Cube, in LEO orbit (about  $50^\circ$  of inclination) with LOF attitude law
3. Cube plus two plane plates, in LEO orbit (about  $50^\circ$  of inclination) with LOF attitude law. The two plane plates represent the solar panels and are pointed towards the Sun.
4. Complete satellite in LEO orbit (about  $50^\circ$  of inclination), with yaw steering attitude law
5. Body of a satellite in EOR orbit, with LOF attitude law. The EOR orbit is characterized by a very low perigee and a very high apogee, and it is almost equatorial.

Also for the aerodynamic perturbation, each case has been studied in three different initial dates:

- (a) Spring equinox (21<sup>st</sup> March) 2001

(b) Summer solstice (21<sup>st</sup> June) 2001

(c) Winter solstice (21<sup>st</sup> December) 2001

The selected cases have different orbits and attitude laws, which allows a complete validation of the tool.

### 14.2.1 ESABASE - TAPAS comparison for aerodynamic perturbation

The geometrical model chosen for the example shown in this section is the one in fig. 14.2. The initial date of this simulation is again the 21<sup>st</sup> June 2001 at 00:00:00 UTC. The simulation covers a complete orbit period. The orbit has the following features:

1. altitude of 700 km
2.  $\Omega = 180^\circ$
3.  $\omega = 0^\circ$
4.  $i \simeq 50^\circ$
5.  $e = 0$
6.  $\nu = 0^\circ$

The values of the normal and tangential coefficients for the analysis are  $C_n = C_t = 2.2$ . These are the values that ESABASE uses by default. Furthermore, it has been chosen a strong intensity of solar activity.

#### Aerodynamic force

The fig. 14.7 and 14.8 show the aerodynamic force for this analysis, obtained respectively with ESABASE and TAPAS.

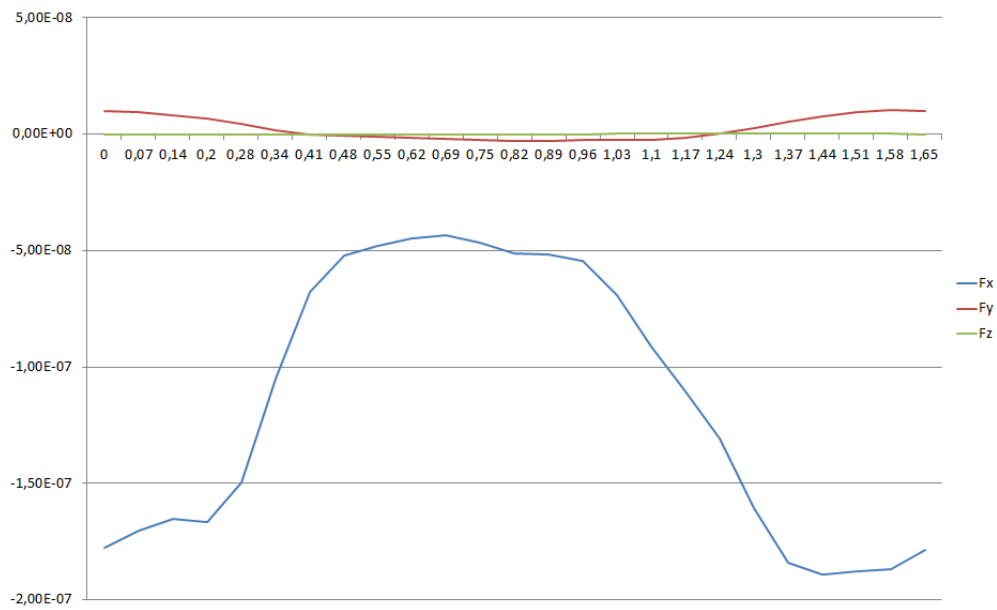


Figure 14.7: ESABASE results of the aerodynamic force, expressed in the satellite reference frame. The x-axis of the diagram is the time in hours, while the y-axis is the force in Newton.

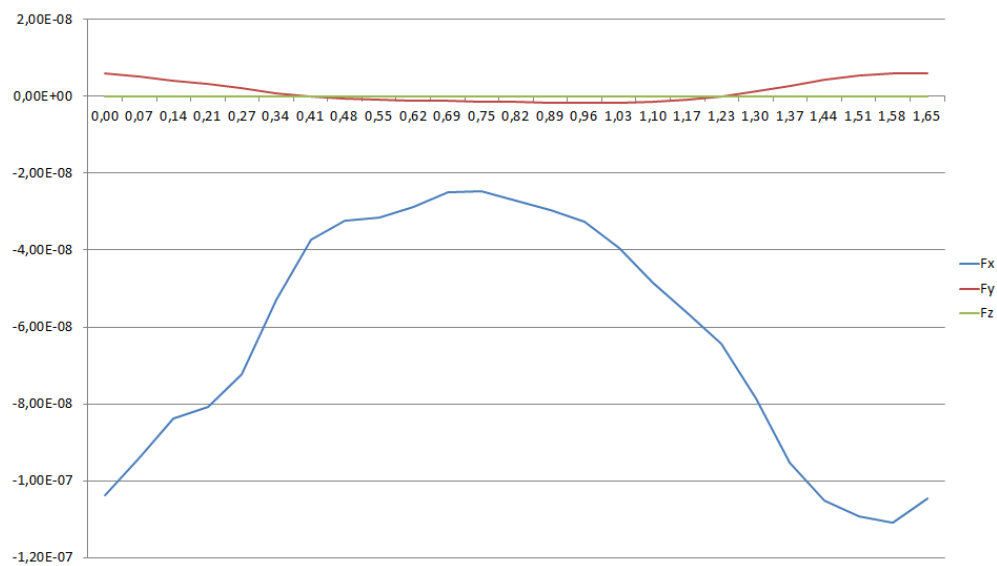


Figure 14.8: TAPAS results of the aerodynamic force, expressed in the satellite reference frame. The x-axis of the diagram is the time in hours, while the y-axis is the force in Newton.

### Aerodynamic torque

The fig. 14.9 and 14.10 show the aerodynamic torque for this analysis, obtained respectively with ESABASE and TAPAS.



Figure 14.9: ESABASE results of the aerodynamic torque, expressed in the satellite reference frame. The x-axis of the diagram is the time in hours, while the y-axis is the torque in Newton meters.

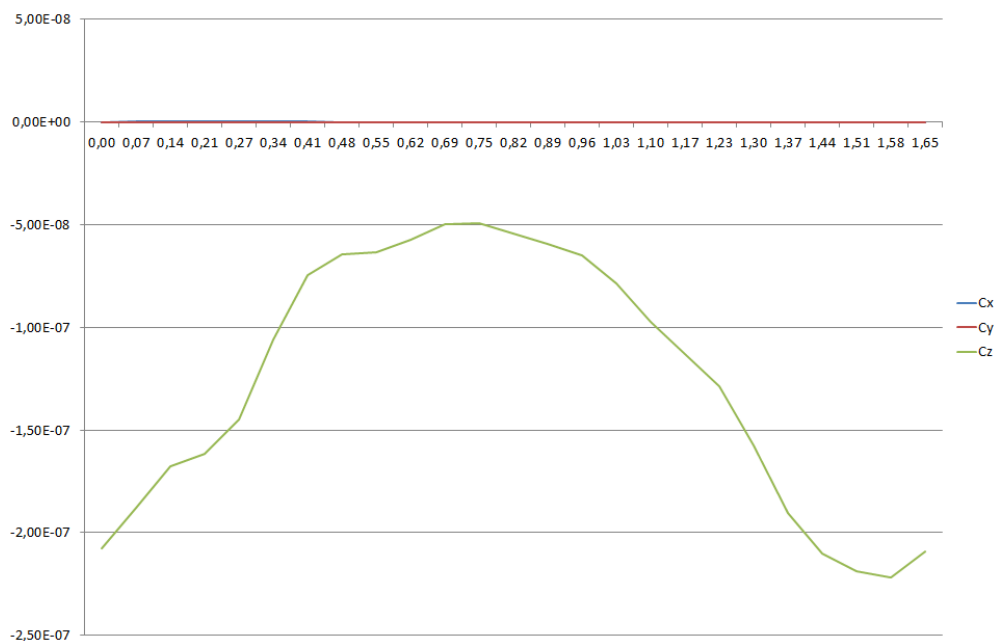


Figure 14.10: TAPAS results of the aerodynamic torque, expressed in the satellite reference frame. The x-axis of the diagram is the time in hours, while the y-axis is the torque in Newton meters.

Also for the aerodynamic perturbation, the shape of the diagrams of ESABASE and TAPAS are very similar. The values differ a bit and it is due to a different calculation of the atmospheric density between the two software. Indeed, ESABASE uses the model MSISE-86 [41], while TAPAS uses the NRLMSISE-00, which is the update of the MSIS-

86. If TAPAS results are balanced with the ESABASE atmospheric density, the ratio of the results between ESABASE and TAPAS becomes close to 1 (with 10 % of margin) for all simulation time instants. This is shown in tables 14.3 and 14.4, where the comparison between the two software is made taking into consideration the same atmospheric densities.

The validation showed good results for all the case studies analyzed.

t [h]	Fx ESABASE [N]	Fx TAPAS [N]	Fy ESABASE [N]	Fy TAPAS [N]	Fz ESABASE [N]	Fz TAPAS [N]
0	-1,78E-07	-1,78E-07	1,00E-08	1,00E-08	-3,79E-25	6,74E-23
0,07	-1,70E-07	-1,70E-07	9,30E-09	9,31E-09	-5,90E-11	-5,98E-11
0,14	-1,65E-07	-1,65E-07	8,08E-09	8,10E-09	-1,06E-10	-1,08E-10
0,2	-1,67E-07	-1,67E-07	6,65E-09	6,67E-09	-1,40E-10	-1,43E-10
0,28	-1,50E-07	-1,50E-07	4,21E-09	4,23E-09	-1,39E-10	-1,42E-10
0,34	-1,05E-07	-1,05E-07	1,52E-09	1,53E-09	-9,51E-11	-9,71E-11
0,41	-6,76E-08	-6,76E-08	-1,38E-11	-5,57E-12	-5,33E-11	-5,46E-11
0,48	-5,23E-08	-5,24E-08	-7,77E-10	-7,71E-10	-3,24E-11	-3,33E-11
0,55	-4,80E-08	-4,80E-08	-1,37E-09	-1,36E-09	-2,08E-11	-2,16E-11
0,62	-4,50E-08	-4,50E-08	-1,80E-09	-1,80E-09	-1,21E-11	-1,28E-11
0,69	-4,32E-08	-4,32E-08	-2,12E-09	-2,12E-09	-6,28E-12	-6,73E-12
0,75	-4,66E-08	-4,66E-08	-2,54E-09	-2,54E-09	-2,86E-12	-3,07E-12
0,82	-5,13E-08	-5,12E-08	-2,89E-09	-2,89E-09	-1,24E-13	4,02E-15
0,89	-5,17E-08	-5,17E-08	-2,80E-09	-2,81E-09	2,96E-12	3,45E-12
0,96	-5,47E-08	-5,47E-08	-2,65E-09	-2,66E-09	7,83E-12	8,66E-12
1,03	-6,94E-08	-6,94E-08	-2,73E-09	-2,75E-09	1,88E-11	2,01E-11
1,1	-9,12E-08	-9,13E-08	-2,50E-09	-2,53E-09	3,99E-11	4,18E-11
1,17	-1,10E-07	-1,11E-07	-1,52E-09	-1,56E-09	6,88E-11	7,11E-11
1,24	-1,31E-07	-1,31E-07	1,25E-10	7,80E-11	1,04E-10	1,06E-10
1,3	-1,61E-07	-1,61E-07	2,50E-09	2,45E-09	1,45E-10	1,49E-10
1,37	-1,84E-07	-1,84E-07	5,37E-09	5,32E-09	1,70E-10	1,74E-10
1,44	-1,89E-07	-1,89E-07	7,70E-09	7,66E-09	1,57E-10	1,61E-10
1,51	-1,88E-07	-1,88E-07	9,28E-09	9,26E-09	1,17E-10	1,20E-10
1,58	-1,87E-07	-1,87E-07	1,03E-08	1,02E-08	6,11E-11	6,33E-11
1,65	-1,79E-07	-1,79E-07	1,01E-08	1,01E-08	-2,61E-13	-2,42E-12

Table 14.3: Comparison between the results of the aerodynamic force components of ESABASE and TAPAS. The comparison is made taking into consideration the same atmospheric densities.

t [h]	Cx ESABASE [Nm]	Cx TAPAS [Nm]	Cz ESABASE [Nm]	Cz TAPAS [Nm]
0	-4,28E-18	-1,35E-22	-3,56E-07	-3,55E-07
0,07	1,18E-10	1,20E-10	-3,41E-07	-3,41E-07
0,14	2,12E-10	2,15E-10	-3,31E-07	-3,31E-07
0,2	2,81E-10	2,86E-10	-3,34E-07	-3,34E-07
0,28	2,78E-10	2,83E-10	-2,99E-07	-2,99E-07
0,34	1,90E-10	1,94E-10	-2,10E-07	-2,11E-07
0,41	1,07E-10	1,09E-10	-1,35E-07	-1,35E-07
0,48	6,48E-11	6,66E-11	-1,05E-07	-1,05E-07
0,55	4,17E-11	4,32E-11	-9,59E-08	-9,59E-08
0,62	2,43E-11	2,56E-11	-8,99E-08	-8,99E-08
0,69	1,26E-11	1,35E-11	-8,64E-08	-8,64E-08
0,75	5,71E-12	6,15E-12	-9,32E-08	-9,32E-08
0,82	2,48E-13	-8,05E-15	-1,03E-07	-1,02E-07
0,89	-5,91E-12	-6,90E-12	-1,03E-07	-1,03E-07
0,96	-1,57E-11	-1,73E-11	-1,09E-07	-1,09E-07
1,03	-3,75E-11	-4,01E-11	-1,39E-07	-1,39E-07
1,1	-7,97E-11	-8,35E-11	-1,82E-07	-1,83E-07
1,17	-1,38E-10	-1,42E-10	-2,21E-07	-2,21E-07
1,24	-2,07E-10	-2,13E-10	-2,61E-07	-2,61E-07
1,3	-2,91E-10	-2,98E-10	-3,22E-07	-3,22E-07
1,37	-3,40E-10	-3,49E-10	-3,69E-07	-3,69E-07
1,44	-3,14E-10	-3,22E-10	-3,78E-07	-3,78E-07
1,51	-2,34E-10	-2,41E-10	-3,75E-07	-3,75E-07
1,58	-1,22E-10	-1,27E-10	-3,74E-07	-3,74E-07
1,65	5,23E-13	4,84E-12	-3,58E-07	-3,58E-07

Table 14.4: Comparison between the results of the aerodynamic torque x and z components of ESABASE and TAPAS. The comparison is made taking into consideration the same atmospheric densities.

# Part VI

## Conclusions

# Chapter 15

## Conclusions

### 15.1 Current state of the TAPAS tool

At this stage, the TAPAS tool is capable of calculating the solar and aerodynamic perturbations on a generic satellite. It is simple to use and it allows the user to carry out disturbance forces and torques analysis quickly.

### 15.2 Way forward

Possible improvements of TAPAS are listed hereafter:

1. Making the tool more flexible as regards the pointing of the movable parts of the satellite. Nowadays, TAPAS can take into consideration two different attitude laws, one for the satellite's central body and one for the rotation of its solar panels around one axis. Possible future developments may improve this aspect of the tool, adding, for instance, the possibility of analyzing satellites which have rotating solar panels along two different axis, or which have movable antennas.
2. Taking the geometric model of the satellite from a step file (with .stp extension) instead of creating it with the TAPAS Gmsh routines. This file might be provided by the CAD department of TAS. Gmsh remains a necessary software for the mesh of the satellite, but taking a step file has the advantage of saving time in the creation of the satellite's model. Furthermore, the step file would be a more detailed representation of the satellite shape than the model created by the TAPAS Gmsh routines, thus allowing more precise analysis. Since Gmsh can read step files, this improvement should be quite straightforward.
3. Moving the TAPAS environment from Matlab to Python. Indeed, Python has the convenience of being an open source code, therefore free of licenses.

# Acknowledgements

I would like to thank all the people who have helped me reach the goals of this internship, in particular the engineers of the *Multi-physics analysis and modelization* team of Thales Alenia Space: Andrea Sita (my internship tutor), Véronique Perrin Bailly (responsible of the team), Vincent Dubois, David Nguyen Van Sang, Jean-François Plantier and Sylvie Brosse. They actively participated to my internship and answered all my questions. I am also grateful to Emmanuelle Benoist, who is the head of the department where I did my internship.

Open

# Appendices

# Appendix A

## Other space environment models

### A.1 Earth's gravitational field

The Earth is not perfectly spherical, and its mass density is not uniform. The fig. A.1 shows the geoid height with respect to the mean sea level, according to the EGM2008 model.

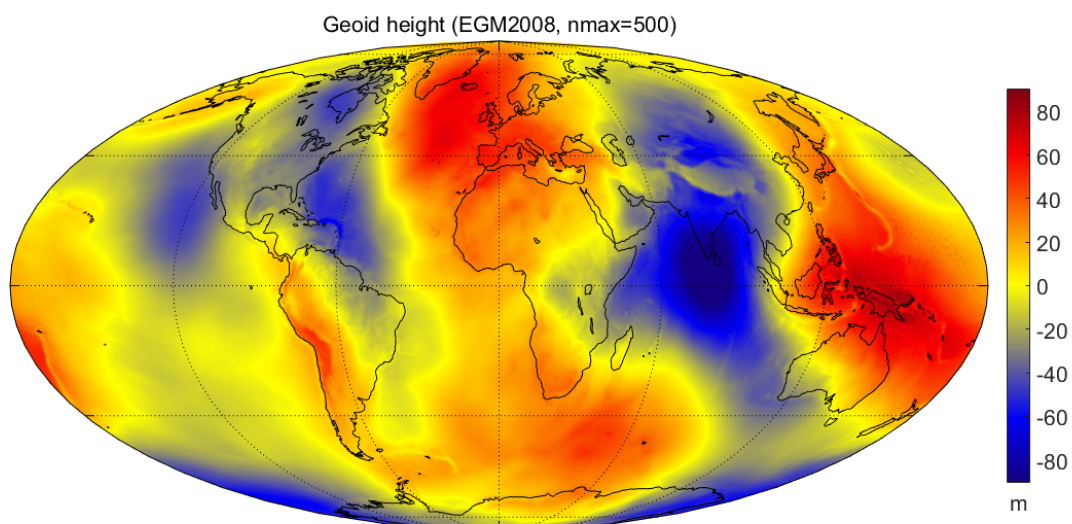


Figure A.1: Geoid height with respect to the mean sea level, according to the EGM2008 model [18].

The Earth's gravitational potential  $U$  can be written as a series expansion [42]:

$$U(\phi, \lambda, r) = -\frac{\mu}{r} \left\{ 1 + \sum_{n=1}^{\infty} \left( \frac{r_{eq}}{r} \right)^n \left[ -J_n P_n(\sin \phi) + \sum_{m=1}^n l_{n,m}(\lambda) P_{n,m}(\sin \phi) \right] \right\} \quad (\text{A.1})$$

where

1.  $\phi$  is the geodetic latitude (see chapter 4.3.2) of the considered point.
2.  $\lambda$  is the longitude of the point taken into account.
3.  $r$  is the distance between the center of the Earth and the point under consideration.
4.  $\mu$  is the Earth's standard gravitational parameter,  $\mu = GM_{Earth} = 398600 \text{ km}^3/\text{s}^2$ .

5.  $r_{eq}$  is the equatorial radius of the Earth, approximately 6378 km.
6.  $J_n$  is the Earth's zonal harmonic constant of order  $n$ .
7.  $P_n$  is the Legendre polynomial [43]. For any real number  $x$ ,  $P_n(x)$  is

$$P_n(x) = \frac{1}{2^n n!} \frac{d^n}{dx^n} [(x^2 - 1)^n] \quad (\text{A.2})$$

8.  $l_{n,m}$  is the following expression

$$l_{n,m}(\lambda) = C_{n,m} \cos(m\lambda) + S_{n,m} \sin(m\lambda) \quad (\text{A.3})$$

where  $C_{n,m}$  and  $S_{n,m}$  are other Earth's harmonic constants of degree  $n$  and order  $m$ . If  $n \neq m$  they are called tesseral harmonic constants, otherwise they are called sectoral harmonic constants.

9.  $P_{n,m}$  is the associated Legendre function [43], defined as

$$P_{n,m}(x) = (1 - x^2)^{m/2} \frac{d^m}{dx^m} P_n(x) \quad (\text{A.4})$$

where  $P_n$  is the Legendre polynomial (eq. A.2).

The fig. A.2 explains the terms zonal, tesseral and sectoral.

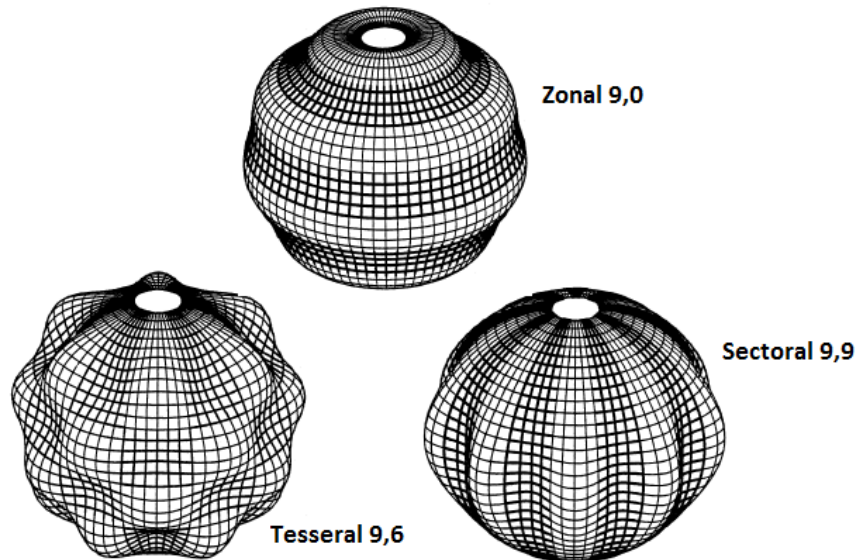


Figure A.2: Three different spherical harmonics.

The most important term in the equation A.1 is the term  $J_2 = 1.0826 \cdot 10^{-3}$  which is associated to the Earth flattening.

The differential equation that governs the motion of a satellite around the Earth is

$$\ddot{\vec{r}}(t) = -\nabla U(\phi(t), \lambda(t), r(t)) \quad (\text{A.5})$$

where  $\vec{r}$  is the position of the satellite in the EME2000 reference frame and  $t$  is the considered instant of time. To solve the eq. A.5, one needs to know the initial position and velocity of the satellite. TAPAS uses the Orekit library [33] to propagate the satellite's orbit and attitude. The most precise propagator of the Orekit library used in TAPAS implements the equation A.1 truncated to  $n = m = 10$ .

## A.2 Earth's magnetic field models

The Earth's magnetic field lines have a similar shape to the one represented in fig. A.3.

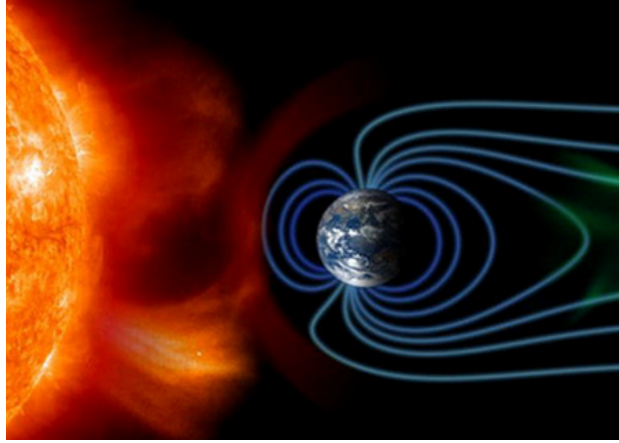


Figure A.3: Shape of the Earth magnetic field lines [19]. The Sun and the Earth are not to scale.

This field is not constant over time. The magnitude of the magnetic field at the Earth's surface ranges from 25 to 65 mT. For a first order approximation, nearby the Earth's surface the Earth's magnetic field can be described as the field of a dipole. For more accurate estimations, there are two standard numerical models: the IGRF (International Geomagnetic Reference Field) and the WMM (World Magnetic Model). They have two very similar formulations. Both models are defined by means of truncated series expansions which fit data from surveys, observations and satellites' instruments [44]. All the models presented herein are valid from the Earth's surface up to an altitude of about 800 km.

### A.2.1 Dipole magnetic field

As already mentioned, up to an altitude of about 800 km, the Earth's magnetic field can be approximated as the field of a dipole currently tilted at an angle of  $11^\circ$  with respect to Earth's rotational axis. The south pole of the Earth's field is actually at the northern hemisphere and vice versa [45].

The equation that best approximates the Earth's magnetic field as that of a dipole is the following

$$\vec{B} = B_0 \left( 3(\vec{e}_r \cdot \vec{M}_E)\vec{e}_r - \vec{M}_E \right) \left( \frac{R_E}{r} \right)^3 \quad (\text{A.6})$$

where  $B_0$  is the mean value of Earth's magnetic field at the equator, defined as  $B_0 = 3 \cdot 10^{-5}$  T,  $\vec{e}_r$  is the unit vector of the Earth-to-satellite direction in EME2000,  $\vec{M}_E$  is the magnetic moment in the EME2000 frame ( $\vec{M}_E = [0, 0, -1]$ ),  $R_E = 6371.2$  km is the geomagnetic conventional Earth's mean spherical radius and  $r$  is the norm of the satellite position vector [21]. Moving away from the Earth's surface, the dipole approximation is no more valid because the lines of the Earth's magnetic field are deflected by the solar wind, as shown in fig. A.3.

### A.2.2 IGRF (International Geomagnetic Reference Field)

The IGRF model is a standard mathematical description of the Earth's magnetic field [46]. On and above the Earth's surface, the magnetic field  $\vec{B}$  is defined in terms of a magnetic scalar potential  $V$  as

$$\vec{B} = -\nabla V \quad (\text{A.7})$$

As already mentioned, the magnetic scalar potential is represented by a truncated series expansion, as follows

$$V(r, \varphi, \lambda) = R_E \sum_{n=1}^N \left( \frac{R_E}{r} \right)^{n+1} \sum_{m=0}^n (g_{n,m} \cos(m\lambda) + h_{n,m} \sin(m\lambda)) \hat{P}_{n,m}(\cos(\varphi)) \quad (\text{A.8})$$

where  $r$  is the distance between the center of the Earth and the considered point,  $\varphi$  and  $\lambda$  are the co-latitude and longitude of this point,  $t$  is the time,  $R_E$  is the geomagnetic conventional Earth's mean spherical radius,  $N$  is equal to 13 and  $g_{n,m}$  and  $h_{n,m}$  are two real, time-dependent empiric coefficients associated to  $n$  and  $m$  values.  $\hat{P}_{n,m}$  is the Schmidt quasi-normalized associated Legendre function of degree  $n$  and order  $m$ . For any real number  $x$ , this function is defined as follows [47]:

$$\hat{P}_{n,m}(x) = \begin{cases} \sqrt{2} \frac{(n-m)!}{(n+m)!} P_{n,m}(x) & \text{if } m > 0 \\ P_{n,m}(x) & \text{if } m = 0 \end{cases} \quad (\text{A.9})$$

where  $P_{n,m}$  is the associated Legendre function (see eq. A.4). In the last version of the IGRF model (IGRF-12), the coefficients  $g_{n,m}$  and  $h_{n,m}$  are provided at epochs separated by 5 years (for instance, 2000, 2005, 2010...). The time dependence of these coefficients is assumed to be linear over 5-year intervals between two epoch dates.

### A.2.3 WMM (World Magnetic Model)

Another standard model of the Earth's magnetic field is the WMM. It is used by the US and UK defense agencies. Its mathematical formulation is the same as the IGRF (see eq. A.7-A.9), but the way the coefficients  $g_{n,m}$  and  $h_{n,m}$  are defined changes. The differences between IGRF and WMM are within expected model inaccuracy. The WMM is a predictive-only model and is valid for the current epoch (2015.0 to 2020.0). The IGRF is retrospectively updated and its latest release is valid for the years 1900.0 to 2020.0. [48]

The fig. A.4 shows the declination of the Earth's magnetic field lines, while the fig. A.5 shows the intensity of this field, according to the WMM model for the epoch 2015.0 [48].

**US/UK World Magnetic Model - Epoch 2015.0  
Main Field Declination (D)**

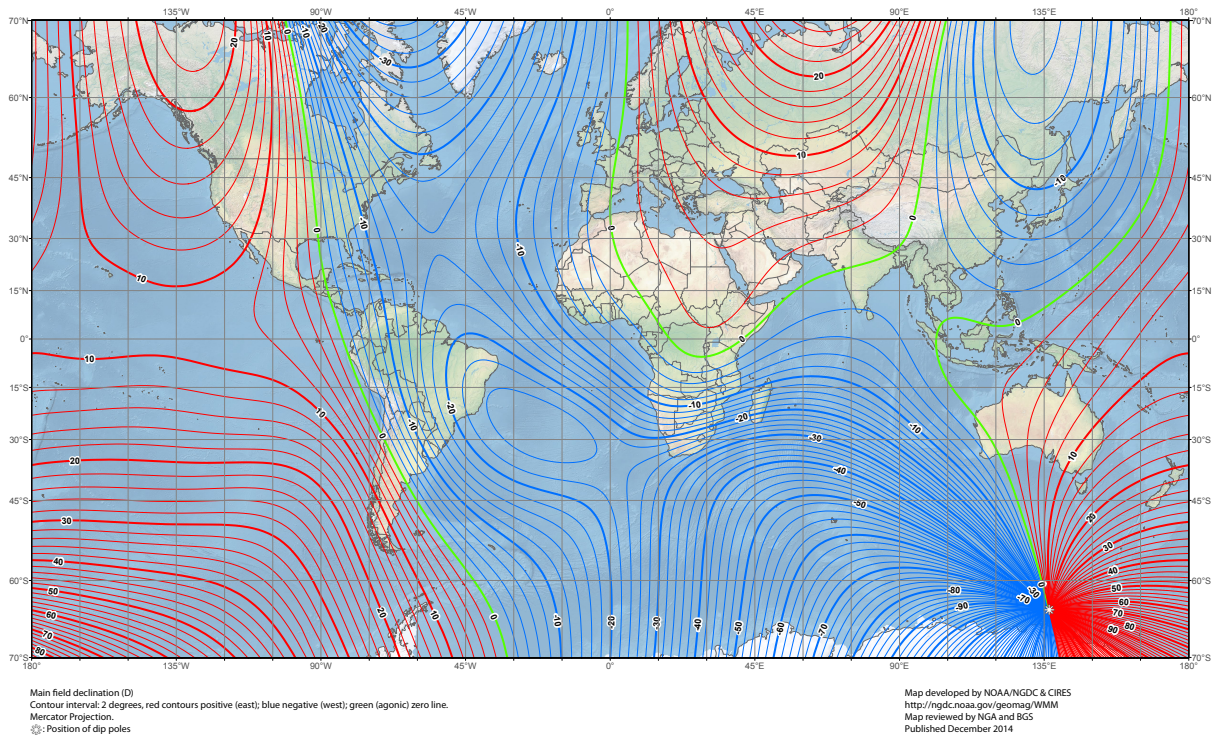


Figure A.4: Declination of the Earth’s magnetic field lines, according to the WMM - Epoch 2015.0.

**US/UK World Magnetic Model - Epoch 2015.0  
Main Field Total Intensity (F)**

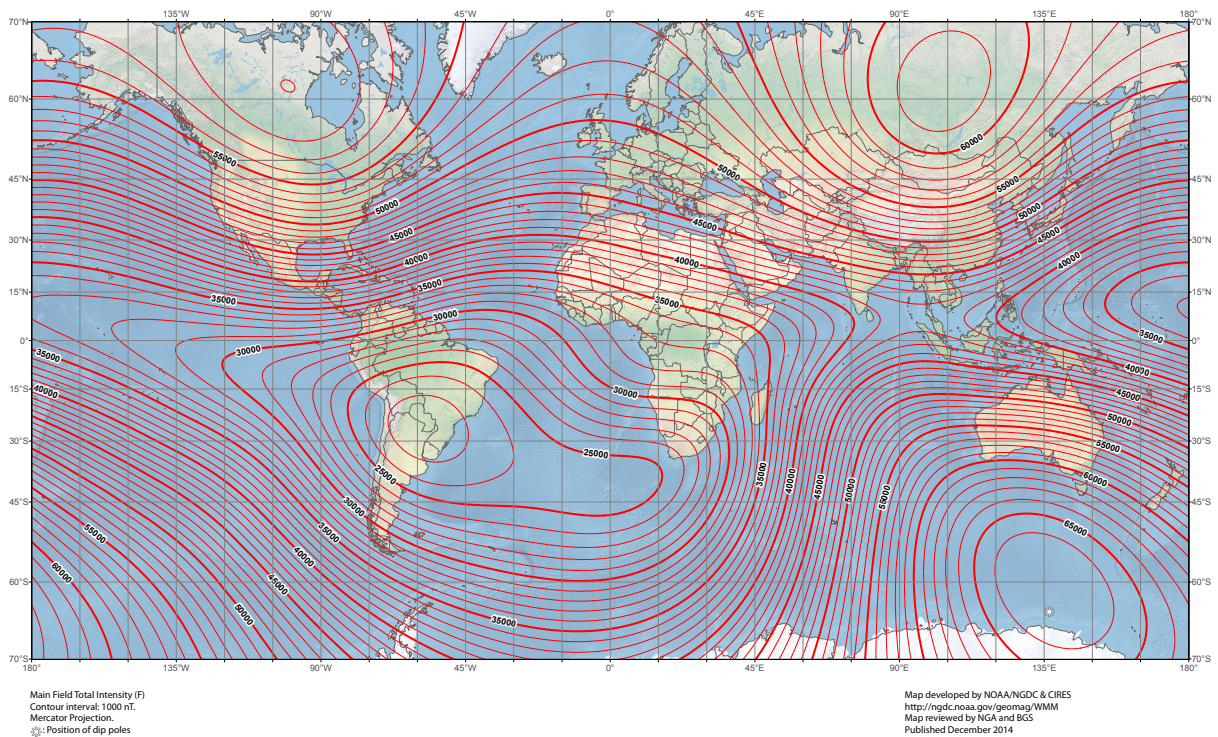


Figure A.5: Intensity of the Earth’s magnetic field, according to the WMM - Epoch 2015.0.

Open

### A.3 Sun ephemeris model

To estimate the solar radiation pressure force and torque, one has to know the position of the Sun with respect to the spacecraft at each instant of time of the simulation. For this, a model of the Sun ephemeris is necessary. TAPAS uses the Jean Meeus model [49], which estimates the position of the Sun with respect to the Earth, in the EME2000 frame, for all time instants from the 1<sup>st</sup> January 1901 to the 31<sup>st</sup> December 2099. The input of this model is the Julian day (in Terrestrial Time) associated to the time instant of the simulation. The starting date to count days is the 1<sup>st</sup> January 4713 BC of the proleptic Julian calendar [27]. Then, the position of the Sun with respect to the satellite is given by the following expression

$$\vec{v}_{sat-Sun}^{[EME2000]} = \vec{v}_{Earth-Sun}^{[EME2000]} - \vec{v}_{Earth-sat}^{[EME2000]} \quad (\text{A.10})$$

where  $\vec{v}_{sat-Sun}^{[EME2000]}$  is the position of the Sun with respect to the satellite's center of gravity,  $\vec{v}_{Earth-Sun}^{[EME2000]}$  is the position of the Sun with respect to the Earth, and  $\vec{v}_{Earth-sat}^{[EME2000]}$  is the position of the satellite with respect to the Earth. All these vectors are expressed in the EME2000 reference frame. Since the disturbing forces and torques are calculated in the satellite reference frame, the vector  $\vec{v}_{sat-Sun}$  must be expressed in the satellite reference frame. This can be done by multiplying this vector by the transformation matrix associated to the attitude of the satellite with respect to the EME2000 reference frame.

## Appendix B

# Different ways of defining the attitude of a satellite

### B.1 Cardan angles

Cardan angles express the attitude of an object in space by means of three elemental rotations, i.e. rotations around the axis of a coordinate system [50]. It is important to specify the order of the three rotations, because rotation operations are not commutative. For classical Cardan angles, the order of the three rotations is z, y and x and the related angles are called yaw, pitch and roll. The fig. B.1 shows the Cardan angles of a satellite around the Earth.

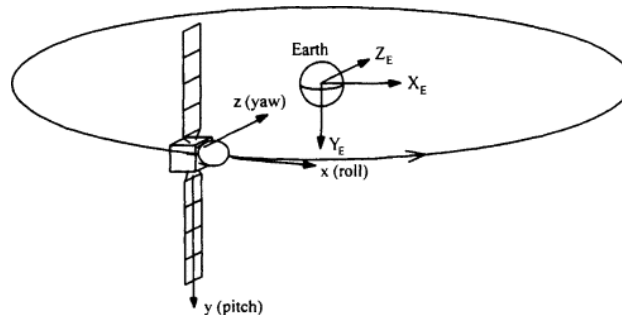


Figure B.1: Cardan angles of a satellite around the Earth [20].

The advantage of using Cardan angles for the definition of the attitude of a body is that they have a straightforward physical meaning. On the other side, the big drawback of this kind of attitude representation is the presence of a singularity when the pitch angle (around y axis) is  $90^\circ$ . This phenomenon is known as gimbal lock. For the applications in which TAPAS uses this kind of attitude definition, the tool makes a check on the value of the second Cardan angle. If it is  $90^\circ$ , TAPAS modifies slightly the attitude of the satellite to avoid the singularity.

### B.2 Rotation matrix

Another way of defining the attitude of a rigid body in space is by means of a rotation matrix. Taking into consideration two reference frames F1 and F2, and calling  $x_1^{[F2]}$ ,  $y_1^{[F2]}$

and  $z_1^{[F2]}$  the three unit column vectors of the reference frame F1, expressed in F2, one can write the following relationship

$$X^{[F2]} = M \cdot X^{[F1]} = \begin{bmatrix} x_1^{[F2]} & y_1^{[F2]} & z_1^{[F2]} \end{bmatrix} \cdot X^{[F1]} \quad (\text{B.1})$$

where  $X^{[F2]}$  is a vector expressed in the F2 reference frame,  $M$  is the rotation matrix, and  $X^{[F1]}$  is the same vector expressed in the F1 reference frame. The rotation matrices do not present any singularity, but they have the downside of being difficult to use and computationally heavy.

### B.3 Quaternions

In spacecraft dynamics, quaternions are widely used to define the attitude of a satellite with respect to a given reference system. Quaternions present the advantage of having no singularities and being simple to use. The fundamental idea behind the definition of a quaternion is that to pass from a reference system to another, one only needs a single rotation around a specific axis, which, in general, does not coincide with any of the three Cartesian axis of the two reference frames. This means that, to define the attitude of an object in space, one just has to define the unit vector  $\vec{n}$  related to the axis of rotation and the angle of rotation  $\theta$ . So, the quaternion corresponding to a rotation of  $\theta$  around  $\vec{n}$  is defined as the following vector of four components

$$q = \begin{bmatrix} \cos\left(\frac{\theta}{2}\right) \\ \sin\left(\frac{\theta}{2}\right) \vec{n} \end{bmatrix} \quad (\text{B.2})$$

For spacecraft orbiting around the Earth, the starting reference frame is usually the EME2000, while the reference frame of arrival is the satellite reference system.

# Appendix C

## The Runge-Kutta 4 method

The Runge-Kutta 4 is a method to solve ordinary differential equations numerically. A generic initial value problem has the following expression:

$$\begin{cases} \dot{y} = f(t, y) \\ y(t_0) = y_0 \end{cases} \quad (\text{C.1})$$

where  $y$  is an unknown function of time  $t$  ( $y$  can be scalar or vectorial),  $\dot{y}$  its time derivative and  $f$  a generic function of  $t$  and  $y$ . Taking a time step  $dt > 0$  and denoting  $y_n = y(n dt)$  and  $t_n = n dt$ , where  $n$  is a positive integer number, the Runge-Kutta 4 method consists in approximating the function  $y$  at the time instant  $t_{n+1}$  with the following expression [51]

$$y_{n+1} = y_n + \frac{1}{6} dt (k_1 + 2k_2 + 2k_3 + k_4) \quad (\text{C.2})$$

where

$$\begin{cases} k_1 = f(t_n, y_n) \\ k_2 = f\left(t_n + \frac{dt}{2}, y_n + \frac{k_1}{2}\right) \\ k_3 = f\left(t_n + \frac{dt}{2}, y_n + \frac{k_2}{2}\right) \\ k_4 = f(t_n + dt, y_n + k_3) \end{cases} \quad (\text{C.3})$$

A graphical explanation of the previous equations is given in fig. C.1

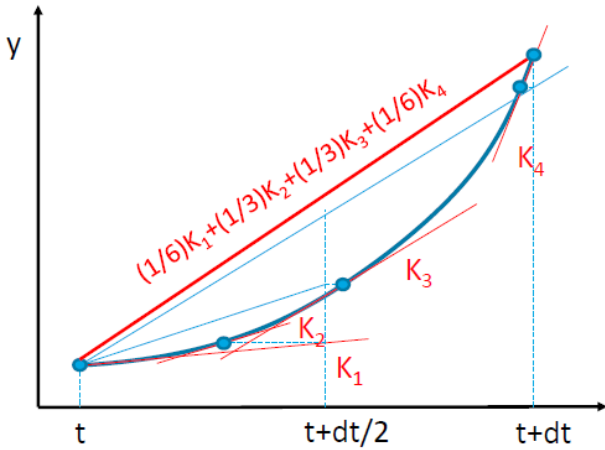


Figure C.1: Runge-Kutta 4 method [21].

# Bibliography

- [1] Wikipedia, “Solar Time.” [https://en.wikipedia.org/wiki/Solar\\_time](https://en.wikipedia.org/wiki/Solar_time).
- [2] USGS, “USGS science for a changing world.” <https://landsat.usgs.gov/landsat-8-data-users-handbook-appendix-a>.
- [3] “what-when-how.” <http://what-when-how.com/gps-with-high-rate-sensors/ecef-coordinate-systems-gps/>.
- [4] Wikipedia, “Latitude.” <https://en.wikipedia.org/wiki/Latitude>.
- [5] SUMUS Tracker, “Conversion to Geodetic Coordinates.” <http://www.stltracker.com/resources/equations>.
- [6] NOAA National Oceanic and Atmospheric Administration, “National Geodetic Survey.” <https://www.ngs.noaa.gov/TOOLS/XYZ/xyz.shtml>.
- [7] S. Jayaram and D. Pais, *Model-based Simulation of Passive Attitude Control of SLUCUBE-2 Using Nonlinear Hysteresis and Geomagnetic Models*.
- [8] Storyblocks VIDEOBLOCKS. <https://www.videoblocks.com/video>.
- [9] SlidePlayer, “External Disturbance Torques.” <https://slideplayer.com/slide/4773365>.
- [10] Wikipedia, “Right-hand rule.” [https://en.wikipedia.org/wiki/Right-hand\\_rule](https://en.wikipedia.org/wiki/Right-hand_rule).
- [11] what-when how, “Precision orbit determination for earth observation systems.” <http://what-when-how.com/space-science-and-technology/>.
- [12] Quora, “What is the beta angle with respect to sun-synchronous satellites?.” <https://www.quora.com/>.
- [13] A. Allahviridizadeh, J. Asgari, and A. Amiri-Simkooei, “Investigation of GPS draconitic year effect on GPS time series of eliminated eclipsing GPS satellite data,” *Journal of Geodetic Science*, 2016.
- [14] “SpaceWeatherLive.” <https://www.spaceweatherlive.com/en/solar-activity/solar-cycle>.
- [15] NASA Marshall Space Flight Center, “Solar Activity Forecast.” <https://sail.msfc.nasa.gov/>.
- [16] D. R. Weimer, “A comparison of the JB2008 and NRLMSISE-00 neutral density models,” *GEM Meeting*, 2014.

- [17] University of Virginia, “Equinoxes and solstices.” [faculty.virginia.edu](http://faculty.virginia.edu).
- [18] ASU, “Matlab script for 3d visualisation.” [https://www.asu.cas.cz/~bezdek/vyzkum/rotating\\_3d\\_globe](https://www.asu.cas.cz/~bezdek/vyzkum/rotating_3d_globe).
- [19] Science of cycles, “Solar Wind and Earth Magnetic Field.” <https://scienceofcycles.com>.
- [20] O. Tekinalp, Y. Tulunay, and O. Uslu, “An Attitude Control System Design Based on the Turksat-1b Geostationary Satellite,” *ScienceDirect*, 2007.
- [21] J. Michaud and L. Tomasini, *Workshop on small satellites design*. ISAE-Supaero.
- [22] Wikipedia, “Sidereal Time.” [https://en.wikipedia.org/wiki/Sidereal\\_time](https://en.wikipedia.org/wiki/Sidereal_time).
- [23] Wikipedia, “Universal Time.” [https://en.wikipedia.org/wiki/Universal\\_Time](https://en.wikipedia.org/wiki/Universal_Time).
- [24] Wikipedia, “Coordinated Universal Time.” [https://en.wikipedia.org/wiki/Coordinated\\_Universal\\_Time](https://en.wikipedia.org/wiki/Coordinated_Universal_Time).
- [25] Wikipedia, “Terrestrial Time.” [https://en.wikipedia.org/wiki/Terrestrial\\_Time](https://en.wikipedia.org/wiki/Terrestrial_Time).
- [26] Wikipedia, “International Atomic Time.” [https://en.wikipedia.org/wiki/International\\_Atomic\\_Time](https://en.wikipedia.org/wiki/International_Atomic_Time).
- [27] Wikipedia, “Julian day.” [https://en.wikipedia.org/wiki/Julian\\_day](https://en.wikipedia.org/wiki/Julian_day).
- [28] Sidi, Marcel J., *Spacecraft Dynamics and Control*. Melbourne, Australia: Cambridge University Press, 1997.
- [29] A. Heidecker, “Development of algorithms for attitude determination and control of the AsteroidFinder satellite,” Master’s thesis, Technische Universität Braunschweig, Braunschweig, 2009.
- [30] F. Romano, “System Analysis and Test-Bed for an Air-Breathing Electric Propulsion System,” *ResearchGate*, 2014.
- [31] CNES - Centre national d’études spatiales, *Cours de technologie spatiale : Techniques et Technologies des Véhicules Spatiaux*. CNES and CILF, 1999.
- [32] Wikipedia, “Gmsh.” <https://en.wikipedia.org/wiki/Gmsh>.
- [33] CS Systèmes d’information, “Orekit.” <https://www.orekit.org/>.
- [34] M.C. Eckstein, H. Hechler, “A reliable derivation of the perturbations due to any zonal and tesseral harmonics of the geopotential for nearly-circular satellite orbits,” 1970.
- [35] R. Mukundan, “A procedure for the estimation of solar radiation torque components considering multiple shadow regions and surface reflectance properties,” *Math/Comput. Modelling, Vol. 13, No. 4, pp. 1-6*, 1990.
- [36] ECSS European Cooperation for Space Standardization, *Space engineering - Space environment*. ESA Requirements and Standards Division, 2008.

- [37] NorthWest Research Associate, Inc., “Geomagnetic Disturbance Index.” <https://spawx.nwra.com/spawx/ap.html>.
- [38] J. M. Picone, A. E. Hedin, D. P. Drob, and A. C. Aikin, “Nrlmsise-00 empirical model of the atmosphere: Statistical comparison and scientific issues,” *Journal of geophysical research*, 2002.
- [39] Wikipedia, “NRLMSISE-00.” <https://en.wikipedia.org/wiki/NRLMSISE-00>.
- [40] M. Mahooti, “NRLMSISE-00 Atmosphere Model.” <https://it.mathworks.com/matlabcentral/fileexchange/56253-nrlmsise-00-atmosphere-model>.
- [41] S. North, Pergamon TSI, *ESABASE Users Reference Manual*. ESA-ESTEC, 1988.
- [42] B. Escudier and J.-Y. Pouillard, *Mécanique spatiale*. ISAE-Supaero, 2008.
- [43] Wikipedia, “Associated Legendre Polynomials.” [https://en.wikipedia.org/wiki/Associated\\_Legendre\\_polynomials](https://en.wikipedia.org/wiki/Associated_Legendre_polynomials).
- [44] Wikipedia, “International Geomagnetic Reference Field.” [https://en.wikipedia.org/wiki/International\\_Geomagnetic\\_Reference\\_Field](https://en.wikipedia.org/wiki/International_Geomagnetic_Reference_Field).
- [45] Wikipedia, “Earth’s magnetic field.” [https://en.wikipedia.org/wiki/Earth%27s\\_magnetic\\_field](https://en.wikipedia.org/wiki/Earth%27s_magnetic_field).
- [46] E. Thébault *et al.*, “International geomagnetic reference field: the 12th generation,” *Earth, Planets and Space*, vol. 67, no. 1, 2015.
- [47] D. E. Winch, D. J. Ivers, J. P. R. Turner, and R. J. Stening, “Geomagnetism and Schmidt quasi-normalization,” *Geophysical Journal International*, 2005.
- [48] NOAA National Oceanic and Atmospheric Administration, “Geomagnetism.” <https://www.ngdc.noaa.gov/geomag/>.
- [49] J. Meeus, *Astronomical Algorithms*. Willmann-Bell, Inc., 1999.
- [50] Wikipedia, “Euler angles.” [https://en.wikipedia.org/wiki/Euler\\_angles](https://en.wikipedia.org/wiki/Euler_angles).
- [51] Wikipedia, “Runge-kutta methods.” [https://en.wikipedia.org/wiki/Runge%E2%80%93Kutta\\_methods](https://en.wikipedia.org/wiki/Runge%E2%80%93Kutta_methods).